vicomtech
your R&D partner for smart digital solutions

POLITECNICO DI MILANO
DEPARTMENT OF ELECTRONICS, INFORMATION AND BIOENGINEERING
DOCTORAL PROGRAMME IN BIOENGINEERING

# DECISION-SUPPORT SYSTEM FOR STEREOELECTROENCEPHALOGRAPHY TRAJECTORY PLANNING

Doctoral Dissertation of:
**Davide Scorza**

Supervisors:
**Elena De Momi, PhD**
**Álvaro Bertelsen Simonetti, PhD**
**Francesco Cardinale, MD**

Tutor:
**Prof. Emanuela Teresa Raimondi**

The Chair of the Doctoral Program:
**Prof. Andrea Aliverti**

2019 – XXXI – Executive PhD

# Abstract

STEREO-ELECTROENCEPHALOGRAPHY (SEEG) is a minimally invasive technique which allows the exploration of brain's activity in patients affected by focal epilepsy, helping the identification of the epileptogenic zone (EZ). The procedure requires to implant a variable number of intracerebral electrodes through small holes drilled in the patient's skull and must accomplish the accurate targeting of the desired intracerebral structures, while minimizing the risk of complications. Traditionally, SEEG planning is performed by a neurosurgeon, who manually selects entry and target points by visually inspecting multi-modal images. Due to the usual number of electrodes (up to 18 per hemisphere) and the need of high accuracy, the planning procedure is complex and very time consuming (2-3 hours per procedure). Therefore, there is a clear clinical need not covered by commercial planning solutions, that do not provide any advanced assistance nor quantitative information regarding the risk of the planned trajectories.

In this context, the PhD work focuses on the development of a surgical planning decision support system to assist the surgeon during the planning phase of intracerebral electrode trajectories.
In particular, the contributions of the thesis are:

1. *The identification of the clinical and technological requirements to model the decision-making process in SEEG surgery, providing a generalization of the problem for the analysis of generic image guided percutaneous interventions (**C1**).*

In this phase, we provided the formalization of the planning procedure of percutaneous interventions, as well as we identified the main clinical requirements in terms of safety and efficacy, to be translated into quantitative values with respect to medical image processing and optimization theory. Accordingly, we developed a set of tools which allow the automated definition of optimal trajectories in SEEG by maximizing the distance from vessels, the insertion angle and guarantee anatomy driven explorations. A retrospective quantitative validation showed that optimized trajectories improved manual planned ones in $98\%$ of the cases in terms of quantitative indexes, even when applying more conservative criteria with respect to actual clinical practice.

2. *A novel methodology to exploit retrospective data and manual plans from patient who underwent SEEG procedures in the clinical center (**C2**), to improve the optimization strategy previously developed.*

   According to the results obtained by C1, we hypothesized that the analysis of retrospective data could support the optimization procedure, providing new information and an objective and reliable method to acquire and transmit the clinical center experience. We developed and analyzed a retrospective database, collecting the data and manually planned trajectories from past cases. Data analysis and machine learning techniques allowed us to obtain the most common paths used by the center to explore specific anatomical brain regions (61 mean trajectories), as well as combinations of trajectories for macro-areas explorations (8 planning strategies). We developed a specific interface to help the surgeon in the definition of trajectories for new patients, selecting among those obtained by their own data.

3. *The development of a decision support system able to exploit the information from past cases and adapt to the specific workflow of the clinical center (**C3**).*

   The third contribution assembles the development of C1 and C2, since it integrates and extends the two modules. The final system allows the surgeon to define a new patient plan by using the interface developed in C2 and to automatically transfer the trajectories to the target patient anatomy. These initialized trajectories act as spatial and anatomical priors, guiding the optimization procedure initially developed in C1. The latter has been updated through iterative experiments with our

clinical partners, and includes different optimization strategies based on the trajectory type provided by the initialization module. The validation of the system showed that the initialization module was able to reproduce $95\%$ of manually planned trajectories, that were subsequently optimized on the patient anatomy. Two surgeons revised 201 optimized trajectories, and considered as clinically feasible $81\%$ of them, while another $7\%$ would have required minor manual adjustments to be used.

The development and results presented in this PhD thesis raised from a strict collaboration between surgeons and engineers, mixing clinical knowledge with medical image analysis, machine learning and optimization theory. The system proposed has been designed to reduce and simplify the interaction between the application and the final user and, therefore, to reduce the planning time while improving precision and safety. The results showed a robust system, able to provide a considerable number of clinically feasible trajectories that only required the surgeon's revision and approval. It is worth to notice that the implemented system is the result of many iterations and empirical experiments in collaboration with our clinical partners, that allowed us to better model, implement and identify the combination of clinical requirements and optimization parameters that best fit their workflow.

This work set the basis of an adaptable surgical decision support system for SEEG planning, with a modular design and a rich documentation to be continuously improved by the people who has yet to come.

# Sommario

La StereoElettroEncefaloGrafia (SEEG) é una chirurgia minimamente invasiva che permette l'esplorazione dell'attivitá cerebrale, d'ausilio nei pazienti affetta da epilessia focale per l'identificazione della zona epilettogenica (dall'inglese *Epileptogenic Zone*, EZ). La procedura prevede l'impianto di un numero variabile di elettrodi intracerebrali attraverso piccoli fori praticati mediante trapanazione del cranio, che permettono il mappaggio dell'attivitá cerebrale tanto nelle zone corticali che in strutture cerebrali profonde.
Tradizionalmente, la pianificazione della chirurgia di SEEG viene effettuata da un neurochirurgo, che definisce manualmente, in base all'esplorazione di immagini multimodali del paziente, i punti di inserzione e bersaglio che definiscono le traiettorie degli elettrodi. A causa della numerositá degli elettrodi (fino a 18 per ogni emisfero) e la grande accuratezza richiesta, il processo di pianificazione risulta complesso e richiede molto tempo (2-3 ore per procedura). Risulta evidente una necessitá clinica che non trova risposta tra i prodotti disponibili in commercio, che non forniscono alcun tipo di assistenza avanzata né informazioni quantitative sul rischio delle traiettorie pianificate.

A questo proposito, il lavoro di dottorato si é focalizzato sullo sviluppo di un sistema di supporto alla decisione orientato alla pianificazione chirurgica, in grado di aiutare il neurochirurgo nella definizione di traiettorie ottime per l'impianto di elettrodi intracerebrali.
In particolare, i contributi della tesi sono:

- *L'identificazione dei requisiti clinici e tecnologici per modellare il*

*processo decisionale nella pianificazione della chirurgia di SEEG, e la descrizione delle base teoriche volte al modellamento di chirurgie percutanee in generale (**C1**).*

In questa fase é stata proposta una formalizzazione del problema di pianificazione per chirurgie percutanee, e sono stati identificati i principali requisiti clinici legati alla sicurezza e all'efficia dell'intervento al fine di essere tradotti in indici quantitativi, utilizzabili nell'ambito dell'elaborazione delle immagini e teoria dell'ottimizzazione. Di conseguenza abbiamo sviluppato una serie di strumenti che permettono la definizione automatica di traiettorie ottimali per SEEG, massimizzando la distanza dai vasi, minimizzando l'angolo di inserzione e rispettando l'anatomia delle strutture esplorate. Una validazione quantitativa retrospettiva ha dimostrato che le traiettorie ottimizzate migliorano la pianificazione manuale nel 98% dei casi in termini di indici quantitativi anche applicando criteri piú conservativi rispetto alla pratica clinica attuale.

- *Un nuovo metodo in grado di elaborare i dati retrospettivi e le pianificazioni manuali di pazienti sottoposti a chirurgia di SEEG nel centro clinico, al fine di migliorare la procedura di ottimizzazione (**C2**).*

  Dai risultati ottenuti in **C1**, abbiamo ipotizzato che l'analisi dei dati retrospettivi avrebbe potuto migliorare la procedura di ottimizzazione fornendo nuove informazioni, oltre ad essere un metodo oggettivo per acquisire e trasmettere l'esperienza clinica del centro. Abbiamo sviluppato e analizzato retrospettivamente una base di dati, raccogliendo i dati e le traiettorie pianificate manualmente di vecchi casi. L'analisi dei dati e le tecniche di apprendimento automatico ci hanno permesso di ottenere le traiettorie piú comunemente utilizzate dal centro per esplorare delle specifiche regioni anatomiche cerebrali (61 traiettorie principali), cosí come le combinazioni di quelle traiettorie per l'esplorazione di macro aree (8 strategie di pianificazione). Abbiamo sviluppato un'interfaccia specifica per aiutare il chirurgo nella definizione delle traiettorie per nuovi pazienti, selezionandole tra quelle ottenute dai loro stessi casi.

- *Sviluppo di un sistema di supporto alla decisione in grado di sfruttare le informazioni estratte dall'analisi di casi retrospettivi e adattabile alle preferenze del centro clinico (**C3**).*

  Il terzo contributo rappresenta la fusione degli sviluppi di C1 e C2, integrando ed estendo entrambi i module. Il sistema finale permet-

te al chirurgo di pianificare un nuovo paziente utilizzando l'interfaccia sviluppata in C2 e di trasferire automaticamente le traiettorie ai bersagli anatomici del paziente. Queste traiettorie definiscono dei requisiti spaziali e anatomici, permettendo di guidare gli algoritmi di ottimizzazione sviluppati in C1. Questi ultimi sono stati modificati per mezzo di diversi esperimenti in collaborazione con i nostri partnes clinici, includendo diverse strategie di ottimizzazione in funzione del tipo di traiettoria definita nel modulo di inizializzazione. La validazione del sistema ha dimostrato che il modulo di inizializzazione é in grado di riprodurre il 95% delle traiettorie pianificate manualmente, che sono state successivamente ottimizzate sull'anatomia del paziente. Due chirurghi hanno controllato 201 traiettorie proposte, giudicandole applicabili nell'81% dei casi, mentre nel 7% dei casi necessitavano piccoli aggiustamenti manuali per poter essere utilizzate.

Il lavoro di sviluppo ed i risultati presentati in questa tesi di PhD nascono dalla stretta collaborazione tra chirurghi ed ingegneri, dalla fusione di conoscenze cliniche con l'analisi di immagini mediche, teorie di ottimizzazione e tecniche di apprendimento automatico. Il sistema proposto é stato pensato per ridurre e semplificare l'interazione tra l'applicazione e l'utente finale e, di conseguenza, diminuire il tempo di pianificazione mentre vengono aumentati criteri di precision e sicurezza. I risultati dimostrano che si tratta di un siatema robusto, in grado di fornire un considerevole numero di traiettorie clinicamente valide che richiedono solo la revione e l'approvazione del chirurgo. E' comunque degno di nota il fatto che il miglioramento del sistema é il risultato di molte discussioni ed esperimenti empirici con i nostri partners clinici, che ci hanno permesso di sviluppare e implementare un sistema che soddisfacesse le richieste cliniche con il loro modo di lavorare.

Questo lavoro getta quindi le basi di un sistema di supporto alla decisione chirurgico per la pianificazione di SEEG, con un disegno modulare e una ricca documentazione con l'intenzione che possa essere migliorato da futuri ricercatori.

# Acknowledgements

This PhD thesis is the result of 4 years of intense work, during which I counted on the support of many people around me: all of you have made this thesis possible.

First, a great thank goes to Ivan, Elena and Cico, which trusted me and gave me the opportunity for developing this research through a collaboration between Vicomtech, Politecnico of Milano and Niguarda hospital. I'm really grateful for your support along these years.

A special thank goes to Luis, who supervised the first part of this PhD, and to Álvaro, which helped me going through the last part of this journey.

A heartful thank goes to the Niguarda medical team, in particular to Cico, Michele, Laura, Pier, Giuseppe, Giorgio, Luciana, Roberto, Stefano. All of you have teached me something, and many of the developments and ideas presented in this manuscript came from your advices.

A great thank goes to Camilo, a friend and collegue that has always supported me along the years and taught me a lot. As well, I need to remember Roberto, Arkaitz, Andoni, Naiara, Nekane, Alba, Karen, Inma and the rest of the department at Vicomtech. Thank you for the morning coffees, the padel games, the great time we spent at conferences and, in general, for these years.

I can not forget my lab members and students: Sara M., Sara EH., Alberto, Gaetano, Lisa, Andrea, Giuseppe, Tiziano. All of you are part of this work.

Equally important have been my friends, amici, kuadrilla, that always made me feel like time and distance do not matter.

Many things have changed during this time, and nothing of this could have been possible without the support of my family. No matter the distance, you are always there for me. Similarly, I need to thank my Spanish family to make me always feel at home.

Finally, I've have to thank my wife. As I already said in the past, I could not leave Spain without you. You have made this possible, as many other things in my life. I love you.

To all of you, and probably there are more people:
Thank you, Grazie, Gracias, Eskerrik Asko!

# Contents

CHAPTER 1

# Introduction

## 1.1 Problem Statement and Motivation

The planning of a surgical intervention, meaning the study of the patient anatomy and the definition of the strategy to perform the surgery, has a crucial role for the safety of the patient and the outcome of the treatment. While this statement may apply for any surgical intervention, percutaneous procedures enhance these requirements since no clear view of the surgical site is available during the operation.

Image processing, optimization theory, machine learning, visualization techniques and many other disciplines can provide useful tools to reduce the clinicians' load with respect to the planning task, increasing the time they can dedicate to patients' care. In this context, the PhD research investigates the decision-making process which guides the surgical planning of minimally invasive intervention, focusing on epilepsy surgical treatment. The final aim is to provide surgeons with a decision-support system able to reduce the planning time and to provide a customized solution based on the patient anatomy and the medical workflow of the clinical center.

## 1.2 Medical Background: Epilepsy

The World Health Organization (WHO) estimates that "*around 50 millions people worldwide have epilepsy, making it one of the most common neurological diseases globally*[1]". The first descriptions on epileptic seizures have been traced back to 2000 B.C., in ancient Assiryian texts, and described also in the Greek Hippocratic collection [129]. The International League Against Epilepsy (ILAE) conceptually defined epilepsy in 2005 as a "disorder of the brain characterized by an enduring predisposition to generate epileptic seizures and by the neurobiologic, cognitive, psychological, and social consequences of this condition", and an epileptic seizure as "*a transient occurrence of signs and/or symptoms due to abnormal excessive or synchronous neuronal activity in the brain*" [70], [69].

Seizure initiation is characterized by the simultaneous occurrence of high frequency burst of action potentials and an hypersynchronization of the neuronal population [24]. At cellular level, the so-called paroxysmal depolarizing shift (PSD), reported in figure 1.1, consists in a prolonged membrane depolarization, resulting in repetitive action potentials not followed by the usual refractory period, causing the propagation of electrical discharge to other cells [94].

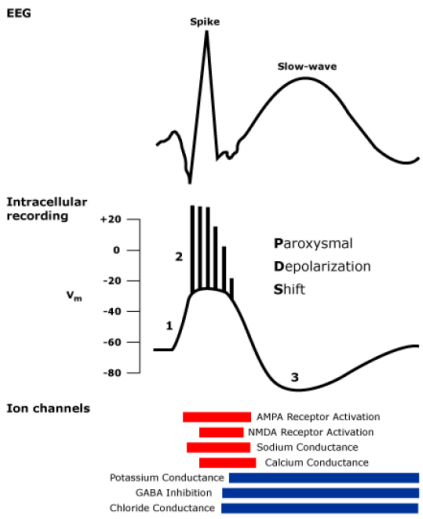


**Figure 1.1:** *Paroxysmal Depolarizing Shift (PSD): it is characterized by the prolonged depolarization, followed by an hyperpolatization. In the EEG signal, this caused a typical spike of epileptic neurons, followed by a slow wave.*

[1] https://www.who.int/news-room/fact-sheets/detail/epilepsy

The classification of epilepsies is an evolving subject, based on the evolution of our understanding of the disease. The diagnosis of epilepsy consists in the classification of the seizure type [71], the epilepsy type [69] and finally the epilepsy syndrome [169], based on the results from investigation in neuro-imaging and electroencephalography (EEG) studies. With respect to the purposes of this thesis, we report the characterization of the seizure type presented in [71], which identify three main categories based on its initial manifestation:

- *Generalized onset*: it may originate at "*some point within and rapidly engaging, bilaterally distributed networks*". Cortical and sub-cortical structures can be involved during the seizure. Even if the seizure may appear localized, the location and lateralization are not consistent between multiple occurrences.
- *Focal onset*: it originates limited to networks within one hemisphere, including subcortical structures. The ictal onset is consistent between seizures, presenting preferential patterns for propagation, which can involve the ipsilateral and/or controlateral hemisphere.
- *Unknown onset*: generally, seizures are characterized as generalized or focal onset. However, there may be cases in which the onset can be clearly state, being categorized as unknown.

As presented in Figure 1.2, each seizure type can be further categorized based on the specific features of the case.

Generally, the diagnostic steps involve different type of non-invasive tests. EEG is the most common method used to define the epileptogenic cortex, providing information of the brain cortical activity [148]. Since EEG is a non-invasive test, many studies have been performed involving healthy populations [97] and the interpretation of EEG signals has been largely documented [193]. This makes EEG an important diagnostic tool for epilepsy, since epileptic patterns are well-known and can be recognized at normal state, as trace of inter-ictal spiking and other abnormalities.

Imaging has also played a key-role in the understanding and diagnosis of epilepsy. Structural and functional neuro-imaging techniques provide valuable information regarding the activation areas, lesions and ipermetabolism which characterize the epileptogenic network. Jointly with EEG, they may provide a rich picture of the patient state [55, 189]. The most used imaging techniques in epilepsy studies are reported as follows:

- *Magnetic Resonance Imaging* (MRI): is a medical imaging technology able to create imaging of body organs by the application of strong

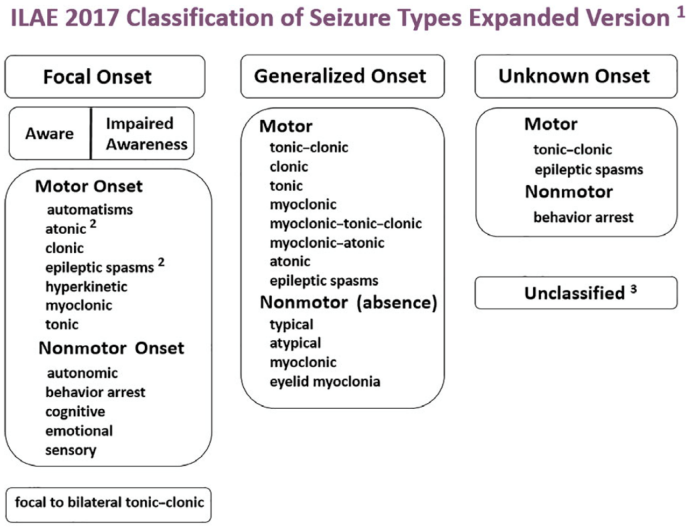


**Figure 1.2:** *ILAE characterization of seizure types. [169]*

magnetic field sequences, magnetic gradients and radio waves, which modify the orientation of tissues' water molecules. It is especially sensitive to soft tissue, making this technology the most used image acquisition technique for brain analysis.

- *Positron Emission Tomography* (PET) and *Single Photon Emission Computed Tomography* (SPECT): images are created by recording the emission of photons from radio-traces previously injected and trapped within the brain tissue, providing a measure of the blood flow in the brain. A more intense region means an increased blood flow, usually correlated with the epileptogenic network.

Most of patients diagnosed with epilepsy are treated by administration of anti-epileptic drugs. However, around $\sim 60\%$ of these suffer partial seizures and $\sim 25\%$ of these are medically refractory to anti-epileptic drug treatments, being potential candidates for surgery [53, 166].

The surgical treatment is based on the epileptogenic zone (EZ) concept, defined as "*the site of the beginning and of primary organization of the epileptic seizures*" [144]. The surgical treatment consists in removing or disconnecting the EZ. For that purpose, a crucial requirement is to define the EZ position and its limits as more accurately as possible.

When non-invasive pre-operative work-up poorly supports the identification of the EZ, additional surgery can be performed to provide more clear

information. For decades, especially in the United States, ElectrodeCorticoGraphy (ECoG) grids have been the primary approach for mapping seizures. ECoGs consists in strips and grids of equally spaced electrodes, which are placed on the subdural space by means of traditional open surgery (cranyotomy), able to map the electrical activity of a precise zone on the cortical surface. However, it requires the patient to undergo to an invasive surgery, and it does not provide any information about the activity of mesial and internal structures.

StereoElectroEncephaloGraphy (SEEG) represents a minimally invasive alternative able to record the brain activity from multiple internal and cortical structures [211], that will be presented in details in the following section.

## 1.3 StereoElectroEncephaloGraphy

SEEG has been shown as a reliable and safe approach to provide distributed spatio-temporal data about electrical brain activity [27, 33, 143]. SEEG is a methodology developed by Talairach and Bancaud since late 1950s at Saint'Anne Hospital, Paris [14]. It is based on accurate analysis of anatomo-electro-clinical correlations, being electrical signals recorded directly from within the brain by means of multi-lead intra-cerebral electrodes (figure 1.3). Such electrodes, stereotactically implanted according to a patient-specific topographical strategy, sample both superficial and deep brain structures.

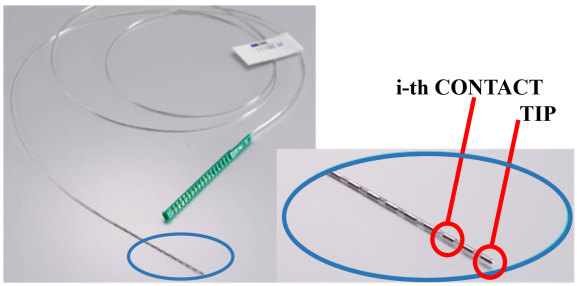


**Figure 1.3:** *Typical SEEG multi-lead electrode implanted for intracerebral recordings of the brain electrical activity.*

The procedure can be divided into four major blocks, as presented in Figure 1.4:

1. *Images fusion*: registration and processing of all biomedical scans required to plan the intervention.

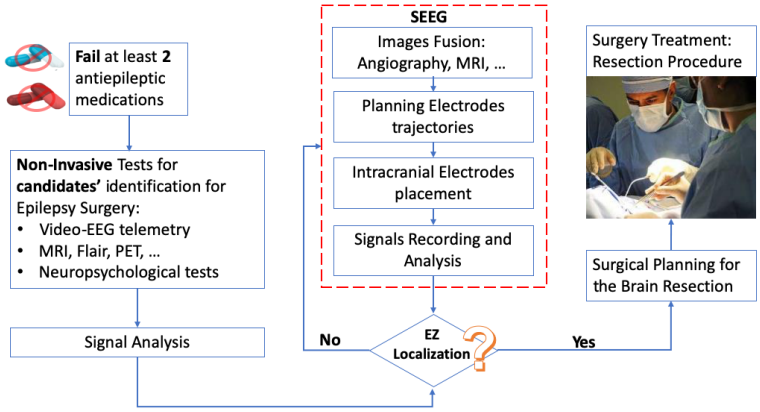


**Figure 1.4:** *Typical Workflow of focal epilepsy surgical intervention using SEEG. Sometimes, non-invasive tests are informative enough to identify the EZ. On the contrary, the SEEG procedure allows to collect meaningful data from cortical and sub-cortical structures, which increase the probability of localize the EZ.*

2. *Planning of electrodes trajectories*: surgeons, using the available images, plan the electrodes trajectories respecting various constraints (e.g. vessels and sulci avoidance, grey matter recording maximization and others).

3. *Intracerebral electrodes placement*: following the trajectories previously planned, the surgeon perform the stereotactic procedure with the help of a stereotactic frame or a robotic assistant.

4. *Signal record and analysis*: the EEG captured from the intracerebral electrodes implanted is analysed to localize the EZ.

The surgical technique has evolved throughout the years with the introduction of robotic assistants, image guided platforms and Computer Assisted Planning (CAP) [29, 32, 59]. In the following paragraphs, the SEEG steps will be briefly described.

### Image fusion

The major concern in relation to SEEG regards intracerebral hemorrhages [200] due to the insertion of multiple electrodes without a clear view of the surgical site. Therefore, additional imaging, such as Contrast-Enhanced

Cone Beam Computed Tomography (CE-CBCT) Digital Substracted Angiography (DSA) [29], T1W MRI with gadolinum contrast medium, Magnetic Resonance Angiography (MRA) and others is usually required for the enhancement of vascular structures.

Both the diagnostic step as the SEEG trajectory planning require the multi-modal images acquired to be registered, allowing the visualization of different type of information in the same space. Additional processing, aimed to an advanced visualization of those data, has been shown to directly influence the decision making process regarding surgical planning [153].

Even if the registration, processing and visualization of such images can be performed by the use of commercial platform such as Voxim™ (IVS Technology GmbH, Chemnitz, Germany) or NeuroInspire™ (Renishaw Mayfield), more advanced analysis can be performed by means of research software such as Freesurfer [66], FSL [99], SPM [8] and general purpose applications as 3D Slicer [159].

A multi-disciplinary team composed by neurologists, epileptologists and neurosurgeons analyzes all the available information provided by imaging, EEG and video-telemetry, and neuro-psychological tests. An EZ localization is formulated, around which the number and the desired position of intracerebral electrodes is defined.

### Planning of electrodes trajectories

Based on the EZ location hypothesis, one or more neurosurgeons carefully study the patient anatomy in order to find the safest path which fits with the requirements expressed by the multi-disciplinary team.

The surgical planning of such procedure remains cumbersome and time-consuming, since the surgeons need to determine optimal trajectories for the patient-specific anatomy. The number of electrodes to be implanted varies from each case but it may be up to 18 just for a single hemisphere. As we will see along the thesis, different research teams have been and are continuously working on advanced solution to provide assistance during this phase.

However, nowadays most of commercial CAP solutions (e.g. Voxim™ (IVS Technology GmbH, Chemnitz, Germany) or NeuroInspire™ (Renishaw Mayfield)) limit the user to iteratively plan trajectories through the visualization of patient images, without providing any further assistance or quantitative information regarding the risk and efficacy of those trajectories. The user is generally required to manually place entry and target points (EP and TP respectively) in the patient's scan and iteratively review

the whole trajectory slice by slice to avoid crossing vascular and other critical structures. Additionally, other constraints such as the insertion angle with respect to the normal to the skull, the quantity of recorded grey matter (GM), and possible unreachable zones depending on the implantation method must be addressed without being explicitly expressed in the images analyzed.

### Electrode stereotactic placement

Electrodes can be surgically implanted through different approaches, depending on the hardware available (a complete review of SEEG implant methodologies was described in [27]. As reported, among the stereotactic devices available, the Talairach frame is the most popular frame for SEEG electrode implantation, while other reported options are the Leksel frame [79] and the StealthStation™ (Medtronic; Minneapolis, MN, USA) in frame-less conditions. However, in the last years numerous robotic assistants [64] focused on stereotactic interventions (e.g. Neuromate® (Renishaw Mayfield, Nyon, Switzerland) or ROSA® (Medtech, Montpellier, France)) gained popularity, overcoming the limitation of previous techniques. Robotic devices represent an ideal assistant for this kind of interventions, allowing the user to freely implant trajectories without any constraints in position and orientation and being free of tremors and fatigue. Image examples of the stereotactic devices are reported in figure 1.5.

The intraoperative scenario may change among clinical centers, depending on the image modalities available and the hardware used for implantation. However, it generally requires the registration of the preoperative image data set used to plan the surgical trajectories and, in case of a robotic device, the registration of the latter to correctly align with the planned trajectories. Recent tools as the NeuroLocate (Renishaw Mayfield, Nyon, Switzerland) [32] allow the frame-less registration of the robotic assistant. Hence, the robot is able to align with the planned trajectories, assisting the surgeon during the drilling of the skull. Drilled holes are usually around $\sim 2.1$ mm of diameter, and a guiding screw is placed based on the skull width drilled. Once all the screws have been positioned, the intracerebral electrodes are inserted.

Finally, before the end of the surgery, each electrode functionality is tested and a post-operative scan is performed to verify the electrodes positions. Figure 1.6 provides a graphical overview of the intraoperative workflow described, used at Niguarda Hospital, Milan.

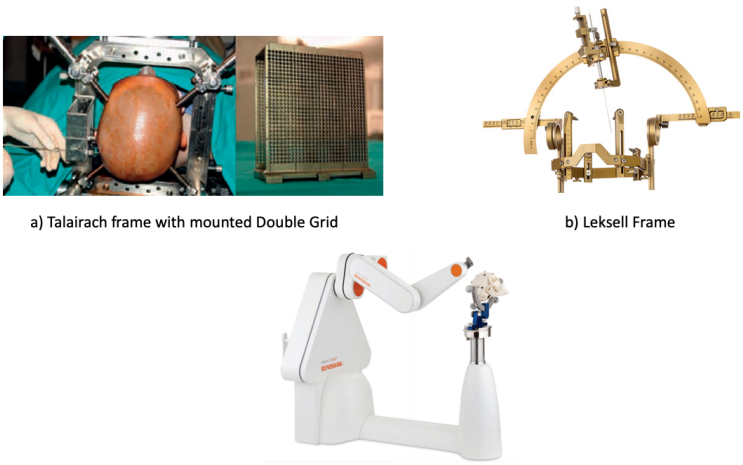


**Figure 1.5:** *Examples of sterotactic frames for electrodes implantation: a) the traditional methodology with the Talairach frame and the double grid mounted [30]; b) the Leksell stereotactic Frame; c) The Neuromate robotic assistant, commercialized by Renishaw Mayfield.*

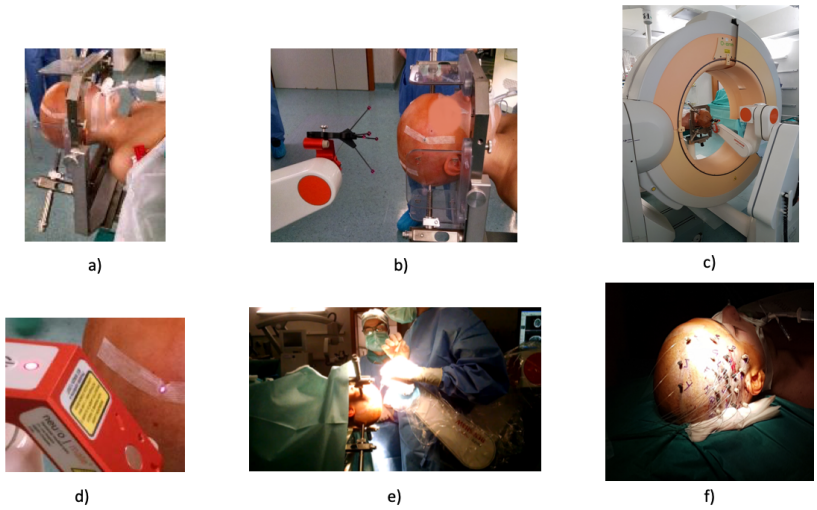


**Figure 1.6:** *Intraoperative scenario at Niguarda Hospital: a) the patient's head is fixed with the talairach frame; b) the Neurolocate, hold by the surgical assistant, is placed close to the patient head; c) an intraoperative O-Arm (Medtronic; Minneapolis, MN, USA) acquisition allows the registration of the preoperative images and the robotic system; d) the quality of the registration is checked by meas of skin markers, which are used targets with which the robot must align; e) the surgeon performed the skull-drilling with the assistance of the robot; f) the screws and electrodes wires implanted.*

### Signal recording and analysis

After implantation, the patient keeps the electrodes from a period that usually ranges between 1 and 2 weeks [79], during which he is kept under observation and constantly video-recorded. When a seizure occurs, a technician offers assistance to the patient and describe the entire scene to provide the maximum information to the neurologist, which will analyze signals and video. Usually, a tagging system to report seizures, sleeping hours and others is available in the recording platform.

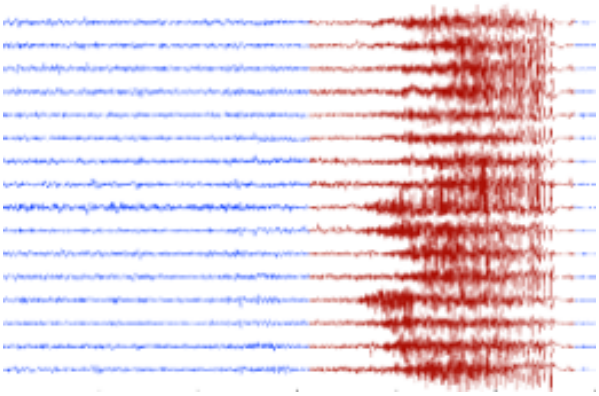

**Figure 1.7:** *The image report a typical SEEG recording at seizure beginning. Constant video-recording allows the neurologists to analyze signals and motor response during seizures, leading to a more precise definition of the EZ.*

Because of the number of possible implanted electrodes and the number of contacts in each of them (between 10 and 18), the neurologist defines a subset of signals that can be recorded and visualized, corresponding to the most relevant contacts following the EZ hypothesis. The implanted electrodes can be also used for provoking seizures and stimulate specific brain zones, as well for performing radio-frequency thermocoagulations [84]. The latter can be used to confirm the EZ hypothesis, in terms of reduction of seizures occurrences after the ablation. In rare cases, thermocoagulation avoided the resection surgery. All the information obtained by the different techniques applied are fusioned and, hopefully, a precise definition of the EZ can lead to an accurate resection surgery.

## 1.4 Aim of the thesis

Planning a SEEG intervention is a time-consuming and complicated task, which consumes many hours to surgeons and medical staff. In this PhD work, we aimed to implement a surgical decision support system able to assist the surgeons during the planning phase finding optimal trajectories and reducing the time required. The PhD work lies on the following hypothesis:

1. *Hypothesis 1* (**H1**): A minimally invasive percutaneous intervention can be modelled as a set of constraints, representing the clinical requirements.
2. *Hypothesis 2* (**H2**): Image processing and optimization techniques can automatically provide optimal trajectories, adapted to the specific anatomy of the patient.
3. *Hypothesis 3* (**H3**): The optimization model can be further improved by the analysis of retrospective data, increasing the specificity of our system.
4. *Hypothesis 4* (**H4**): The complete system is able to combine the knowledge extracted by past cases with the optimization strategy used to plan new patients' cases.

This PhD dissertation describes the methodology developed along these hypothesis, describing the iterative procedure which led to the definition of the final system.

### 1.4.1 Structure of the thesis

The dissertation is organized following the hypothesis presented:

- Chapter 2 proposes a systematic review on the state of the art regarding planning assistance applications for minimally invasive percutaneous interventions. We collected articles from different applications, analyzing and classifying the methodology adopted and providing a generic overview of the planning process (**H1**).
- Chapter 3 presents the first prototype built on the basis of **H1**, adapting the model to the specific domain of SEEG. We present the architecture of the application and the tools defined in collaboration with the surgeons (**H2**). A quantitative validation compares the proposed trajectories with the ones planned by the surgeons.

- Chapter 4 focuses on **H3**, presenting a novel method which exploits retrospective data to build a surgical model for SEEG, representing the most common exploratory patterns used by the center.
- Chapter 5 presents the complete system developed (**H4**), result of iterative experiments in collaboration with surgeons. We report a quantitative and qualitative validation of the global system, performed on a set of retrospective patient data sets.
- In Chapter 6, we remark the contribution of the thesis, as well as we analyze the future direction and ethical and philosophical issues related to this work.

A graphical abstract of the thesis is report as following:

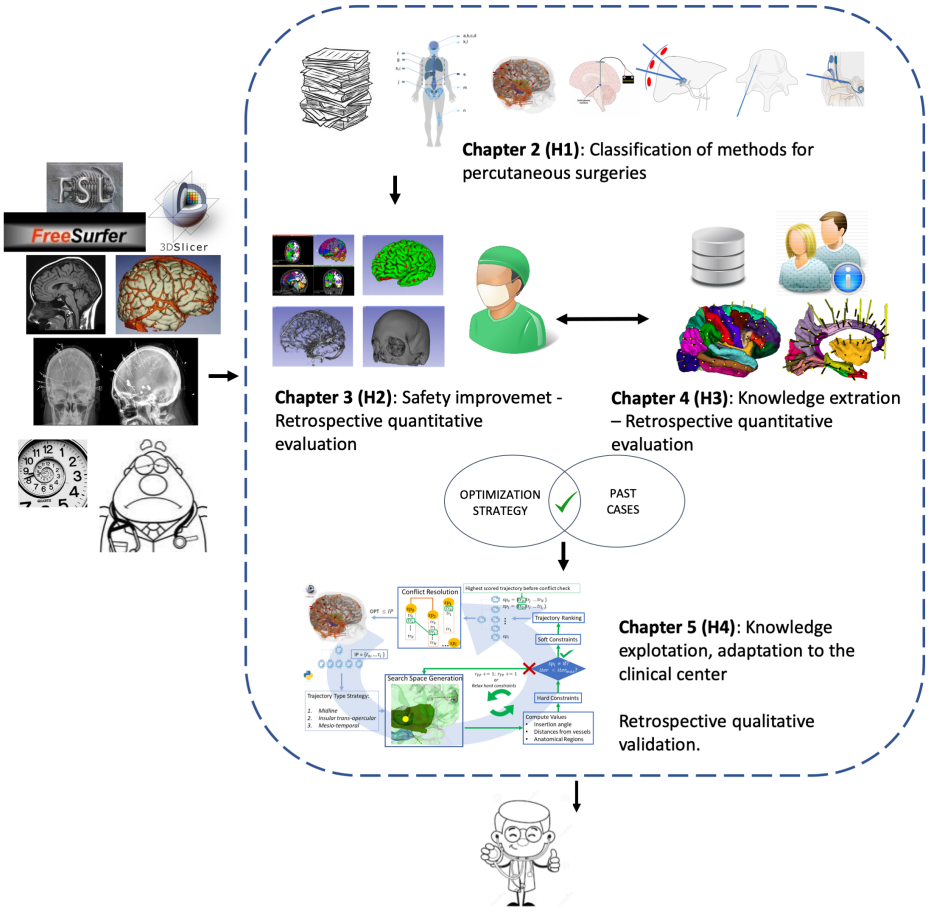


**Figure 1.8:** *Graphical abstract of the thesis, representing the structure of the chapters. The developed system is the contribution of different parts, including an extended revision of the state of the art (Chapter 2), the development of a preliminary prototype (Chapter 3, the analysis of retrospective data provided by the clinical center (Chapter 4 and the final decision-support system developed based on the previously mentioned contributions (Chapter 5)*

CHAPTER 2

# Surgical planning assistance in keyhole minimally invasive surgery: a systematic review

Chapter 1 reports a systematic literature review regarding surgical planning assistance solutions in percutaneous surgeries. It provides the theoretical basis related to the modelling of the decision making process in percutaneous surgical planning, as well as a wide panorama over the different clinical applications that have been object of study by researchers. Finally, the reported articles are classified based on the assistance provided to the final user, and a qualitative description of the algorithms is presented.

A journal article based on this work will be submitted to *Medical Image Analysis* as: Scorza, D., El Hadji, S., Cortés, C., Bertelsen, À., De Momi, E. "Surgical planning assistance in keyhole minimally invasive surgery: a systematic review".

## 2.1 Introduction

Minimally Invasive Surgeries (MIS) are commonly accepted as representing a group of surgical procedures "*associated with a lower post-operative patient morbidity compared with a conventional approach for the same operation*" ( [156]). In general, MIS procedures present for the patient a reduced number of cuts, a faster healing time, reduced pain and bleeding after the operation, limited scarring and shorter hospitalization ( [128]). Therefore, they have known a growing interest in the past decades, in the medical community but as well in the field of computer science, where the development of multiple computer-assisted techniques has seen a proportional growth.

Many MIS are performed accessing patient's body through one or more small incisions or a natural cavity and require the insertion of surgical instrumentation. In some interventions, the surgeon has the possibility to insert an endoscope, which provides a direct visual feedback of the operating scenario (e.g. laparoscopy). In case of endovascular procedures, the surgical instrumentation is inserted through a catheter, which limits the movements to the main vascular tree. Such procedures are also supported by intraoperative fluoroscopy, ultrasound imaging or tracking methods, which provide a continuous feedback to the surgeon about the catheter position.

Percutaneous keyhole surgeries (e.g. tumour ablation) and stereotactic procedures (e.g. keyhole neurosurgery) usually do not provide a clear view of the surgical scenario, and the positioning of the instruments requires to be accurately planned to guarantee an effective and safe procedure. Therefore, preoperative surgical planning has a crucial role. However, it can be complex and time consuming due to the numerous aspects that have to be taken into account. Surgeons have to accurately study the patient's anatomy and define one or more trajectories along which inserting the tool to maximize the efficacy of the intervention while ensuring the safety of the patient.

Most of existing commercial Computer Assisted Planning (CAP) solutions limit the user to an interactive definition of the trajectories by navigating the preoperative images and do not provide suggestions or quantitative information regarding the safety of the trajectory path, the access point or the target coverage.

In the recent years, different research groups have focused their efforts on the development of semi-automated or automated planners and decision support systems to assist surgeons during this phase. Figure 2.1 reports the number of publications per year that focused on surgical planning assistance for percutaneous interventions and were published in the last

two decades (search details are described in appendix). To the best of our knowledge, available literature reviews in keyhole surgery are mainly focused on methods to model needle-tissue interaction ( [1]) or on specific procedures (e.g. [174, 218] entirely focused on percutaneous liver tumour ablation). Despite the growing interest to this topic, a comprehensive literature review which analyzes the decision-making process of surgical planning from a methodological point of view, providing a generalization of the problem and enhancing differences and similarities of the methods proposed is still lacking.

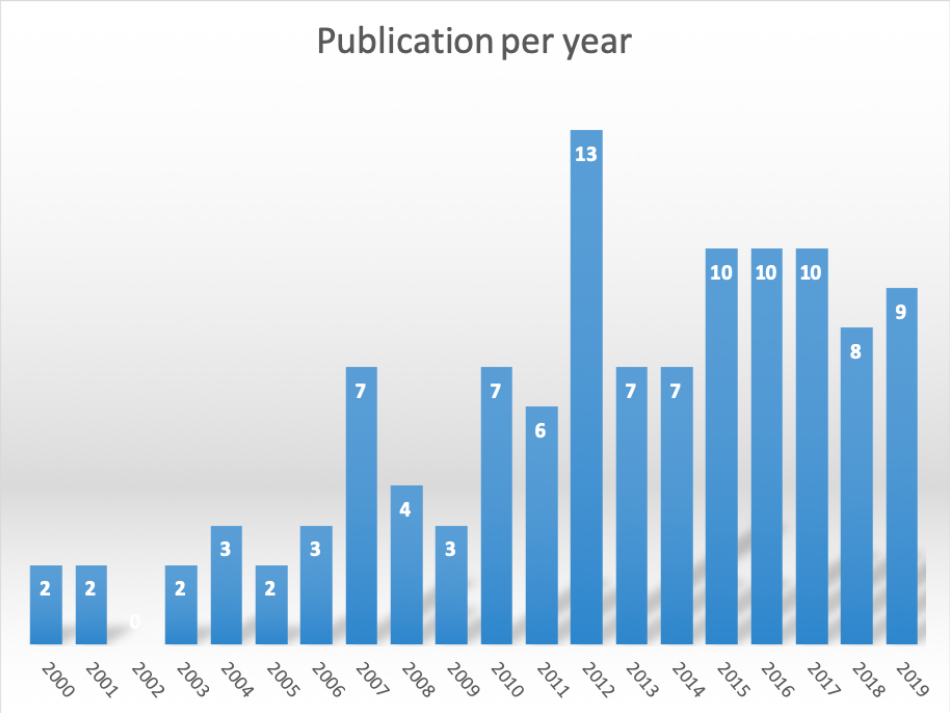


**Figure 2.1:** *Graph reporting the number of publications per year in surgical planning assistance solutions.*

In this work, we provide a generalized view of the surgical planning problem related to keyhole procedures and, independently from the application, we describe the necessary steps to model the intervention, the approaches used to assist the surgeon in the decision process of planning straight trajectories, and the experiments carried out to verify the clinical effectiveness (section 2.2).
In section 2.3, we report all the clinical applications that have been object

of study for the development of surgical assistance tools, describing their clinical aspects and identifying the anatomical site involved.
In section 2.4, we classify the different algorithms based on the type of assistance provided to the final user, focusing on the technical aspects of their implementation. From our systematic search, we included a total of 116 articles related to planning assistance solutions in different keyhole surgeries. This review is intended for researchers and engineers from universities and companies approaching the surgical planning in percutaneous surgeries. It provides a panorama on different surgical interventions, enhancing the transversality of the methods proposed in literature, which may be translated to new surgical fields. Along the article, we link the reader to additional papers regarding more specific topics, such as segmentation methods for specific anatomies and optimization strategies providing technical and practical tips that can help in the development of surgical planning assistance methods.

## 2.2 General problem formulation

Planning a keyhole intervention is a complicated and time consuming task, where multiple requirements need to be considered simultaneously. Depending on the surgical application, clinicians may have to define the optimal access path to reach a target, the optimal set of parameters to perform an ablation and/or the best target point position to place an implant or to perform a biopsy. The requirements to meet safety and efficacy vary depending on the surgical intervention, the anatomical zone, and the medical workflow.

An accurate specification of the characteristics of the intervention, or clinical requirements, is the preliminary step to model the decision process that guides the planning procedure. Usually this phase requires a strict collaboration with, at least, one clinical group and to interact with surgeons with expertise in planning such interventions. Understanding the entire surgical workflow, from the preoperative image acquisition to the postoperative follow-up, can be useful to decompose the surgical procedure in different phases and provide additional information about how the procedure is performed, the hardware used and the type of imaging available.

A straight *trajectory* can be defined as a set of 3D Euclidean coordinates, corresponding to an Entry Point (EP) and a Target Point (TP) in the image space, that completely identify the path of a surgical instrument. They constitute the *variables* of the problem. The planning is the choice of the trajectory that fits the best all the predefined clinical requirements. This

| Constants | Variables | Objectives | Operators |
|---|---|---|---|
| Organs | | Avoid | Distance |
| Tissues | EP | Reach | Angle |
| Functional areas | TP | Maximize | Coverage |
| | | Minimize | |

**Table 2.1:** *Common requirements for the modelling of percutaneous surgical planning interventions*

is usually achieved using an optimization model that tries to calculate this path by translating clinical requirements into *geometric constraints* to be satisfied and optimized. A geometric constraint is the combination of constants and variables using *operators* to describe relative geometric relations between them, the *constants* being the anatomical structures of interest extracted from the preoperative images.
For instance, an optimal surgical path will usually try to avoid all the dangerous structures and maximize its distance from them, to allow for sufficient space around those obstacles and account for the dimensions of the tool and possible insertion errors. The trajectory direction must also often follow other practical considerations regarding its feasibility on the considered anatomical structures, such as slippery organs boundaries or specific anatomical Regions Of Interest (ROIs) that have to be crossed a certain way. Similarly, depending on the type of application, a trajectory planning algorithm should account for the effects and characteristics of the instrument inserted. For example, in the case of percutaneous thermal ablations, the probe and TP positions are chosen based on the coverage of the targeted structure by the ablation volume. Most of the clinical requirements can be translated using a limited set of geometrical variables, constants and operators that will represent the majority of the constraints. Table 2.1 provides a summary of the most common ones.

Independently from the application, we can identify four main components when designing a planning assistant:

1. *Image processing*: it defines the processing of patient's preoperative images such as multimodal image registration and segmentation of relevant anatomical structures. Generally, this preliminary processing is needed to obtain the structures of interest reported in Table 2.1 as *constants*.

2. *Formalization*: it defines the objectives of a planning strategy and how to combine the operators, constants and variables to represent the surgical rules.

3. *Optimization strategy*: it defines the way in which the different constraints should be taken into account and how to explore the available solution space in order to reach the optimal ones.

4. *Performance metrics and experimental design*: it defines a set of experiments and the validation protocol to compare the results proposed by a planning assistant with respect to the real clinical benchmark. Depending on the maturity level of the system, different experiments can be performed to test and improve the implemented strategy.

In the following sections we describe each component in detail, providing to the reader an overview of the methods and mathematical formulation at the base of planning assistance solutions. In Section 2.2.1, we provide a brief generic overview on the type of images commonly used in MIS, and focus on the image processing required to obtain the planning constants described in Table 2.1. In Section 2.2.3, we provide a formalization of the planning problem as an optimization procedure, with an overview on the strategies and methods used in literature. Finally, in Section 2.2.4, we classify the different types of experiments used to validate a planning assistance, enhancing their respective advantages and drawbacks.

### 2.2.1 Image processing

Acquired medical images vary according to the type of information the surgeons have to visualize, and can be categorized into two main groups: *structural imaging*, aiming to visualize the patient anatomy, and *functional (or physiological) imaging*, which measures changes in the metabolism, oxygenation, blood flow or chemical components of a target tissue. At least one structural image (usually a Computed Tomography (CT) or Magnetic Resonance Imaging (MRI)) must be acquired based on the type of tissues and organs intended to visualize. In some cases, a second acquisition with the use of contrast medium is performed to enhance additional structures (e.g. vessels) that were not visible with the normal acquisition. Especially in neurosurgery, functional imaging (mostly functional MRI (fMRI)) and Diffusion Tensor Imaging (DTI) are widely used to map the functionality and connectivity of the different brain areas.

Accordingly, the segmentation of all the relevant structures is a required step to correctly quantify the risk associated to a specific trajectory. Anatomical segmentation is a very wide topic and there are many different methods proposed in the literature which varies based on the anatomical structure and specific image modalities. Some of them are very specific for a target

anatomy, while others are more generic and can be interactively used to segment a variety of structures. The description of the different segmentation methods is out of the scope of this review. Nevertheless, we provide a generic categorization based on the interaction level required to the user:

- *manual segmentation*: the user delineates and labels the relevant structures through the use of a CAP workstation or similar software;
- *interactive segmentation*: generic algorithm where the user provides limited and simple input to segment a structure (e.g. thresholding or region growing);
- *automated methods*: complete pipelines of algorithms aiming to segment specific organs or structures in full autonomy. This includes for instance atlas-based methods, machine learning and deep learning techniques.

Depending on the anatomical complexity of the surgical site, a combination of those methods may be used. More detailed information is provided in Section 2.3.

### 2.2.2 Formalization

Once the critical or targeted structures have been identified and segmented, operators should be chosen to specify the relative position of the trajectory, e.g. the distance or the angle, the positioning or the coverage of the target. Some of them require preprocessing steps to be performed on the images.

The distance from critical structures is one of the main operators commonly considered in percutaneous interventions, determining the minimum or maximum distance at which an instrument can be placed from a critical structure. By providing a binary mask of all relevant anatomical regions, an efficient way to compute distances is through the use of distance Euclidean transform algorithms: in [45] and [177], the authors computed a distance map volume based on the method proposed by Danielsson [42], while in [150] they used a fast marching algorithm [180] to compute the distance from surrounding surfaces and binary structures. Other authors [173, 175] combined different anatomical structures such as lungs, bones, cartilages and vessels into a single mask and then computed the Euclidean distance transform. Such approaches are computationally convenient since they require to compute the distance once at the beginning, with respect to a binary mask provided by the user. Similarly, in [183, 184] the authors used a set of distance maps to build a so-called risk volume, asking the surgeons to

define a risk for each segmented structure. This approach allows to aggregate structures with the same risk in a unique mask, reducing the number of distance maps to be computed. In [214], they used the distance map to provide a preferential sampling of target points around the center of the target structure. Segmented structures are commonly transformed into triangular meshes [126] to work with their surface representation. Therefore, different authors (e.g. [146, 163, 187]) exploited mesh properties to efficiently compute intersections and distances by the construction of bounding boxes and bounding volume hierarchies [103]. In [138, 206], a more geometrical approach is computed to determine safe corridors based on specific anatomical consideration on the structure to operate (e.g. vertebras or pelvis).

Operator Angle has different possible usages in trajectory planning: in [177], [186], and [10] the authors computed the angle between the trajectory and the surface normal of an organ, to avoid tangential trajectories that can be too slippery; others [61, 62] computed the angle between the trajectory and the main axis of the targeted structure, to provide the correct alignment at the target point; in [179] they computed the angle of the trajectory with respect to one of the main anatomical planes, to ensure a good visualization during the intervention.

Target coverage indexes are generally computed as the overlapping region between two volumes. The first volume represents the targeted structure, while the second volume simulates the effect of a surgical instrument to predict its efficacy. Examples of simulated volumes are the ablation volume [11], or the recording capacity of an electrode [187, 214].

Finally, the accurate positioning of a target is a fundamental requirement, which is generally influenced by all the previous variables. However, some applications as for example deep brain stimulation often uses functional data to provide additional information and define the target position of the tool inserted [48, 50, 51, 85].

### 2.2.3 Optimization strategy

The optimization strategy is an approach to find the best values of EP and TP, based on an evaluation of the constraints and their associated objectives. Thanks to the previous formalization step, we can consider the optimization process as independent from the specific anatomy or the surgical procedure. The surgical planning process can be modeled as a constrained optimization problem, subject to a series of so-called hard (strict) and soft constraints ( [63]) defined as:

- *Hard (or strict) constraints*: set of binary conditions that must be sat-

isfied to generate the space of possible solutions (e.g. critical structure avoidance);

- *Soft constraints*: set of requirements that must be satisfied at best, usually defined by numerical cost functions (e.g. maximize the distance from vascular structures)

While hard constraints determine the available space of solutions, soft constraints guide the optimization strategy in the search for the optimum values. Depending on the complexity of the problem, it may be necessary to model it by defining one aggregative cost function (single-objective approach) or multiple independent cost functions (multi-objective approach). Some authors modelled the surgical problem by a so-called constrained single-objective optimization problem, constituted by a single cost function subject to a set of equality and inequality constraints. However, such approaches usually focus on specific part of the whole planning problem such as the coverage at the target point ( [47, 127]) or distance to a critical structure ( [2, 91]).
However, in the majority of the cases, surgical trajectory planning requires to be modeled as a constrained Multi-Objective Optimization (MOO) problem, defined as:

$$
\begin{aligned}
&_{x\in\Re^k}\mathbf{F(x)} = [f_1(\mathbf{x}), f_2(\mathbf{x}), ..., f_N(\mathbf{x})]^T \\
&\text{subject to:} \\
&\quad G_i(\mathbf{x}) \leq 0 \quad \text{where } i = 1, \ldots, M \\
&\quad H_j(\mathbf{x}) = 0 \quad \text{where } j = 1, \ldots, E
\end{aligned}
$$

where $F(\boldsymbol{x})$ represents a vector of $N$ objective functions, $G_i(\boldsymbol{x})$ and $H_j(\boldsymbol{x})$ express the set of $M$ and $E$ inequality and equality constraints, respectively. The vector of decision variable is $\boldsymbol{x} \in \Re^k$, where $k$ represents the number of independent variables. Satisfying equality and inequality constraints defines the so-called *feasible design space* (or *feasible decision space* or *constraint set*) $\boldsymbol{\chi} = \{\boldsymbol{x} \mid G_i(\boldsymbol{x}) \leq 0 \text{ with } i = 1, \ldots, M \quad \text{and} \quad H_j(\boldsymbol{x}) = 0 \text{ with } j = 1, \ldots, E\}$. The corresponding *feasible criterion space* (or *feasible cost space* or *attainable set*) $\boldsymbol{Z} = \{F(\boldsymbol{x}) \mid \boldsymbol{x} \in \chi\}$ determines all the possible solution points with respect to the cost functions [135]. The definition of optimal solution in MOO problems leads to the concept of *Pareto Optimality* (Vilfredo Pareto, 1906), defined as the vector of solution $\boldsymbol{a} \in \boldsymbol{\chi}\ if \nexists \boldsymbol{b} \in \boldsymbol{\chi} \mid \boldsymbol{F(b)} \leq \boldsymbol{F(a)}\ and f_i(\boldsymbol{a}) \leq f_i(\boldsymbol{b})$ for,

at least, one cost function. Explicitly, Pareto optimal solutions represent all the solution vectors in the criterion space $\boldsymbol{Z}$ that cannot be improved with respect to one cost function without deteriorating the value of another cost function (*Pareto front*). Several methods were developed and studied for the exploration of the criterion space and the identification of the optimal solutions in different engineering fields ( [40]), and, as the authors proposed in [135], we can identify two main categories: *scalarization methods* and *vector optimization methods*. Scalarization methods reduce the problem to a single equation, composed by the independent cost functions opportunely weighted. The most common approach in surgical planning, probably because of its simplicity and intuitiveness, is the *weighted sum method*[1], mathematically expressed as:

$$F(x) = \sum_{i=1}^{N} \omega_i * f_i(x) \tag{2.1}$$

(with respect to the definition of $f_i$ a few lines above)

with $0 \leq \omega_i \leq 1$ and $\sum_{i=1}^{N} \omega_i = 1$. The weights have to be defined *a priori*, based on the importance of each constraint. Similar techniques have been used by the authors in [90, 173], where the authors used a *weighted product* method to combine the cost functions, or in [150] where each cost function is represented through a logarithmic scale in order to make comparable very different values.
Other authors [44, 182, 183, 196] used a single cost function based on the distance to critical structures, however they gave them different weights based on the suggestions of clinicians. While this technique may be very effective from a practical point of view, especially because surgeons are usually able to express the priority of each constraint, the definition of those weights may not be straightforward. The majority of the approaches define them empirically based on surgeons' suggestions and iterative experiments. In [214] they used a questionnaire filled by three clinicians to define the weights and hard constraints values, while in [125] they extrapolated them by studying iterative experiments on 10 trajectories by two surgeons and trying to identify their preference. In [60, 61], the authors presented a method for the optimal definition of weights by the analysis of retrospective Manually Planned (MP) trajectories, and reverse-engineering of the weights.
Another method to weight multiple criteria is the *analytic hierarchy pro-*

[1] [4,5,9,12,16,20–22,26,45,46,61,62,86,112,124,125,150,154,161,176,177,186,187,197,199,214,215,219]

*cess* [167], that has been used in [185]. The method consists in the definition of a pairwise comparison matrix, which determines the relative importance of a criterion with respect to another and is used to compute the real weights.

Scalarizing approximations, as well as single cost function problems, are usually solved by means of classical optimization approaches, that can be grouped between *gradient-based* and *gradient-free* methods [6]. Gradient-based methods require the analytical expression of the cost function derivative, which is used at each iteration to determine the search direction and explore the criterion space to reach the optimal solution. The gradient-descent method has been used in [4], and a multi-scale version in [5]. [35] used an *unconstrained steepest descent* algorithm, while [12] used a modified version with limited memory of the Broyden-Fletcher-Goldfarb-Shanno (BFGS) algorithm.
However, since the definition of the cost-function derivative is not always straightforward, gradient-free optimization algorithms are more commonly used. Such algorithms treat the cost function as a *black-box* and implement different strategies usually based on the perturbation of their independent variables. At each iteration, the cost function value is computed and the perturbation strategy updated to minimize this value. Hence, the *Nelder-Mead* algorithm (also known as *downhill simplex* or *AMOEBA*) ( [147]) has been used in [9, 11, 61, 62, 86, 108, 203, 208], and the *Powell* algorithm ( [160]) in [26, 150]. Since each algorithm implements a different optimization scheme, the work presented in [204] tested the previous optimization methods and the *Simulate Annealing* algorithm ( [105]) and compared the results on their specific application. Similarly, in [98] the authors compared the usage of seven gradient-free optimization methods, enhancing their advantages and drawbacks applied to the cryosurgery ablation of liver tumours. These approaches are computationally efficient, but are sensitive to their initial position and require suitable initialization. Many authors[2] preferred to use an *Exhaustive search* method (also called *Brute force* method), consisting in the exploration of the whole search space.

Contrary to scalarization methods, vector optimization approaches consider each cost function as independent, and try to find the optimal set of solutions lying on the Pareto front. The algorithms in this category are usually based on a *a posteriori* definition of preferences and explore the available criterion space to identify the optimal solutions lying on the Pareto front. In surgical planning domain, only few studies have explored *dominance based*

[2] [2, 16, 20–22, 44–46, 57, 65, 87, 91, 117–119, 124, 125, 136, 138, 154, 176, 177, 179, 182, 185–187, 196, 197, 206, 214, 215, 219]

optimization methods, which rely on the concept of *Pareto dominance*: a solution vector $\boldsymbol{a}$ dominates $\boldsymbol{b}$ ($a \prec b$) if $\nexists\, \boldsymbol{b} \in \boldsymbol{\chi} \mid f_i(\boldsymbol{b}) \leq f_i(\boldsymbol{a})$. In other words, we can not improve our solution without deteriorating at least one cost function. A comparison between a weighted sum method and a Pareto-based approach has been presented in [87], showing that the latter is able to propose additional solutions that could not be found with the weighted sum approach, and that those are relevant solutions often chosen by the experts. Pareto dominance methods shows to be very effective in the case of non-convex optimization problems, where the search space can be discontinuous and contain many local minima, such as surgical planning problems. In [179], the authors proposed Pareto-optimal solutions by listing only the best trajectory for each cost function, representing the so-called *Pareto-frontier*. In [175], they extended this concept by locally approximating the Pareto front at different starting points through an hyperboxing Pareto-approximation method presented in [194]. A genetic algorithm approximation has been proposed in [162], where the authors defined a binary expression of chromosomes to represent the planning problem, updated based on an exponential fitness function which account for different clinical requirements. A *particle swarm optimization* (PSO) was used in [80, 81] to explore the search space, assigning to each particle a cost composed by multiple objectives and generating Pareto-optimal solutions by keeping only non-dominated particles.

While the majority of methods exploits optimization theory as the engine of CAP solutions, a different approach has been recently presented in [218], where the authors modeled the surgical planning problem as a Markov Decision Process (MDP) to be solved through a reinforcement learning approach. Even they presented only preliminary results based on simulation, it may represent an interesting area of research for the future.

### 2.2.4 Performance metrics and experimental design

The validation of surgical planning assistance algorithms is a complex task, since there are not unique solutions or standardized performance metrics to identify the *optimal* trajectory. Actually, this definition is very subjective, based on the experience of each surgeon, the quality of available images, and the specific case that is being studied. Accordingly, there are no standardized metrics available to evaluate the performances of a surgical planning assistant.

The solutions proposed are therefore usually evaluated by two main approaches, based on the type of computed indexes:

- *Quantitative validation*: a set of relevant objective metrics are compared with respect to the minimum requirements, or with respect to manually planned (MP) trajectories. There is no need to directly involve the medical staff for this type of evaluation.
- *Qualitative validation*: one or more clinicians assess the trajectories proposed by the system, providing direct feedback on their clinical feasibility, ratings, rankings, or other subjective information.

Since in most of the cases a global and unique ground truth does not exist, the quantitative validation usually compares the value of each relevant constraint that takes a role in the optimization process with respect to its initial value or, if available, the corresponding value of a MP trajectory. However, the direct comparison of manual and proposed trajectories may be misleading, considering that the manual solution may not be the most optimal. Additionally, while this approach provides objective and reliable metrics on the algorithm performances, it assumes that the optimization model and identified cost functions are correctly modelling the problem and the segmentation of the constants is completely reliable. Consequently, a quantitative validation is not able to detect incorrect solutions with respect to additional clinical criteria which may have not been included or segmentation issues (e.g. unsegmented vascular structures or lack of accuracy).

This problem is overcome by a qualitative validation, that directly involves the final user to rate the proposed solutions on the basis of his/her experience. In this case, the user is assessing the proposal globally, and typically many different issues may arise due to sub-optimal or erroneous segmentation, missing or erroneous representation of an objective. On the other hand, qualitative validation may lack of objectivity, since there may be a high variability between surgeons regarding the definition of the "*optimal solution*" (as demonstrated in [199]) and the *inter* and *intra*-operator variability should be taken into account (as in [111]).

In order to perform these validations, three main categories of experimental setups can be used, depending on the type, completeness and realism of available input data:

1. *Simulations*: the algorithms are tested on synthetic data or data obtained from retrospective preoperative images (e.g. a tumour volume). However, these experiments usually lack of realism since, even if target regions and obstacles may have been obtained by clinical images, they usually test algorithms in a simplified and controlled environment, with no ground truth to compare with and where the proposed solution is directly assessed by the user;

2. *Retrospective study*: the algorithm is tested on image datasets of past cases and the results are validated with respect to the surgeon choice (being quantitative, qualitative or both);

3. *Prospective study*: the algorithm is used on new patient cases as an alternative to the traditional planning method. The solution proposed is directly assessed by the user and, if possible, compared with traditional planning methods.

The use of these different setups also often depends on the degree of readiness of the prototype, algorithms and systems that are to be tested. The readiness can be categorized following the Technology Readiness Level (TRL) scale proposed in [133]. In the current usage described in [89], the TRL scale ranges from 1 (Basic Principles Observed and Reported) to 9 (actual system proven in operational environment). Most published surgical planning assistance algorithms and tools can be considered in the 3 (experimental proof of concept) to 7 (system prototype demonstration in operational environment) range.

Simulations are usually used at the preliminary stage of the proof of concept[3]. Constraints values are computed and compared with the corresponding minimum values defined for the application (e.g. minimum acceptable distance from a vessel). The algorithms and systems tested through such experiments usually go from TRL 3 to 4.

A widely used experiment, that does not require to directly involve the medical staff, is the *retrospective quantitative* validation (TRL 4 to 5), where past cases are used to test the behaviour of the system and the trajectories planned by the clinicians represent the ground truth[4]. Because of the drawbacks of quantitative evaluation, *retrospective qualitative* studies are an alternative or complement closer to the clinical scenario, where the system is directly evaluated by one or more clinicians (TRL 4 to 6). The experimental design may vary depending on the case and the availability of the medical staff: in [15, 117, 118, 173, 214], a single surgeon compared the feasibility of the trajectories with respect to the clinical practice, while in [20, 21, 80, 81, 154, 175, 196] multiple surgeons from the same center reviewed and evaluated the proposals. In [45, 46, 179] the authors asked the raters to express a preference with respect to MP trajectories, comparing the proposal with the past clinical practice. The authors from [124] focused the validation in understanding if the weights used in the optimization pro-

[3] [9–12, 47, 54, 100, 101, 121, 127, 136, 191, 192, 217]

[4] [4, 5, 26, 36, 44, 50, 61, 62, 77, 85, 104, 108, 110, 112, 119, 122, 138, 150, 155, 176, 177, 182, 184, 186, 197, 207, 215, 216, 219]

cess effectively captured the clinician's preferences: after calibrating such parameters on a reduced training set, raters were asked to pick up between a MP trajectory and the one optimized by the system, blinded to their identity. Similarly, in [16] they asked a clinician to rate trajectories coming from different sets, some manually defined by other surgeons, others automatically computed by their system. In [187] a blind surgeon rated the trajectories proposed by their system, without knowing the origin of the plan. Most of the previous qualitative validation experiments reported also present a quantitative comparison with MP trajectories.

Authors from [125] defined their validation as *pseudo-prospective* (TRL 6), since even if they used retrospective data, they planned the trajectories as if they were new patients. Two surgeons adjusted the weights by iterative experiments on a subset of 10 trajectories, and the validation was performed by a third clinician from another institution. Using an external rater as a reviewer for the proposed solution adds information regarding the generalizability of the optimization model. The work in [199] presented a qualitative validation with 5 external raters from different institutions, to which MP trajectories and optimized ones were blindly presented. Is interesting to note that this study showed that a relevant percentage of MP trajectories was considered as unfeasible by other clinicians, enhancing the fact that the surgical planning problem cannot be reduced to a unique optimal solution. Similarly, [201] presented solutions to blinded external raters for evaluation. In [111], two independent surgeons planned the same set of trajectories manually two times, allowing to estimate for intra and inter raters variability, and the results were compared to automatically computed trajectories.

While retrospective qualitative validations are very effective to understand the capability of the method to reflect the clinical practice, the limitation lies in their retrospective nature. During the trajectory ratings, clinicians do not usually remember the whole clinical history of the patient and usually base the evaluation only on anatomical and bio-mechanical considerations. Such bias is intrinsically avoided in a *prospective study* (TRL $\geq$ 7), were the planning assistance is used on new patients cases, considering all the clinical aspects involved and usually compared with traditional planning method. These studies need to be approved by an ethical committee, and require the medical staff to use the new system for planning future interventions and compare its benefits with respect to traditional planning methods. In [50], the authors reported a complete study which included retrospective and prospective validation experiments. The latter has been performed on 12 patients, and the clinicians compared the proposed solution to

the planned one and judged if it was acceptable or not. The work from [19] presented a prospective study on a pilot group of 5 patients, were the surgeons directly used the proposed software to plan the surgery. In [22], the authors demonstrated how their solution influenced the surgeon's decision making for 7 out to 8 cases, when comparing with the traditional planning method. In [90], they included 33 patients in their study along a year and evaluated the whole workflow, including the implemented segmentation methods. The semi-automatic proposals were rated by surgeons and, if found comparable to the expert solution, an equivalent trajectory was used. Recently, the work from [198] presented a prospective study for the evaluation of CAP assistance with respect to traditional manual planning. The CAP platform was used to generate automated proposals, but also to modify the trajectories when necessary to meet surgeon criteria. Manual planning was conducted in parallel, and the plan with the lowest risk score was finally implanted. Planning times were reported, showing that CAP can considerably speed up the process.

The TRLs reported here are purely indicative, however we assume that experiments closest to the clinical practice present robust and more advanced prototypes, at least at an algorithmic level.

## 2.3 Clinical Applications

Our systematic search revealed that various clinical applications have been subjects of study in the development of trajectory planning assistance systems for the percutaneous insertion of one or more needle-shaped instruments. All the articles included in the review have been classified "*per application*" and "*per anatomical district*". A schematic representation of the classification is reported on figure 2.2. Almost $45\%$ of the works have been focusing on neurosurgical applications, among which Deep Brain Stimulation (DBS, $14\%$), StereoElectroEncephaloGraphy (SEEG, $10\%$), or generic interventions such as biopsies ($15\%$) and Laser interstitial Thermal Treatments (LiTT, $4\%$) used for the ablation of specific brain zones or tumoral masses. Abdominal procedures represent almost $30\%$ of the articles found, the majority of which for hepatic interventions ($20\%$). Most of them are related to tissue ablation techniques, representing almost $32\%$ of the articles, and divided between Radio-Frequency Ablation (RFA, $17\%$), Cryoablation (CRYO, $7\%$), Microwave ablation (MW, $3\%$) and LiTT ($4\%$). Screw placement (SP, $18\%$) papers focus on the percutaneous insertion of screws into a bony structure, which could be potentially located everywhere in the body. However, the majority of them addresses the problem of vertebral fixation

for spinal fusion, and only a few articles are on pelvis screw placement applications [78, 88, 138]. Finally, the systematic search revealed some interesting works regarding Maxillo and ENT surgery ($6\%$), for the safe access of internal parts of the ear or skull-base puncture for biopsies.

In the next sections, we provide an overview of the main identified clinical applications. In particular, for each application we report a brief description of the clinical requirements to be considered for the development of an advanced CAP system, as well as the segmentation methods used by the authors to account for the surrounding anatomical structures.

### 2.3.1 Neurosurgery

Several neurological disorders, such as Parkinson's disease, epilepsy or tumors, happen to be resistant to drug therapy and thus require to be approached surgically through minimally invasive procedures for advanced investigation, e.g. biopsy and diagnosis, or treatment. These procedures are not trivial as they require precise targeting of lesions or anatomical landmarks with a probe or a needle inside the brain. An incorrect positioning of the surgical tool can result in severely harmful neurological complications, e.g. ineffective treatment, intracranial hemorrhage, temporary or permanent neurological deficit. Hence, they require an intensive pre-operative planning to identify specific critical structures to avoid and/or to target.

We identified three major types of neurosurgical applications that use preoperative CAP: (1) DBS, that requires the implantation of electrodes to release electrical impulses in specific brain regions, generally called deep brain nuclei, and reduce the symptoms due to movement disorders, e.g. Parkinsonâs Disease; (2) SEEG, which consists in implanting several multilead intra-cerebral electrodes recording electrical signals in order to identify the epileptogenic zone of the brain that requires to be surgically resected ( [190]); and (3) biopsy or generic stereotactic techniques that require the insertion of a needle-shaped instrument for tumor/lesion histological analysis or ablation. Figure 2.3 presents an example of DBS (left) and SEEG (right) implant sites, with the main anatomical regions to be considered.

Considering the main objective of the above mentioned applications, it is possible to highlight some differences which also influence the constraints that must be fulfilled. DBS aims at targeting a specific anatomical structure: a key requirement to guarantee the efficacy of the treatment is the optimal selection of the stimulation point. In fact, according to different studies, the symptom improvement strongly depends on how accurately the stimulated brain area is targeted ( [93, 130, 168, 195]). Changing the location of the

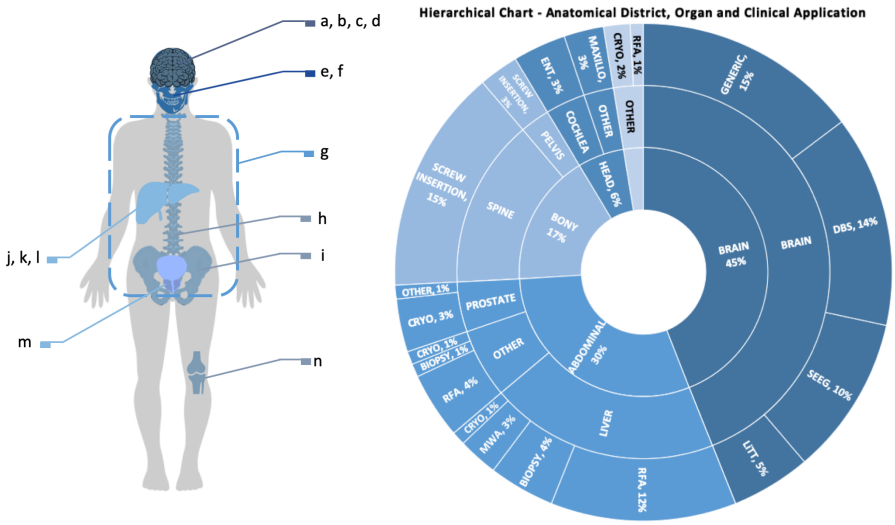


**Figure 2.2:** *The figure reports the articles found by the systematic search, associated to the anatomical district and the application described. On the right, the pie-charts presents the distribution of our results with respect to the anatomical district, the organ and the intervention.*

[a] *Biopsy: [2, 13, 23, 44, 65, 91, 92, 134, 136, 146, 155, 163, 181–184, 196]*
[b] *DBS: [20–22, 25, 48, 50, 51, 60–63, 85–87, 124, 125]*
[c] *SEEG: [45, 46, 154, 176, 177, 186, 187, 198, 199, 214, 215, 219]*
[d] *LiTT or other type of ablation: [80, 81, 95, 119, 197, 201]*

[e] *ENT: [3, 76, 150, 207]*
[f] *Maxillo: [15, 16, 75]*

[g] *Generic - Ablation: [26, 57, 104, 121, 161, 162, 210]*

[h] *SP: [41, 77, 107–113, 117, 118, 122, 185, 202, 206, 208, 217]*
[i] *SP: [78, 88, 138]*

[j] *Biopsy: [?, 17, 90, 171–173]*
[k] *RFA: [4, 5, 9–11, 35, 36, 54, 175, 203, 204, 209]*
[l] *MWA/CRYO: [19, 98, 123, 216]*

[m] *CRYO: [12, 127, 191, 192]*
*OTHER: [100]*

[n] *Bone ablation: [101]*

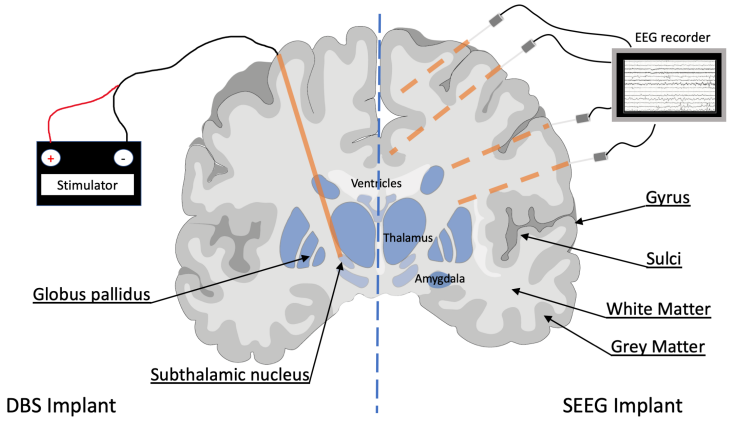


**Figure 2.3:** *Example of DBS (left) and SEEG (right) implants. DBS usually requires the implant of an electrode connected to a stimulation device for the electrical inhibition of specific brain zones such as the subthalamic nucleus or the globus pallidus. On the contrary, SEEG requires to implant multiple intra-cerebral electrodes, aiming at recording the electrical activity of different cortical and deep-located regions. Insertion EPs are commonly located on gyri, while sulci zones are avoided.*

active contact within or around the nucleus may provide different positive or negative clinical outcomes. The signal coverage of some brain tissues can even cause severe side effects ( [139]). Based on this observation, the solutions provided in [48, 50, 51, 85] used functional data to optimize the target positioning of the inserted tool. Moreover, the anatomical structures to be targeted are only a few millimeters long, which makes targeting accuracy even more crucial. Other structures such as thalamus, amygdala or hippocampus can be used as an electrophysiological landmark when targeting, for example, the subthalamic nucleus (STN) and thus require to be segmented.

In SEEG, the goal of intracerebral electrode implantation is to maximally record EEG from a given volume. Electrode arrangements are planned in order to both maximize cortical coverage and pass through safe, avascular planes. For example, in case of mesial temporal lobe epilepsy, which is the most common type of refractory epilepsy, the main suspected regions are hippocampus (HC), the amygdala (AG) or the temporal neocortex. Therefore, it is important to guarantee not only the accurate recording from deep structures, but also a good coverage of the surrounding cortical regions. This could be obtained by ensuring electrodes pass through the maximal amount of grey matter (GM), since it is generally the component of brain tissue that generates seizures [214]. SEEG is also the

only neurosurgical procedures that requires the planning of multiple electrodes simultaneously, which increases the algorithm complexity and requires specific solution to manage different possible combinations of trajectories [45, 177, 187].

Precise targeting of a lesion or tumour is also a fundamental requirement for biopsies and general stereotactic neurosurgical procedures, but on the other hand these applications demand a careful assessment of the functionality of the tissue surrounding the target. Mapping the brain activity and connectivity around the targeted lesion can reduce the likelihood of adverse outcomes of the stereotactic procedure. To this end, no-go zones could be defined to avoid severe cognitive, perceptual, motor, or language deficits by including and processing multiple brain imaging modalities (e.g. fMRI and DTI), as proposed in [2, 13, 196].

In general, all the previously described procedures share also other common constraints and requirements that guarantee the safety of the procedure. In particular, some anatomical structures must be avoided, such as:

- *vessels*, to avoid intracranial bleeding;
- *ventricles*, to prevent leakage of cerebrospinal fluid (CSF);
- *sulci*, to decrease the probability of hitting vessels, as they can be located at any depth within a sulcus.

One of the major risks related to these procedures is intracranial hemorrhage [18, 120, 143]. To prevent that risk, 3D visualization and assessment of the cerebrovascular tree play an important role. In general, vessel segmentation methods can be divided into four categories: vessel enhancement, machine learning, deformable models, and tracking methods [141]. Manual, semi-automatic and fully automated thresholding approaches are the most widely used methods when angiography data are available[5]. Otherwise, vessel enhancement filters are also popular approaches[6]. In [154, 186, 187] the authors used a multi-scale, multi-modal tensor voting algorithm proposed in [220]. In [181], they used an Expectation Maximization algorithm initialized by thresholding and post-processed by multi-scale vesselness filter ( [72]) applied to MRA. Level set is then applied for vessel boundary extraction. the work from [178] proposed a 2D automatic vessel segmentation based on Gaussian mixture model (GMM) and Markov random field (MRF) can be applied directly to the MIP image, in order to identify only vessels around the electrode. The authors in [183, 196] employed

[5] [44–46, 91, 92, 124, 125, 146, 177]
[6] [2, 20–22, 25, 214, 215]

the method proposed by [73], which combines an automatic watershed-based method for large vessel segmentation, and a graph-based method for small vessel segmentation and post-processing, which exploits an edge weighting function that adaptively couples voxel intensity, intensity prior, and local vesselness shape prior.

Structural brain segmentation has a large literature and many different algorithms and software have been released for the analysis of MRI images. As a consequence, some of them has been used to generate the required brain structures that must be considered during surgical planning. In [20–22, 215], the authors used a set of different algorithms based on probabilistic and multiple templates based segmentation ( [37–39]) for the identification of left and right caudate, cortical GM, ventricles and sulci. FreeSurfer (FS) is another well-known open source software tool the the analysis and processing of brain images [66], which offers different functionalities for image registration, skull stripping, cortical surface reconstruction and anatomical labelling [67] among others. The results of the FS pipeline have been used as inputs for the automated planning algorithms in [45, 46, 176, 177, 187]. [63] used FS specifically for the volumetric segmentation of the ventricular system, while the scalp and cortical sulci were automatically segmented by through the BrainVISA ( [164]) anatomical segmentation pipeline ( [132]). In [62] the cortical sulci were automatically segmented using an algorithm based on curvature information ( [115]). In [7] Geodesic Information Flows (GIF) presented by [34] is used to perform brain parcellation using the Brain Collaborative Open Labeling Online Resource (Brain-COLOR) atlas ( [106]) to define the anatomical labels of the cortex, GM and sulci. The brain atlas contains 142 possible regions. In [48, 60, 86], the preprocessing of the images was performed using the pyDBS pipeline a fully-integrated and automatic image-processing workflow for planning and postoperative assessment of DBS interventions as described in [56]. pyDBS includes denoising, bias correction on MRI, CT image registration to preoperative MRI, automatic segmentation and 3D mesh reconstructions. In particular after an interactive localization of the anatomical landmarks AC and PC, performs an intensity-based segmentation of the scalp, brain, and cortical sulci, as well as an atlas-based segmentation of the brain ventricles and basal ganglia.

[7] [119, 154, 186, 187, 197, 199]

### 2.3.2 Abdominal surgery and ablation technologies

The placement of needle-shaped instruments in a minimally invasive image-guided framework is a typical intervention performed in the abdominal region, e.g. liver, for biopsies or minimal invasive tumor therapies. Minimally invasive tissue ablation procedures are widely used for the local treatment of primary and metastatic tumor. These procedures allow the destruction of pathological tissue by means of an ablation effect which acts to create of a necrotic zone in the target area. The pre-operative planning of the intervention aims at finding an optimal path which guarantee both the complete ablation of the target volume with a minimum amount of affected healthy tissue and without damaging adjacent vital structures.

Tissue ablation procedures might require one or more ablations to be planned in order to guarantee that the target volume is completely destroyed. In fact an incomplete ablation might increase the risk of tumor recurrence. The major causes which can hinder a complete ablation are the following: i) difficulty in reaching the entire target volume due to technological constraints; ii) difficulty in releasing efficiently the ablative effect to the entire achievable ablated region because of the perfusion of nearby vessels and capillary level microperfusion which interfer with the ablative effect. On the other hand, the ablative effect could affect unforeseen locations, leading to unwanted ablation of healthy tissue. Hence, an ablation procedure is considered successful, if the whole target volume and the additional safety margin are covered by the coagulation and overtreatment is minimized.

In this review we considered only energy-based ablation mechanism in which the ablation instrument is used to destroy the tissue in the target volume by changing the temperature within that region. Hyperthermic ablation heats up the target region and aims at acute coagulative necrosis, which is the case of RFA and MWA. The first technology uses alternating current of RF waves flowing from the electrode tip through the surrounding tissue, while MWA uses electromagnetic waves to implement thermal ablation. Within the electromagnetic field polar molecules, such as water, continuously realign to the continuously changing waves. This oscillating movement generates the heating effect. All tissue within the electromagnetic field is heated simultaneously, which reduces treatment times in comparison to RFA [82, 96, 137, 212, 213]. Hypothermic ablation cools the target tissue which leads to the breakdown of cellular metabolism, formation of ice crystals and osmotic shock. Cryoablation, also referred to as cryosurgery, is the only hypothermic modality. It utilizes a percutaneously

placed instrument called cryoprobe to decrease drastically the temperature in the target region in order to achieve cell death. All thermal ablation interventions are negatively affected by the blood vessel perfusion: nearby macroscopic vessels (larger than 1 mm in diameter) cause the so-called heat/cold sink effect which consists of the dispersion and removal of the heat/cold. This effect will reduce and deform the boundary of the expected coagulation region.

In case of hepatic interventions, the lung or the costo-diaphragmatic recess should be avoided in order to prevent a pneumothorax. Also blood vessels should be avoided: there are several kinds of vessels (hepatic vessels, superior epigastric vessels) that should not be crossed in order to prevent bleeding and pain. Bone structures such as the ribs represent an obstacle which prevents to reach the target. Furthermore, nerves beneath the ribs can cause considerable pain and neurological deficits if injured. Figure 2.4 shows example trajectories aimed to reach a deep-seated location in the liver.

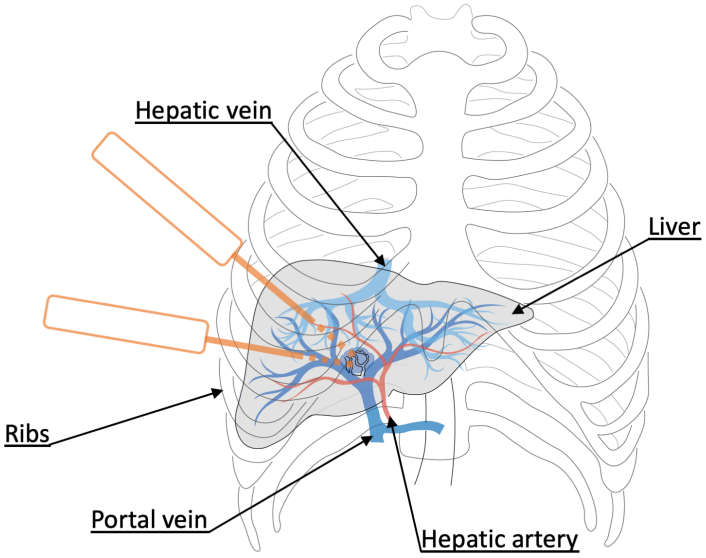


**Figure 2.4:** *Example of liver percutaneous trajectory insertion. The main vascular trees corresponding the hepatic vessels are represented. In case of biopsy, a single trajectory should be planned to reach the tumour region, avoiding ribs and vessels. In case of ablation procedure, depending on the tumour size, it could be necessary to plan more than a single path to guarantee the complete of ablation of the target volume.*

As it regards the feasibility of the procedure, the chosen path should consider four key factors:

- *the length* of the chosen path should be as short as possible in order to minimize deviation from the planned path during the intervention;
- *the angle* between the path and the axial plane (vertical angulation) should be as low as possible, in-plane trajectory are more easy to perform;
- in-plane orientation (i.e., left, anterior, right, posterior) of the selected access paths has to conform to the standard local clinical workflow;
- avoid collision with the scanner, promote comfort of the patient and of the interventional radiologist.

It has been widely noted that the success of these procedure hinges greatly on its pre-operative planning [10, 11], which requires the identification of the anatomical structures of abdominal cavity and the location of the tumor for its histopathological evaluation or for its ablative treatment.

The identification and reconstruction of extra-hepatic structures (including the rib, celiac artery/vein, spine, lung, stomach, and spleen) and intra-hepatic tissues (including the liver, liver vessel, and liver tumor) is of utmost importance for the pre-operative planning of these procedures. The authors in [36] segmented liver, bone, skin and hepatic tumors by a region-appearance-based adaptive variational model proposed in [157]. Thresholding and region growing techniques were used in [57, 90, 175]. A semi-automatic segmentation method was applied in [162], using the ITK-SNAP program's geodesic active contour method [213] to identify the key structures including the tumor and structures that should not be traversed such as the ribs, liver vasculature, and adjacent critical anatomical structures.

### 2.3.3 Spinal Fusion

Vertebral fixation is a surgical procedure for the treatment of different types of spinal column disorders including neurological deficits or severe pain caused by ruptured or slipped discs, degenerative disc disease, vertebral fracture, stenosis, spondylolisthesis, and spinal disc herniation. The spinal fixation is used for fusing together and/or mechanically immobilizing vertebrae of the spine and one of the most used technique is pedicle screw placement. It consists in the insertion of screw from the posterior side, by drilling a canal into the vertebra pedicle [131]. During the procedure, however, clinically relevant screws that are 4.5-8.0mm in diameter, should be inserted into the lumbar pedicle of the vertebra, which only has a diameter of about 6-10 mm. Failure in doing so may cause unrecoverable damage to the spinal cord, resulting in serious injury to the patient [52].

Determining the proper size and orientation of pedicle screws in an operating room environment is challenging. If a mistake is made in selecting an appropriate size and/or orientation of the pedicle screw, the consequences for the patient may be severe and cause great injury. In fact, fracturing the pedicle can damage nerve roots, the dural sac, vascular structures, and pleura, while medial breach of the spinal canal is particularly dangerous and can cause paralysis. Figure 2.5 shows a graphical representation of a pedicle screw insertion procedure.

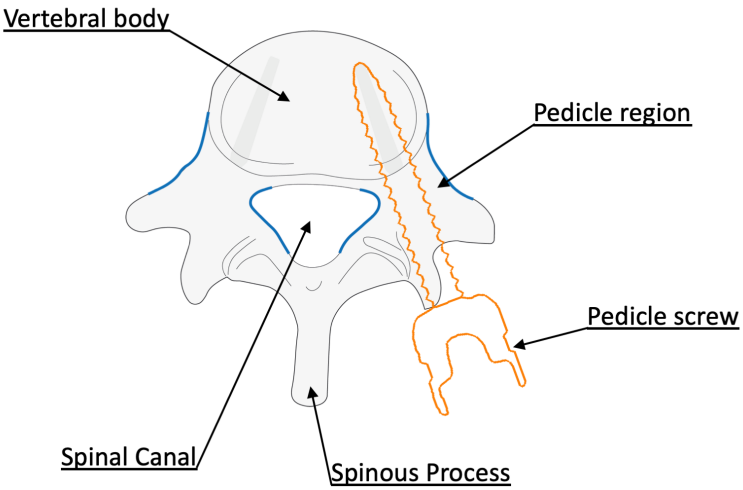


**Figure 2.5:** *Example of pedicle screw insertion. The screw is inserted to a previously drilled canal in the pedicle region. The screw must be correctly positioned to avoid the breach of the anterior cortical bone and pedicles boundaries.*

Surgical planning algorithms for pedicle screw insertion are bounded to the specific anatomy of the vertebra, and require the identification and segmentation of the different vertebral segments. Some authors working on trajectory planning have also proposed their own pipelines for the segmentation of those structures: in [206, 208] they applied a thresholding method for the segmentation of a single vertebral spine segment, exploiting the large gap between bone and soft tissue intensity values. Further surface extraction was performed via edge detection technique such as sobel, prewitt filters. In [116] the authors proposed a method for the identification of the vertebra, of the center point of the spinal canal and the spinal pedicle, based on a three steps algorithm which included: i) a dynamic thresholding, ii) an edge matching step and iii) a connected component analysis to isolate only-spine regions from the rest of the structures. A morphological

thinning operator was applied to identify the spinal canal, which allowed for the subsequent identification of pedicles. This methodology have been used in [117, 118]. The authors in [108–112] used a parametric modelling based on superquadrics. The 3D vertebral body shape model was represented in the form of an elliptical cylinder, and deformed by introducing additional shape parameters and aligned to the observed vertebral body in the CT image by maximizing the similarity between the 3D model and the corresponding anatomy. A analog procedure is applied to obtain the 3D pedicle models.

### 2.3.4 Maxillo-facial and ENT surgery

Articles focused on Maxillo and ENT surgery constitute a minor part of the results, however they follow the general principles related to surgical planning modelling. While only [75] is focused on cranio-facial surgery, the remaining articles present methods for lateral skull based interventions [15, 16], which include cochlea implant surgery [3, 76, 150, 207]. The minimally invasive percutaneous access to the cochlea requires the drilling of a small tunnel from the outer surface of the mastoid, passing through the facial recess and reaching the cochlea without damaging any sensitive surrounding structure as the facial nerve, the external of the auditory canal, the chorda tympani and the ossicles (the malleus, incus and stape). Figure 2.6 report an example of cochlear implant.

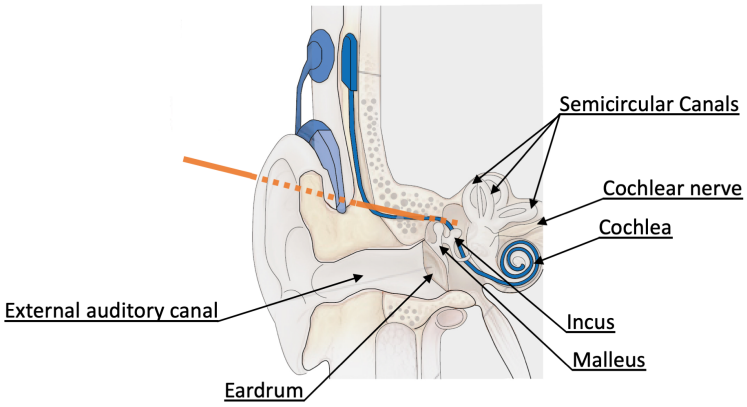


**Figure 2.6:** *Example of cochlear implant surgery. The drilled trajectory must reach the entrance of cochlea without damaging the surrounding structures. In the anatomical image some of the most sensitive anatomical structures are reported.*

From the mastoid surface to the cochlea, all of the above mentioned crit-

ical structures are contained within a region which ranges between 1.0 - 3.5 mm in diameter [150], through which the trajectory must also pass. Previous studies demonstrated that a drilling accuracy of at least 0.5 mm would be sufficient to safely drill through the facial recess without causing any damage to surrounding structures [170]. Therefore, the identification and segmentation of those anatomical regions is mandatory for the development of automated surgical planning algorithms.

In [15,16], a simple thresholding method were used for the segmentation of the cranial bone, however all the interal structure were manually labelled from the analysis of CT images. In [76], the authors used semi-automatic methods, manual thresholding and morphological operators. In [207] ossicles, cochlea, the vestibulum, and the semicircular canals were segmented using a region growing algorithm, and manual refinement to remove outliers in the bony labyrinth. With the exception of [150], which localized the relevant structure using an atlas-based strategy ( [43, 165]) and specific segmentation pipelines ( [149, 151, 152]), all the reported works require the manual intervention of the user.

## 2.4 Planning Assistance

The previous section has analyzed the theoretical basis of surgical planning modelling, and presented the clinical requirements as well as segmentation techniques related to different applications and anatomical district. In this section, we classified the different solutions based on the interaction level required with the user and the type of problem they approximate (figure 2.7). As stated at the beginning (section 2.2), at the algorithmic level many approaches may be relevant for different clinical problems. Therefore, in this section we will provide a qualitative description of the algorithms used from a general perspective, when possible without focusing on their original application.

### 2.4.1 Interactive Planning

Because of the difficulties in the definition of the *optimal* trajectory and the parameters that define it, some authors focused their work on the augmentation of the information presented to the surgeon by CAP platforms. Through the usage of those system, the clinician is assisted with several risk metrics (reflecting relevant operators with respect to the surrounding anatomy) associated to the planned trajectory, helping him/her in the definition of the optimal path.

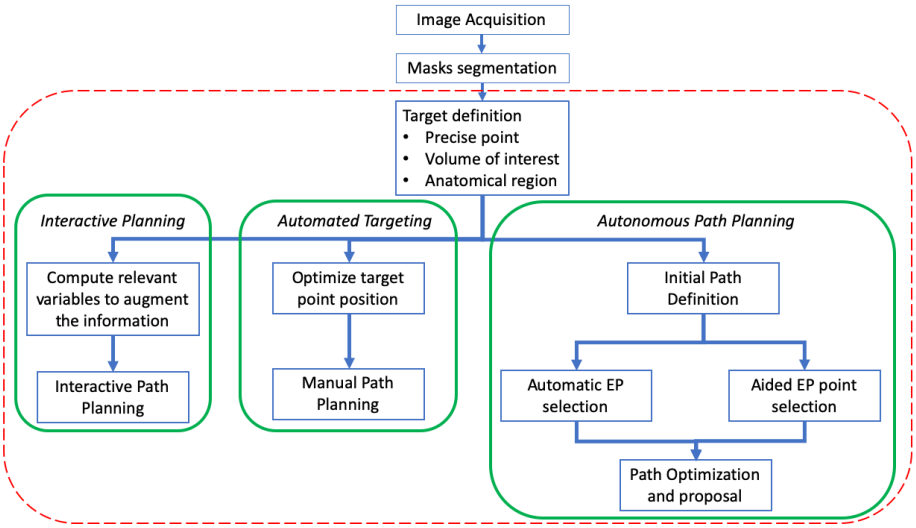


**Figure 2.7:** *Planning assistance division scheme: the articles are presented based on the type of assistance provided to the final user and the problem aimed to solve. Interactive planning is related to methods in which the user manually plans the trajectory using augmented data, or selecting among optimal proposed trajectories. Automated Targeting describes algorithms focused on the optimization of the surgical target, aimed as position or coverage. Autonomous Path Planning focuses on the optimization of the whole path.*

Starting from 2000, Nowinski et al. [155] proposed a pioneer planning assistant, which allowed a multi-atlas visualization for the definition of the target point, continuous navigation and mensuration. The tools provided in the CAP system helped the surgeons to precisely identify the target and the surrounding structures, and measuring distances directly on the medical scan. Following studies have been focused on the computation of those distances and other relevant variables to provide to the user a real time (RT) feedback with respect to the risk of the trajectories. In [76, 207], the software presented the values of distance operators as regards the surrounding critical structures in RT, while the surgeon planned the trajectory. The target point was chosen by the surgeon at the beginning, and the user interactively moved the EP over the surface. The platform computed also the predicted error along the trajectory, represented as a 2D model around the path.

Authors in [92, 146, 163] proposed interactive systems which codified the information through the usage of color-coded maps projected on the outer surfaces of 2D slices. In [92], the system provided a stability map, representing the possible entry regions able to reach a pre-defined target. In [146], the authors used a surface-based rendering technique to compute a series of access maps (a *Direct Impact* map, a *Proximity map* and a *Path Length* map) which were projected on the outer surface and could be used by the surgeon to identify the most feasible entry point (EP). This approach was extended in [163] by exploiting algorithms optimized for Graphical Processor Unit (GPU). In particular, they used *acceleration spatial data structures* based on *bounding volume hierarchy* (BVH) to efficiently represent the critical structure meshes, providing a rapid computation of the risk access maps and RT interaction.

An alternative approach has been proposed in [104], where the authors used a *crepuscular rays* analogy and implemented a voxel-based ray casting solution exploiting GPU performances to compute all available safe paths. They provided a 2 step planning system: first, they used a multi-volume rendering to provide an overview of all available paths through a 3D representation; second, they provided a 2D slice visualization for accurate planning, using cutting planes on the desired orientation, with a color-coded scheme to identify the available paths. Volume rendering techniques were used in many planning assistance solutions: in [172], authors used a direct volume rendering techniques to build a risk structure map based on a user-defined target point and the segmentation masks of critical structures. They used a cube map [83] to store all the paths which intersect risky structures, consisting in six projections obtained by placing a perspective camera centered at the target point. This technique allowed to use high performance

*shaders* developed for computer graphic purposes, which exploits GPU architecture to speed up the computation. The results were projected onto the 2D views navigated by the surgeon, enhancing the available access regions by a color-coded scheme.

GPU accelerated algorithms were used also for the simulation of the ablation necrosis zone [216], allowing a real time estimation of the ablation volume while the surgeon interactively adjusted the trajectory. In [19], the authors proposed an ablation system which automatically provided the ablation parameters based on the specific ablation volume defined.

Other interactive techniques were presented in [183, 184], were the authors pre-computed a risk-volume by assigning a risk factor to each segmented structure, based on the expected damage in case of collision with the clinical probe. The target required to be defined in advance, and all the possible access path were computed and projected through a color-code scheme on the outer surface. Additionally, the CAP system provided the visualization of risk-card containing the values of relevant operators. During the interactive analysis of the trajectories, a geometrical model named *safety zone sleeve* is visualized and corresponds to the positioning uncertainty worst-case scenario estimated, based on localization and target errors. In [181] the authors extended the previous method by introducing an augmented reality system, which presents the quantified trajectories on a 3D physical model, allowing the surgeon to plan the trajectory in the physical space.

While all the previous works focused their assistance in augmenting the information presented to the surgeon, in [25] the authors precomputed all the possible trajectories to reach a predefined target and organized them based on a distance-based criterion. The distance values were used by the user to filter the computed trajectories. Similarly, in [171] the authors computed all the reachable trajectories by using cylindrical projection derived by cube maps. Each projection represented a different operator value, and the results were organized on a parallel coordinate plot. Therefore, the user could filter the trajectories based on his/her preferences with respect to different operator values. An extension of that method was proposed in [175], by normalizing and weighting the cylindrical projection, obtaining a single map. The latter was used for the definition of a set of initial seeds, for optimal trajectory computation. Such seed trajectories allowed to run local optimizations and determine solutions which approximate the Pareto-front, avoiding to fall in local minimum. The user could navigate the approximated Pareto-optimal by the use of Pareto-sliders (one for each criterion).

In [75], the authors implemented a solution for access path determina-

tion based on the visibility of the target point: contrary to the previous reported works, they generate a set of grid points uniformly distributed on a sphere surface and positioned a virtual camera at each vertex, with the focal point set to the target. The results can be navigated by the use of scatter and parallel coordinates plots. A similar application is presented in [15], authors presented their result by color-coded 3D cylinders that could be interactively chosen by the surgeon.

### 2.4.2 Automated Targeting

While many applications require the precise targeting of structures, only tissue ablation techniques and some works on DBS have been focused only on the definition of the optimal target, without accounting for the remaining constraints. Usually, the systems presented in this section require the definiton of the tumour volume of interest (VOI).

Preliminary works [26, 54] simulated the ablation volumes by geometrical primitives (e.g. elliptical and spherical volumes) and experimented the efficacy of different number of probes in the coverage of a tumoural volume. In [205], the authors developed a simulator which account for deformation of the ablation zone caused by surrounding vessels, by approximating the heat-sink phenomenon by stopping it in presence of large vessels. The resulting necrotic zone is represented through a deformed ellipsoid, following the vessel's shape.

In [161], the authors used a *branch and bound* method (integer programming) firstly to compute the minimum number of trajectories to cover the target volume, and secondly to compute the minimal number of ablation along the trajectories. Recently, a PSO-based algorithm was proposed to account for the multi-objective nature of the ablation problem [80, 81], able to determine the number, size and position of ablation spheres to maximize the coverage of the VOI.

While in the previous articles the ablation zone is simulated by geometrical primitives, other solutions used the *bio-heat transfer* equation [158] to model the cooling/heating effects on the surrounding tissues. The latter is used to simulate the temperature distribution in a living tissue influenced by the blood flow effects, represented as a heat sink and sources. Such equation is usually applied through a finite element model (FEM) simulation, which estimates the ablation effects on the surrounding tissues and, consequently, the ablation volume. Based on that, in [12] the authors implemented and tested three objective functions for multiple cryo-probes numerical optimization. In [127], an optimization algorithm based on a *force*

*field analogy* was proposed, where the bio-heat equation was computed at each iteration and forces applied to the different cryo-probes to reach the correct temperature configuration. In [4, 5] the authors focused on the optimal placement of RF probes, computing the estimated electric potential and the heat distribution at target zone and minimizing a temperature-based objective function. Tanaka et al. [191, 192] developed a more mechanical approximation method to deal with the overlapping of multiple probes. They represented the elliptical ablation volumes (bubbles) for each probe, and applied a bubble-packing algorithm where Van der Waals'-like forces are simulated to move these bubbles until a minimum force configuration is found.

All the previous optimization approaches required to compute the heat-transfer simulation at each iteration, to correctly estimate the ablation zone. FEM-based simulations are computationally expensive, increasing the time required for finding a solution and making them unpractical for real situations. Consequently, another study [35] focused on finding more efficient solution by modelling the RFA heat transfer without the necessity of re-meshing.

### 2.4.3 Autonomous path planning

Most authors have tried to completely reproduce the trajectory planning problem by developing algorithms which automatically propose the optimal computed trajectory or set of trajectories to the surgeon. Different algorithm and modalities have been proposed, some of which require the user to only identify the target (section 2.4.3), while others reduced the computation burden by taking advantage of the anatomical region knowledge or requiring additional interaction for the algorithm initialization (section 2.4.3).

#### Automated EP definition

Most of the approaches which require a precise definition of target points, being the coordinates of the target or a complete volume of interest (VOI) definition, proposes techniques similar to the ones described in the previuos sections (section 2.4.1, section 2.4.2). In [204], authors used a voxel-based ray casting procedure to detect the surrounding structures, and optimized the number and position of multiple ablation probes based on the coverage of the target VOI. Since the algorithm was initialized by the definition of the tumour VOI and the outer surface, in [11, 203] they computed and stored all the accessible paths into cube maps to reduce the possible search

space. In particular, in [11] they did not consider a single target point, but computed the cube maps from each voxel on the VOI boundary in order to determine the accessible paths. After removing non-reachable solutions, they optimized the trajectory based on the coverage maximization between the target VOI and the simulated ablation sphere. Since they applied a numerical optimization strategy by the use of Nelder-Mead algorithm, a semi-exhaustive initialization identified all the available connected zones on the outer surface, which were used as starting points for the optimization.

In [179] they exploited computer graphics algorithms for the determination of available entry zones by Z-buffering volume rendering, removing all the occluded vertices on the outer surface. Subsequently, soft constraints regarding the trajectory length, the distance from critical structures and the insertion angle were computed and a Pareto-based optimization scheme is applied to determine Pareto-optimal solutions. Similar approaches were used for DBS application in [62], where they reduced the search space entry zones by the exploitation of GPU rendering algorithm, generating cube maps view from the target point. It is worth notice that in [61, 62], authors deeply analyzed the rules guiding DBS intervention and developed a generic approach based on a meta-language (XML) for the translation of rules into geometrical constraints.

Finally, GPU architecture was exploited also in the development of Epinav [187, 219], a SEEG automated planner which used BVH organization for the computation of intersection and distances with respect to critical structure surfaces and which required only the definition of TPs. The GPU acceleration allowed the usage of an exhaustive search method and efficient removal of unfeasible EPs for each trajectory, based on the hard constraints provided. In [186], the authors introduced the definition of user-specific priors to guide the way a trajectory crosses a specific target region.

As in the interactive planning section, other authors implemented their algorithms without exploiting rendering techniques or GPU architectures. In [210], a multi-purpose system based on the Image Guided Surgery Toolkit (IGSTK) was presented, where the authors developed an automated planning algorithm for tumour ablation in the lung. The whole pleura surface was used as initial entry region, and the number of trajectories and ablation was optimized through a branch and bound method as in [161]. The "*collision-free reachable workspace*" appeared in [123], where the optimization method took into account the workspace of the robot used by including its kinematics in the computation of optimal trajectories. A similar work is proposed in [17], where the available search space defined on the patient skin was determined by taking into account the points that were

reachable by the robot. In [182] the authors implemented an automated version which ranked the trajectories incrementally, based on the risk score. As in the interactive versions [183,184], they computed a risk volume based on risk values assigned by the surgeon and, for each computed trajectory, they presented a risk card reporting additional information. In a following publication [196] the authors studied the efficacy of the automatic method with respect to a traditional planning and an augmented version of their software. The same risk volume approximation was reported in [44], which introduced the usage of fuzzy logic to better transmit to the surgeon the risk associated to a trajectory.

#### Aided EP definition

While the previous algorithms automatically explored the whole search space with respect to the defined target, in [20–22, 124, 125, 214, 215] the authors defined a set of entry regions on an atlas head surface, according with DBS intervention standards. Therefore, they registered the atlas to the new patient scan, reducing the available entry zone by the one previously define. In [45, 46, 177] an automated planning algorithm for SEEG was implemented, in which the surgeon roughly initialized each trajectory by placing EP and TP. Such points where used to generate initial entry and target search space for each trajectory, and the reduced search space allowed the usage of an exhaustive search method in a feasible time span.

Similarly, the algorithm presented by [150] required a manual initialization of EP and TP, or their estimation through an atlas registration procedure [3]. The algorithm presented in [16] implemented a multi-port automated planner for skull-base applications, which optimized the set of the three best trajectories to reach a predefined target. Again, the clinician had to roughly select a set of obvious initial candidate entry points.

Automated planning algorithms focused on screw insertion are strictly bounded to the anatomical characteristics of the surgical site. The majority of these articles are focused on the spine and require a characterization of the pedicular regions to run the optimization, focused on the optimal implant size and orientation (section 2.3.3). Authors in [206] applied a set of geometric considerations for extracting anatomical information from the segmented patient images. By correctly orienting each vertebra, they scanned each slice along the anterior-posterior direction looking for chords which identified four intersections, representing the pedicle regions. Once the pedicles were identified, the authors could estimate the minimum pedicle width by simply computing the Euclidean distance between intersected

points, and build a set of 3D coordinates as the mean points along the pedicle, fitted by a least square algorithm to identify the trajectory. In [117,118], the authors searched for the optimal trajectory by providing a safe margin with respect to the pedicle boundaries and maximizing the insertion depth in order to improve the so-called *fastening strength* between the screw and vertebra interface [114]. Also in [208] they used a set of geometric consideration with respect to the anatomical vertebra planes, and searched for the optimal solution by maximizing the fastening strength computed at the screw boundaries. The authors in [108,109] based the planning of screw on the parametric modelling of pedicles already presented in section 2.3.3. The screw was modelled as a cylinder, and positioned to cross the mid-coronal plane of the pedicle and optimized with respect to the axial and sagital angles. Trajectory and size of the final screw were estimated taking into account the 3D vertebra and pedicle models previously obtained, and maximizing the fastening strength based on the image intensities underlying the screw boundaries (similar as in [208]). The method for the estimation of sacro-iliac screws is similar in [138], which analyzed the voxel-intensity sequence by scanning a correctly oriented CT scan, and defined the maximum screw width and the optimal trajectory.

While all the previous algorithms focused on the optimization of trajectories based on anatomical constraints, in the last years other approximation tried to introduce additional knowledge based on the analysis of past cases. For both spinal [77, 202] and pelvis screw [78, 88] placement applications, the authors proposed a planning method based on the construction of a statistical shape model, containing trajectory annotations. The atlas is constructed from different segmented data sets, containing annotation of expert clinicians regarding screw trajectories. An active shape model registration method was used to register a new CT volume without requiring any previous segmentation. Following a similar concept, the authors in [176] proposed a method for the analysis of retrospective trajectories, and their accumulation in an average brain space based on their spatial position and the anatomical regions crossed. The latter focused on SEEG surgical practice, and the trajectory atlas is shown to be helpful in the initialization of optimization algorithms (e.g. [177]). Atlas based methods represent an alternative approximation to the surgical planning problems, based on the idea of encapsulating expert knowledge which may contain additional consideration rather than only anatomical or bio-mechanical constraints.

## 2.5 Conclusions

An extended overview of surgical planning assistance methods focused on percutaneous keyhole interventions based on the insertion of needle-shaped tools has been presented. The systematic review included 115 articles, which have been classified and analyzed from different perspectives. To the author knowledge, this is the first systematic literature review which covers needle-shape trajectory planning assistance from a methodological point of view, without focusing on a single clinical application.

The problem has been presented from a general perspective, describing the principal phases guiding the modelling of percutaneous applications: *image processing* (section 2.2.1), *formalization* (section 2.2.2), *optimization* (section 2.2.3) and *experimental design and validation* (section 2.2.4). Along the description of each phase, we provided practical examples by including the references to the articles.

Focusing on optimization schemes, the review revealed that the majority of the works represented the surgical planning problem with an aggregative approach, probably because of its intuitiveness defining the importance of each constraint. Only few works have explored Pareto-based and evolutionary approaches, which are stated to be more efficient in the resolution of non-convex optimization problems and represent an interesting research area.

We classified the validation experiments based on the type of evaluation performed and the data used, providing a brief description and references of the most relevant experiments. In many cases, the authors passed through many different validation steps (e.g. authors of Epinav$^{TM}$, which represent the most advanced platform in terms of validation experiments), indicating how surgical planning modelling consists in a long and iterative process. However, using the validation provided as an indicator of the TRL, only few systems can be considered close to their inclusion in the clinical practice. In [199], the authors demonstrated the enormous variability in the definition of a safe and optimal trajectories, at least in the SEEG domain. The same problem has been reported for other neurosurgical scenario, which represent almost 50% of the available literature. There are no standard rules to directly compare the quality of the proposed assistance, that is also greatly influenced by the different medical workflows of clinical centers (which include medical image scans, segmentation methods, the hardware used for the interventions and others).

Different clinical applications have been found from the literature research, presented in section 2.3. While each clinical intervention has its

own requirements, it can be state that they share a common base and many of the algorithm could be translated to other applications. Actually, a general framework (similar to the one proposed in [11]) could provide a solution adaptable to many of the interventions reported. Accordingly, in section 2.4 we presented many similar algorithms applied to different applications (especially abdominal and neurosurgical procedures).

In our opinion, a fundamental requirement of those systems is their usability: accurate anatomical segmentation seems to be one of the major problems, which is directly bounded to the anatomy of interest and from which the results of a planning assistant are deeply influenced. While neurosurgical and abdominal applications can take advantage of a wide literature on segmentation algorithm, spine, maxillo and ENT applications may require to implement their own solutions. Especially the latter, which requires the precise segmentation of small anatomical parts, did not present a robust segmentation pipeline and manual intervention was often required, which may prevent those systems to be widely used in the near future.

Finally, all the articles reported in this work assume perfectly straight needle trajectories, with no deformation occurring during the insertion. This specific problem has been faced only in [86].

## Appendix - Systematic search

We searched for publications on the topic of automatic planning in surgery on PubMed, Scopus, ISI Web of Science. The research included all the different combination of 4 groups of words, reported in table 2.2.

| group 1 | group 2 | group 3 | group 4 |
|---|---|---|---|
| Automat(ic, ed)<br><br>Computeri(s/z)ed<br><br>Computer - assisted, aided | surgical<br>surgery<br>percutaneous<br>needle(s)<br>screw(s)<br>keyhole<br>biopsy(ies)<br>probe(s) | plan<br><br>planning | trajectory(ies)<br><br>path(s) |

**Table 2.2:** *Combination of words used in the systematic review. The words within each group where searched with an 'OR' connection, while between groups we applied an 'AND' connection.*

The choice of such strict queries was determined by the specific topic covered by the review. To guarantee that all the relevant works were con-

sidered, we revised the bibliography of each accepted paper and manually add to the list the important ones.

### Inclusion/Exclusion Criteria

In the review, we included all the papers which describe a software application able to assist the surgeons during the planning phase of percutaneous surgeries. Automated, semi-automated or interactive approaches aiming to simplify the trajectory definition have been considered. We intended as assistance all software solutions able to provide a quantitative feedback regarding the safety and effectiveness of the trajectory, or methods aimed to optimize specific parameters of the surgery based on clinical considerations. The search was limited to the last 19 years (from 2000) and only papers written in English were taken into account. We voluntarily discarded all the articles focused on steerable needles or describing the modeling approaches about needle-soft tissue interaction. We considered those works to be related on the implementation of new prototypes for robotic surgery, or to provide a realistic simulation between tissues and needles. The aim of this survey is to revise the actual state of art in modeling and automatize the planning phase procedure based on the clinical requirements of percutaneous interventions.

The results of the literature search are presented in 2.8, which reports the diagram representing the workflow based on PRISMA [142].

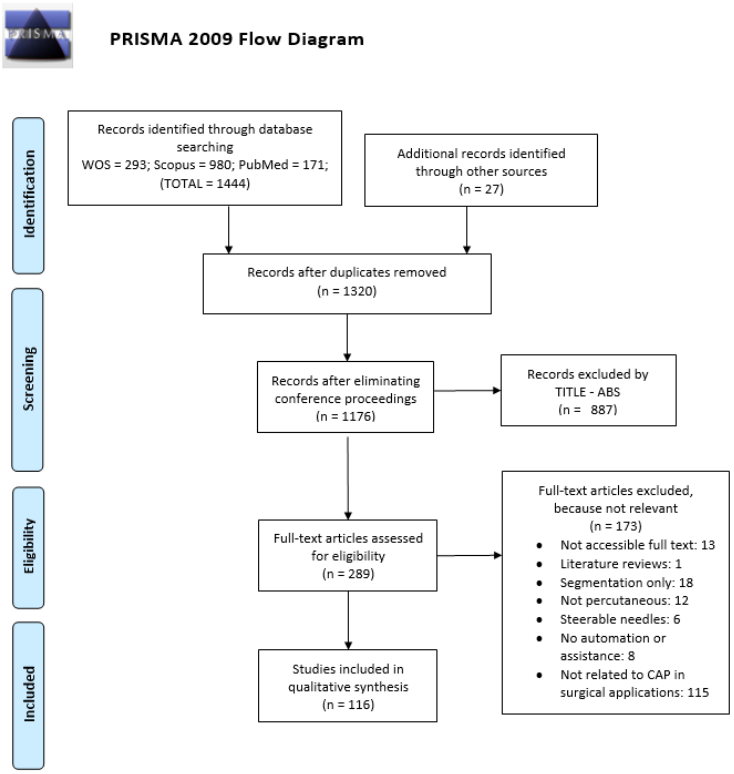


**Figure 2.8:** *PRISMA (Preferred reporting item for systematic reviews and meta-analysis) diagram for the systematic identification, screening and included articles in the review.*

CHAPTER 3

# Retrospective Evaluation and SEEG Trajectory Analysis for Interactive Multi-trajectory Planner Assistant

In this chapter, we present the first prototype based on the analysis of the constraints that guide SEEG surgical treatment and the methodology presented in the literature review presented in chapter 2. The system described has been designed to be modular, accounting for possible future modifications. An image processing module allows additional processing for planning purposes, and an anatomy-driven optimization algorithm is able to adapt the electrode trajectories on the specific anatomy of the patient. A graph-based heuristic approach to efficiently combine the electrode optimal states is presented. The method reduces the computational complexity of a classical brute force approach, without preventing the system to reach the global optimum. A quantitative retrospective validation shows that the solution is able to maximize the values of operators related to safety requirements, reaching values superior than manually planned trajectories.

Based on this work, a journal paper has been published as [177]: Scorza, D., De Momi, E., Plaino, L., Amoroso, G., Arnulfo, G., Narizzano, M., ...

Cardinale, F. "Retrospective evaluation and SEEG trajectory analysis for interactive multi-trajectory planner assistant". In *International journal of computer assisted radiology and surgery*, 12(10), 1727-1738, 2017.

## 3.1 Introduction

Different automatic algorithms have been proposed for minimally invasive neurosurgery, mainly for SEEG, Deep Brain Stimulation (DBS) and needle biopsies. The ultimate goal is to assist surgeons during the planning phase and find feasible and safe trajectories according to the application constraints. In [92], the authors presented a biopsy planner to reach deep seated brain tumors, which interactively assists surgeons during manual trajectory assessment through the interactive visualization of trajectory risks. Another group [183, 184] proposed a method which assigns risk values to each segmented critical structure based on the estimated damage that could be caused by crossing them. Results are visualized as color maps, and risk cards associated to trajectories provide quantitative information when making the final choice. An alternative method was presented in [146], which generated access maps to guide surgeons during the selection of an entrance point to access specific regions and target anatomical structures. In [163], the estimated risk associated to accessing path was visualized interactively thanks to GPU optimized methods.

Other approaches automatically compute trajectories and select the best set based on the maximization of different constraints. In [63], the authors proposed a hybrid approach for DBS planning by providing information in the form of a color map and then automatically proposing a trajectory plan. Similarly, other authors ( [20–22, 124, 125]) implemented approaches for DBS which take into account different restrictions as vessels and sulci avoidance, precision on target, ventricle avoidance, etc.

In relation to SEEG planning, in [46], the authors presented a multi-trajectory automated planner which optimizes electrode trajectories and operates serially in the event of electrode conflicts, making the final plan biased by the electrode optimization order. In [45] they overcame this problem by computing all possible combinations of electrode configurations. However, this approach is computationally inefficient, requiring too much time or forcing the user to decrease the number of solutions to be taken into account. Another implementation was presented in [187, 188], where the authors developed an automated MT planning algorithm that considers the distance to critical structures, trajectory length, insertion angle, gray matter (GM) ratio and the interference between trajectories. Dynamic pro-

gramming and a depth first search algorithm speed up the search strategy, leading to an optimal plan which takes into account all electrode positions simultaneously. In [214], the authors centered the study on the localization of the electrode contacts in order to maximize the coverage of the region of interest.

Most of the presented methods are based on constraints which have been defined beforehand in collaboration with surgeons and medical staff. Moreover, these parameters are usually applied to all the trajectories that have to be optimized, without considering different values based on additional factors such as the anatomical region explored. To the best of our knowledge, only in [60] the authors have retrospectively analyzed the planned trajectories to define the optimal weights for their cost function. A retrospective quantitative analysis of manually planned trajectories was performed in order to better understand routine clinical practice. Parameters have been collected and stored on a database and these will be used to improve the optimization constraints. Furthermore, we present an improved planning assistant built in 3D Slicer 4.5.0-1 [102] which improves the functionalities described in previous works [45, 46]. This planner version allows the optimization of electrode trajectories based on the following constraints:

1. Vessel avoidance
2. Sulcus avoidance
3. Insertion Angle with respect to the skull surface
4. Initial entry and target brain region definition
5. Electrode conflicts avoidance by means of a selective brute force approach

With respect to our previous work, we introduced two main innovations. The first one is that an atlas is used to limit our search space to the anatomical structures in which the neurosurgeon placed EPs and TPs. This feature is fundamental in order to respect the epileptological strategy of the implantation. The second new development is that we have overcome the computational limitations which affected our previous version in the case of electrode conflicts. Instead of considering all possible combinations of trajectories, a new selective brute force approach based on a graph construction was implemented. This method allowed us to run our optimization algorithm in a reasonable time using 3D Slicer platform which, as far as we know, does not natively offer the possibility of multi-core parallelization or GPU acceleration.

Our work is structured as follows: section 3.2 presents the implementation details and the retrospective validation. A description of each planner module is provided, with an explanation of its usage and the optimization strategy applied. Subsequently the characteristics of the experiment performed on retrospective patient data, illustrating methods, images used and indexes that have been evaluated are given in 3.2.4. Section 3.3 presents the results of the retrospective validation on 20 patients, for a total of 253 trajectories and compares the Manual Planning (MP), Optimized Single Trajectory Planner (OSTP) to the Optimized Multi-Trajectory Planner (OMTP) strategy. Finally a discussion and description of future work is provided in section 3.4.

## 3.2 Materials and Methods

The SEEG-Planner extension built using 3D Slicer is composed of three different modules, each providing a different interaction level and assisting surgeons during a specific phase of the planning procedure. The *Image Processing Module* (section 3.2.1) allows the user to load and interactively prepare patient images required during the optimization procedure. The *Optimization Module* (section 3.2.2) enables neurosurgeons to select desired entry and target brain regions to initialize electrode trajectories and automatically computes the optimal ones according to chosen constraints. Finally, in the *Advanced Trajectories Verification Module* (section 3.2.3) surgeons can assess the surgical feasibility of the proposed plan. This module simplifies this phase with advanced interactive tools for vessel enhancement visualization and provides additional quantitative information about vessels distance.

Once a plan has been defined, information and data on the trajectories are stored in a trajectory database containing relevant information (recorded brain zones, parameter values, etc ...) which will be used for further studies.

### 3.2.1 Image Processing Module

This module initializes the patient planning procedure by loading the required images in 3D Slicer and generating additional data which will be used during the trajectory optimization. The modules uses 4 main inputs:

- CT-Angiography Volume
- Brain cortical surface mesh

- Curvature data relative to the cortical mesh
- CT acquisition of head bone or, alternatively, a T1-MRI

First, the user interactively selects a global threshold to segment vessels, visually guided by a volume-rendered output in the 3D view (Figure 3.1b). The volume is then visually inspected and once the surgeon finds a satisfactory result, a distance map is computed using Danielsson's distance mapping algorithm [42]. Second, the user defines a cortical curvature threshold representing feasible cortical entry points. This threshold is applied to the curvature data and transformed into a new surface which defines whether each vertex represents a feasible or unfeasible entry point (Figure 3.1c). Generally speaking, the curvature, which represents the cortical folding, is an effective index to distinguish between gyrus and sulci. Finally, the user obtains the patient skull or skin surface by thresholding the CT-bone volume or the T1-MRI, respectively (Figure 3.1d).

In our workflow, we used a Cone-Beam CT (CBCT) mobile scanner to obtain a 3D catheter angiography. Prior to administering the contrast medium injection, a preliminary CT volume (CT-bone) is acquired to obtain a bone-mask that will be subtracted from the enhanced dataset, thus keeping only the vascular tree. Therefore, exploiting this 3D CBCT DSA approach, a single threshold approach is sufficient to construct a binary volume containing white voxels representing vessels and black for everything else. In order to obtain surface and curvature data we used Freesurfer (FS) [66], a well-established MRI imaging pipeline that has been proven to reliably segment cortical sheets [28]. It should be mentioned that any other program able to provide such information could be used as an alternative to FS. Additionally, we used the Destrieux Atlas [68] (Figure 3.1a) provided by FS as a probabilistic atlas which will be used during electrode optimization. We choose the Destrieux since it provides a finer representation of anatomical structures compared to Deskian-Killiany. Also in this case, the user can load his/her own preferred atlas.

### 3.2.2 Optimization Module

The Optimization module attempts to find the best combination of electrode models and trajectories that more accurately resemble the investigation strategy that has been planned. The implemented optimization approach is divided into four steps. The first (i) aims to define a set of feasible EP/TP. Subsequently, (ii) we optimize single trajectories constructed by pairing a feasible entry and target points for each electrode. Finally, we

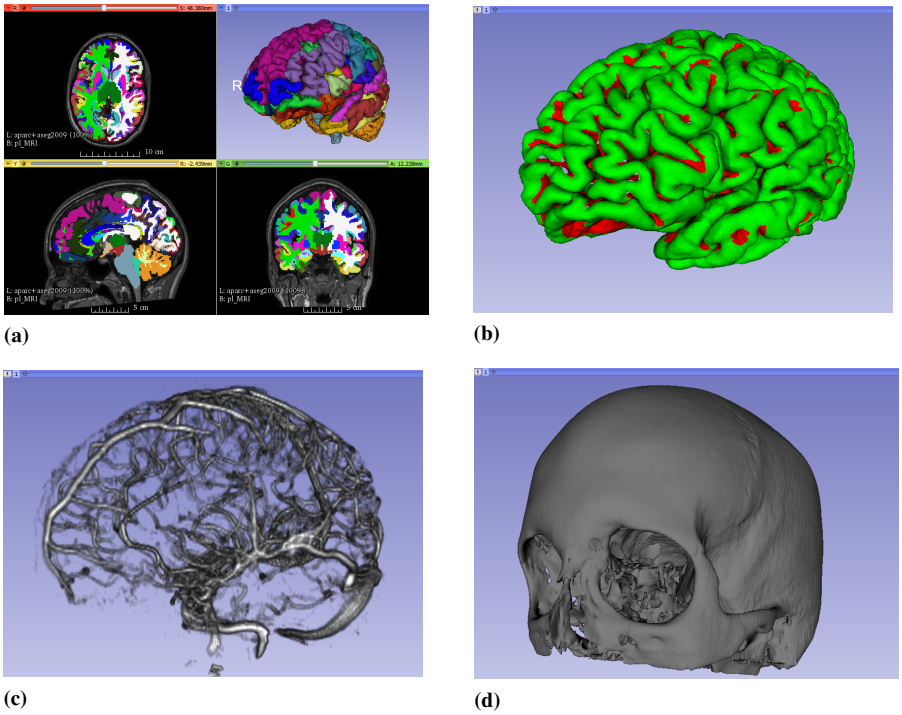

**(a)** **(b)** **(c)** **(d)**

**Figure 3.1:** *Image Processing Module: (a) shows the Destrieux Atlas co-registered to MRI module during FS processing. (b) shows the volume rendering helping surgeons during the threshold selection for vessels binarization. (c) is the cortical surface divided into possible entry regions (green) and discarded regions (red). (d) is the skull surface obtained from CT acquisition.*

(iii) construct a conflict graph for all optimized trajectories and (iv) correct any potential conflicts if found.

Initially, the user defines a set of EP and TP to represent the desired intracerebral investigation strategy. These points represent the initial 3D coordinates of the seed points that will be used later in the optimization. By defining these seed points, the user also establishes the entry and target anatomical regions, based on the atlas used (i.e. Destrieux atlas). As an initial output, the module provides a suggestion for electrode models based on the total electrode distance measured as the Euclidean distance from EP to TP. In our centre we use Microdeep® (DixiMedical, Besançon, France) or Depth Electrodes Range 2069® (Alcis, Besançon, France). However, we provide a configuration file in json format which contains the geometric information of the electrode models and where it is possible to add other models from different manufacturers.

Subsequently, for any given electrode, the module constructs all possible trajectories starting from the user selected EP/TP pair. For any given pair, the module defines a circular or spherical Region Of Interests (ROI) for EP and TP with a radius of $r_{EP}$ and $r_{TP}$ , respectively. Then, we map all possible entry and target points to the corresponding closest voxel coordinates. We discard all those points contained in the circular ROI that are considered unfeasible based on the curvature surface built during the initialization module as EP candidates. Furthermore, we discard all those voxels which do not belong to the corresponding initial anatomical region selected by the user as EP and TP candidates. The collections of all feasible EP and TP among the possible candidates constitute the accepted EP ($S_{EP}$) and TP ($S_{TP}$) that will be used for optimization.

The optimization strategy is based on four hard constraints that have to be satisfied in order to find the best combination of trajectories. Hence, (1) we define $\theta_{max}$ as the maximum insertion angle with respect to the skull normal acceptable for electrode placement. Regarding vessel distance (2), we split each trajectory into two tracts. Therefore, the user defines a length value $\zeta$ applied from the cortical EP to separate the cortical and distal tract and a distance threshold value of $\delta_v^{EP}$ representing the minimum distance from the closest vessel which has been applied to the first tract of the trajectory (Figure 3.2). The distance from vessels can be relaxed while proceeding in depth. Thus, a different threshold $\delta_v^{TP}$ has to be defined for the second tract, usually satisfying $\delta_v^{EP} \geq \delta_v^{TP}$. This approach arises from the consideration that the first tract, closer to the cortical surface, represents the zone where skull drilling and dura mater ablation are performed. Therefore, safety issues require a higher distance between the trajectory and the clos-

est vessel in that zone while, nearer to TP, this constraint can be relaxed considering that SEEG electrodes are essentially atraumatic [**?**]. The user is allowed to change this parameter in the case of more traumatic devices.

Finally, we define $\gamma_{min}$ as the minimum distance (3) between electrodes not causing any conflict and (4) the weights $\omega_v$ and $\omega_a$ for the final cost function 3.4. The default values applied are shown in table 3.1. A resolution value of $\xi = 0.25$ mm for sampling the trajectories during the optimization procedure was defined according to images resolution and neurosurgeons suggestions.

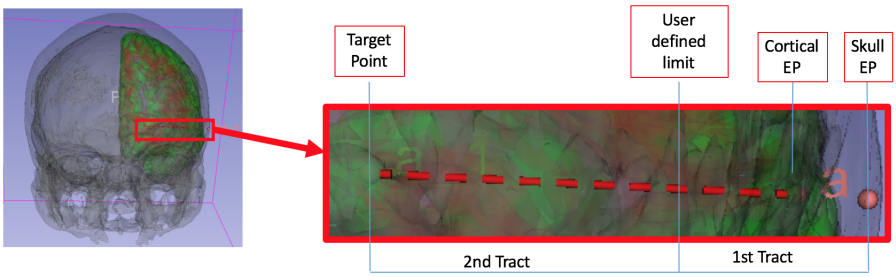


**Figure 3.2:** *Electrode trajectory tracts: in the first tract, a stronger constraint to vessel distance is applied, but this is relaxed reaching the TP. Both values can be manually adjusted.*

| **Hard constraints** | | **Optimization Values** | |
|---|---|---|---|
| Vessel distance first Tract [mm] | 4 | EP search radius [mm] | 7 |
| Vessel distance second Tract [mm] | 1 | TP search radius [mm] | 3 |
| Insertion Angle [deg] | 30 | First tract Length [mm] | 10 |
| Inter-electrodes minimum distance [mm] | 3 | $\omega_v, \omega_a$ [46] | 0.8, 0.2 |

**Table 3.1:** *Default values applied for optimization parameters*

Finally, we run the MT strategy in two phases, starting with a dense search around the user seed points and applying a selective brute force algorithm to avoid conflicts. For each electrode, the total number of possible trajectories $M$ is represented by the combination of all possible EPs and TPs (equation 3.1).

$$M = |S_{EP}| * |S_{TP}| \tag{3.1}$$

where symbols $|S_{EP}|$ and $|S_{TP}|$ represent the cardinality of each set of points.

the insertion angle $\theta(j)$ is computed with respect to the skull normal, with $j = 1, 2, \ldots, M$ and a cost function $f_\theta(j)$ is computed:

$$f_\theta(tr_j) = \begin{cases} discarded & if \quad \theta(j) > \theta_{max} \\ \frac{\theta_{max} - \theta_j}{\theta_{max}} & otherwise \end{cases} \tag{3.2}$$

A higher score is given to those trajectories with a smaller angle with respect to skull normal.

The cost function for vessel distance $f_v$ is computed for each trajectory, based on the distance map generated in the previous module (3.2.1). The trajectory length $len(j)$ is defined by the Euclidean distance between $EP_{skull}(j)$ and $TP(j)$, and trajectory $j$ is divided into a set of control points $N = \frac{len(j)}{\xi}$. The corresponding value on the distance map is checked for each control point, which represents the distance from the closest vessel $d_v$, and the cost function is computed as following:

$$f_v(tr_j) = \begin{cases} discarded & if \quad d_v(i) > \delta^{thresh} \\ \frac{1}{N+1} * (\sum_{i=1}^{N} \frac{d_v(i) - \delta_v^{min}}{\delta_v^{max} - \delta_v^{min}} + \frac{\delta_v^{min} - \delta^{thresh}}{\delta^{thresh}}) & otherwise \end{cases} \tag{3.3}$$

where $i = 1, 2, \ldots, N$, $\delta^{thresh}$ is respectively $\delta^{EP}$ or $\delta$ based on the trajectory tract, $\delta_v^{min,max}$ are respectively the minimum and maximum distance value for trajectory $j$.

Finally, a total cost function is computed as a weighted sum between the two components of each possible trajectory $j$:

$$f(tr_j) = \omega_v * f_v(tr_j) + \omega_a * f_\theta(tr_j) \tag{3.4}$$

A recursive strategy is applied in case all trajectories are discarded, which increases iteratively the search radius at EP and TP and the optimization is restarted.

At this point, each electrode has a total number $A$ of acceptable trajectories that have been computed and sorted in descending order based on the cost function expressed in equation 3.4.

Then, to prevent conflicts, we define an undirected conflict graph $G = (V, E)$ where each node represents an electrode with $A$ possible states corresponding to the accepted trajectories, and edges $E$ represent possible conflicts among them.

At initial state, no possible conflicts have been identified, therefore $G = (V, \emptyset)$.

Then, we compute the Euclidean distance $\gamma_{i,k}$ between nodes $v_i, v_k$ of the conflict graph considering their initial EP and TP. We establish a possi-

ble conflict (create edge $e_l$ between $v_i, v_k$) if:

$$\gamma_{i,k} - (r^i + r^k) < \gamma_{min} \tag{3.5}$$

where $r_i = \max(r^i_{EP}, r^i_{TP})$ and $r_k = \max(r^k_{EP}, r^k_{TP})$. This is equivalent to estimating the area in which electrodes might be placed using the optimization algorithm, and checking whether these areas overlap or have a minimum distance inferior to $\gamma_{min}$. Notice that the existence of an edge $e_l \in E$ represents a candidate conflict between the nodes $v_i, v_k \in V$. Later, it will be verified if a conflict actually exists between $v_i, v_k$. Theoretically, by applying this criterion, there is the possibility to obtain a fully connected graph in which all electrodes mutually influence their final positions. In that case, all possible combinations of all electrode trajectories computed need to be analyzed as in [45]. However, it represents an unlikely situation in which the electrodes are all close to each other. From a clinical point of view, there is no point in placing all the electrodes in a restricted brain zone, since the aim of the surgery is to explore brain activity find the epileptogenic focus. Therefore, we assume such a situation as highly improbable.

A more realistic scenario is to obtain a disconnected graph, in which it is possible to identify one or more subgraphs $G[S] \subseteq G = (V, E)$ comprising connected nodes. Then, we traverse each subgraph checking for conflicts by computing the Euclidean distance between the final position of the electrode pairs in the subgraphs. If a conflict is found, we take into account all possible combinations of electrode trajectories $I = A_1 * A_2 * \ldots * A_{|G[S]|}$ present in the subgraph to find the best conflict-free combination of electrode trajectories in the subgraph. For each combination $q \subseteq I$ it is possible to compute a new cost function $\Gamma(q)$, which evaluates the best combination of electrode trajectories contained in the subgraph $G[S]$ which avoids conflicts:

$$\Gamma(q) = \frac{(1)}{|G[S]|} * \sum_{h=1}^{|G[S]|} S_h(j) \tag{3.6}$$

where $j = 1, 2, \ldots, A$ and $A$ depends on the number of possible states of each node of the subgraphs. Finally, the combination of trajectories which maximize the cost function 3.6 is selected:

$$\Gamma = \max_q \Gamma(q) \tag{3.7}$$

In this way, we are able to split the conflict resolution into smaller subproblems that can be independently analyzed, reducing the time and computational resources required to determine valid solutions, as compared to complete brute-force exploration.

In addition, it should be highlighted that the use of the graph does not imply any degradation of results with respect to a standard brute-force approach. To demonstrate this point, consider a case study of $n = 3$ electrodes $e_1, e_2, e_3$ where $\gamma_{1,2} - (r_1 + r_2) < \gamma_{min}$ , therefore causing a possible conflict between $e_1, e_2$. Once the three electrodes have been optimized, we obtain a pool of possible solutions representing the cost function values of the possible states of each electrode $S_1(j), S_2(j), S_3(j)$. For simplicity, we assume that $j = 1, \ldots, 5$ and then each electrode can have only $J_{max} = 5$ possible states that have been computed during the optimization and are ranked in descending order. Table 3.2 represents the possible states of each electrode of the case study.

| $e_1$ | $e_2$ | $e_3$ |
|---|---|---|
| $S_1(1)$* | $S_2(1)$* | $\boldsymbol{S_3(1)}$ |
| $S_1(2)$* | $S_2(2)$* | $S_3(2)$ |
| $S_1(3)$* | $\boldsymbol{S_2(3)}$ | $S_3(3)$ |
| $\boldsymbol{S_1(4)}$ | $S_2(4)$ | $S_3(4)$ |
| $S_1(5)$ | $S_2(5)$ | $S_3(5)$ |

**Table 3.2:** *Solution Space of case study. We report the possible state of each electrode after optimization. (*) represents the trajectories which creates a conflict. In bold, the best trajectory combination which does not cause any conflict.*

Using the standard brute force approach, the conflict resolution method analyzes all possible trajectory combinations between all electrodes, for a total of $J_{max}^n = 5^3$ possible combinations. After traversing all the solution space, the combination of conflict-free trajectories which maximize the group cost function $\Gamma$ will be selected, $\Gamma = \frac{S_1(4)+S_2(3)+S_3(1)}{3}$. By using our approach (graph), only $e_1, e_2$ solution space is traversed, given that $e_3$ cannot cause any conflict. The use of the graph decreases the number of trajectory combinations to $5^2$ by considering only the first two columns of the solution space (Table 3.2), selecting $\Gamma = \frac{S_1(4)+S_2(3)}{2}$ as the best ranked conflict-free solution. Regarding $e_3$, our approach will select the first state in the table, $S_3(1)$, which is already the best configuration for this electrode. Therefore, our algorithm returns $\Gamma = \frac{S_1(4)+S_2(3)+S_3(1)}{3}$ as the global solution of the problem, which matches with the one provided by the standard brute-force approach.

In the case no conflict can be avoided, the electrodes are placed in their best positions respectively and a warning is displayed. The neurosurgeons are able to manually modify these trajectories.

### 3.2.3 Advanced Trajectories Verification Module

In order to allow surgeons to evaluate the feasibility of the proposed trajectories, we propose an advanced module for their visualization and analysis. The user can select an electrode and apply a probe eye view, which allows the visualization on the plane perpendicular to the electrode trajectory on the original angiography dataset. In addition, a volume portion can be selected to generate Maximum Intensity Projection (MIP) images on that plane and enhance vessel visualization, especially in images with contrast medium (Figure 3.3).

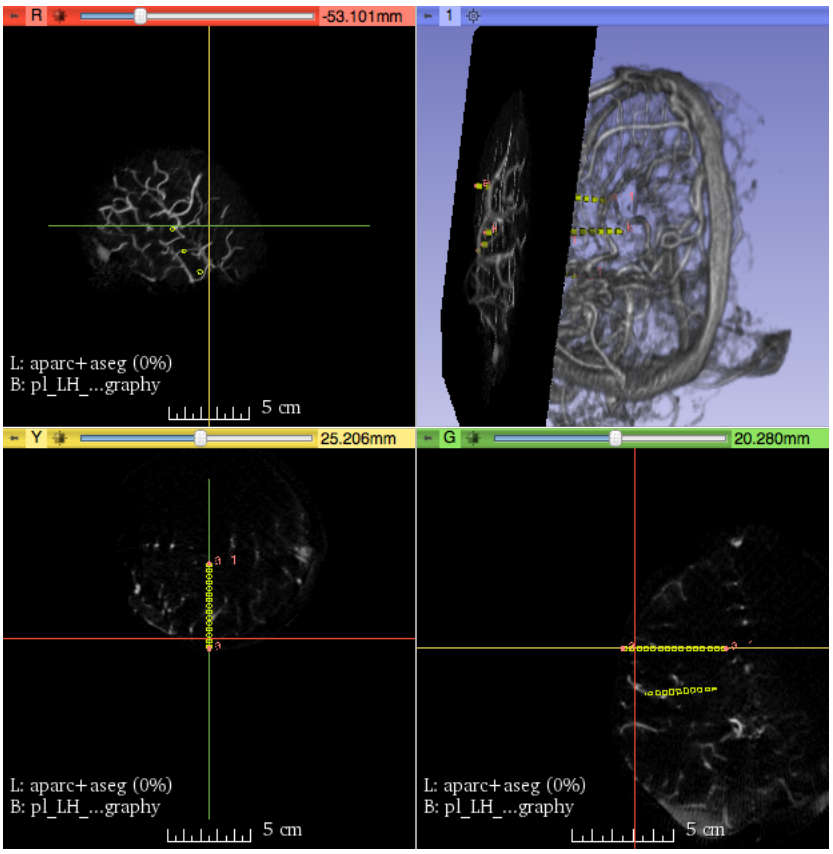


**Figure 3.3:** *Advanced electrode trajectory check with MIP image projection on Probe Eye View. The red slice view shows the plane perpendicular to the electrode on which the MIP has been applied. The other two views (yellow and green) show the two planes orthogonal to the electrode trajectory. These two, jointly with the slice intersection, help the neurosurgeon to understand the view position in relation to the electrode total length. Electrode models are enlarged to allow an easier visualization (yellow contacts).*

Finally, in order to reduce background noise, an automatic vessel segmentation based on Gaussian Mixture Model (GMM) and Markov Random Field (MRF) can be applied directly to the MIP image, in order to identify only vessels around the electrode [178].

### 3.2.4 Retrospective Evaluation

In order to determine if our approach would adapt to real clinical practice we conducted a preliminary evaluation on 20 patients in the form of a retrospective analysis. We collected trajectories that had been planned manually by neurosurgeons and used them as seed points for our optimization. Since these trajectories represented the neurosurgeon's solution and no complications have been reported, we also extracted quantitative information to better understand the viability of our constraints. These data have been stored in a connected database and will be used for future developments. Hence, we collected a total number of $253$ trajectories, and compared the manual planning to the optimized MT strategy and the single trajectory strategy. Even though the planner allows electrode-specific constraints to be selected, in this particular preliminary study we used the same values for all electrodes as a global optimization strategy, as would have been performed at that time.

#### Experimental Protocol

Retrospective validation was performed on patients who underwent the SEEG procedure at "Cladio Munari" Centre for Epilepsy and Parkinson Surgery A.O. Ospedale Niguarda CaGranda, Milan, Italy. No complications have been reported. For each patient, MR images were acquired using the hospital system $1.5T$ (Intera Achieva, Philips Medical System, The Netherlands, T1 3D FFE sagittal images, $0.90mm \times 1.07mm \times 0.90mm$ voxel dimensions, without any inter-slice gap, then reconstructed and reformatted on the axial plane with $560 \times 560 \times 220$ matrix, $0.45mm \times 0.45mm \times 0.9mm$ voxel dimensions). FS pipeline was run to obtain the cortical reconstructed surface and the other structures explained previously. Angiographic images were acquired (O-arm, Medtronic Inc., US, $512 \times 512 \times 192$, $0.4mm \times 0.4mm \times 0.8mm$ voxel) using contrast medium. Bone mask was removed following the procedure presented in [31]. Electrode trajectories were manually planned by neurosurgeons using the Voxim (IVS Technology GmbH, Chemnitz, Germany) software application. All previous steps were done specifically for the use of the automated planning assistant developed but already part of Niguarda Hospital Workflow for SEEG proce-

dures. An experienced neurosurgeon performed the segmentation steps for each patient following the image processing module (section 3.2.1), and saved the results. Subsequently, vessel tree segmentation, possible entry regions and the skull surface have been generated and stored for the optimization step. The threshold values chosen for optimization were defined equally for all electrodes (table 3.1). We compared the performances of three methods: Manual Planning (MP), Optimized Single Trajectory Planning (OSTP), and Optimized Multi-Trajectory Planning (OMTP). The difference between OSTP and OMTP was the management of inter-electrode conflicts: in OSTP, the electrodes that cause a conflict were not optimized and a warning message was displayed to the user. In order to quantitatively compare the methods, we proceeded as follows. For each trajectory and method we quantified the minimum distance from vessels in the first (1) and second tract (2) along with the insertion angle in relation to the skull normal (3). We defined a trajectory to be correctly planned if all the hard constraints (see 3.2.2) had been satisfied. Then, we quantified the trajectory success rate defined as the number of correct trajectories out of the total number.

Furthermore, to evaluate the effects of the optimization approaches, we quantitatively evaluated the indexes defined above for the final electrode positions proposed by OMTP and OSTP in relation to MP trajectories. We performed a Kolmogorov-Smirnov test to check the normality of the computed indexes and, consequently, a two-sample t-test was performed to check for statistical differences. Statistical analysis was performed in Matlab.

Finally, we reported the computation time and the number of trajectories for each electrode that had been taken into account during the optimization procedures (section 3.3.3). To quantify the effect, in terms of computational efficiency, we estimated the number of trajecory combinations analyzed by the selective brute force approach compared to a classical brute force algorithm, as proposed in [45]. Data has been processed on a laptop Acer v5-573G, Intel(R) Cose(TM) i7-4500U CPU @ 1.80GHz with 8GB of RAM DDR3 running Windows 10.

## 3.3 Results

### 3.3.1 Trajectory Success Rate

Our algorithm discarded the majority of the manually planned trajectories by analyzing them without performing any optimization (table 3.3). Al-

most $50\%$ of them reported a minimum $\delta_v^{EP}$ inferior to the threshold applied. Additional experiments showed that by relaxing the first tract threshold $\delta_v^{EP} = 3.8$ mm, the MP discarded trajectories fell to a total of $41\%$, half of them because of a too large insertion angle. As expected, OSTP and OMTP methods improved these trajectories by reaching a success rate of $92\%$ and $98\%$, respectively. The $5\%$ difference represents the OMTP capacity to resolve inter-electrode conflicts.

| | MP | OSTP | OMTP |
|---|---|---|---|
| $\theta$<br>$\delta_v^{EP}$ | 47 (18%)<br>92* (36%) | 5(2%) | 5(2%) |
| $\delta_v^{TP}$ | 34 (13%) | 0 | 0 |
| Conflicts | 0 | 9 (3%) | 0 |
| Total Discarded | 173 (68%) | 13 (8%) | 5 (2%) |

**Table 3.3:** *Discarded trajectories using our algorithm, based on hard constraints used and image processing steps performed, for each method and a total of 253 trajectories. *Trajectories rejected based on $\delta_v^{EP}$ criteria reduced to $8\%$ by relaxing the threshold to $3.8$ mm.*

### 3.3.2 Quantitative Evaluation

Figure 3.4 reports on the final values of the three indexes considered after running the two optimization procedures, OSTP and OMTP. Figure 3.4a shows a general improvement, where the majority of points lie under the bisector representing a decrease in the maximum insertion angle. On the contrary, in figures 3.4b and 3.4c we want to maximize the distance from vessels, subsequently the improvement is represented by points above the bisector. This was not always true, especially for the minimum distance in the second tract $\delta$ (Figure 3.4b). However, it should be noted that all optimized trajectories reported values which satisfied the threshold limits. This was not always accomplished by MP trajectories, as in all three images it is possible to find initial values which exceeded the maximum/minimum thresholds. Table 3.4 reports mean and standard deviation values computed for the three methods and confirms the general improvement provided by the optimization of the MP trajectories. Accordingly, statistical differences have been found between MP and OSTP and between MP and OMTP. No statistical differences have been found between the two optimization methods, however we computed median and inter-quartile range values of the differences found between the alternative trajectories proposed by OMTP in relation to OSTP. For the three indexes, we found a minimum distance from

vessels in the first tract of $0.46(1.06)$ mm, in the second tract of $0.3(0.4)$ and an insertion angle of $1.03(5.86)$ deg.

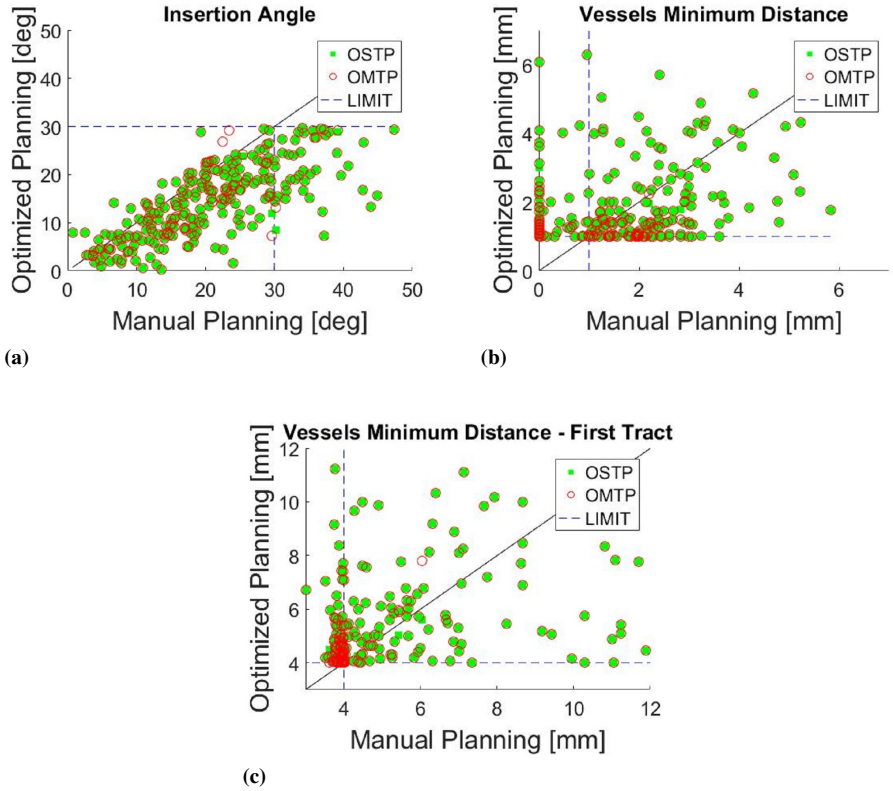


**Figure 3.4:** *Quantitative comparison of the three indexes computed in relation to the MP trajectories. 3.4a shows the values obtained from the insertion angle after the optimization procedures. The same is presented in 3.4b and 3.4c for minimum vessel distance detected and minimum vessel distance in first tract respectively. On each graph, the x-axis reports the MP values, which represent the starting points, while y-axis reports the final values reached. The blue dashed lines represents the optimization hard constraints used in our algorithm.*

### 3.3.3 Computational Efficiency

Regarding computational complexity, we report a mean processing time of $160.5 \pm 102.25$ seconds for a single electrode optimization. For these experiments, all the electrodes were optimized serially, making the total computational time strictly dependent on the electrodes number. For each electrode, entry and target point regions generated a mean number of $25 * 10^3$ possible trajectories. During the optimization, the mean number of

| | MP | OSTP | OMTP |
|---|---|---|---|
| $\theta$ [deg] | $20.65 \pm 9.81$ | $14.44 \pm 7.54$ | $14.53 \pm 7.64$ |
| $\delta_v^{EP}$ [mm] | $4.78 \pm 3.55$ | $5.52 \pm 1.77$ | $5.54 \pm 1.78$ |
| $\delta_v^{TP}$ [mm] | $1.66 \pm 1.30$ | $1.96 \pm 1.35$ | $1.95 \pm 1.35$ |

**Table 3.4:** *Mean and standard deviation values are reported for each method for the indexes computed.*

acceptable trajectories per electrode dropped to $2.7 * 10^3$. With regard to the conflicts graph, the largest subgraph built comprised $4$ nodes, taking into account all patients. Then, in the case of conflicts, the total number of maximum combinations was reduced to an order of $10^{12}$, while with the previous method we would have had a number of around $10^{41}$ (assuming a mean number of 12 electrodes in our patients). However, in the majority of the cases, the final electrode positions did not generate conflicts and the mean time used to traverse the conflict graph was in $0.015 \pm 0.005$ seconds.

## 3.4 Discussion

We have presented an improved automated multi-trajectory planner for SEEG, based on open source software widely used by the scientific community (3D Slicer, Freesurfer, FSL). Compared to our previous planner versions [45, 46], the transformation into a multi-modular architecture improved modularity, flexibility and usability. An additional module implementing MIP images and automatic vessel segmentation was presented, which simplifies the validation of proposed trajectories. Regarding optimization strategy, a dense search around EP and TP has been complemented with the use of an atlas, which restricts the search space to the anatomical regions identified by the initial EP and TP seeds. Compared to other groups [188, 214], the user initializes the electrodes by roughly selecting EP and TP. This is an easy and fast procedure but is closer to the clinical solution and limits exploration only on the surrounding area.

To guide the optimization procedure we defined global optimization parameters and hard constraints values according to surgeon experience and surgical constraints that can be found in literature [45, 188, 214]. However, the analysis of MP trajectories, according to the defined criterion, rejected $68\%$ of them, even though those trajectories were used to perform safe implants without any complications reported.

Furthermore, by lowering the threshold $\delta_v^{EP}$, we considerably reduced the number of MP discarded trajectories, suggesting the neurosurgeon's intention to follow the criterion strictly applied in the planner. Moreover, it

must be considered that such trajectories have been planned with only visual assistance (3D images), without any quantitative information. These results suggest that the thresholds used in the optimization algorithm may need to be revised as it actually happens in real practice, when surgeons decide to be less restrictive in some cases. In addition, we cannot discard that new constraints have to be added to our algorithm, in order to take into account additional requirements that may influence the clinical choice. Nonetheless, OSTP and OMTP were able to optimize these trajectories, reaching a success rate of $93\%$ and $98\%$ respectively. The difference between the two methods underlies the importance of providing an efficient strategy able to manage inter-electrode conflicts. On the contrary, no possible solutions were found in 5 cases. When analyzing those patients' datasets, we found that the initial insertion angle of these MP trajectories was too large in relation to the maximum angle allowed, leading to the impossibility of finding a similar solution even for initialization methods which do not limit the search region. Therefore, as a result of the possibility to define electrode specific constraints, we increased the maximum angle allowed ($40$ deg) specifically for those electrodes. With this new constraint, the optimization method was able to find a feasible solution.

The quantitative analysis showed that both OMTP and OSTP were able to improve the MP trajectories used as initial seeds. When analyzing the graph presented in Figure 3.4a, the insertion angle has clearly been improved by both optimization methods, even when the initial values where further from the threshold defined. Figure 3.4b reports a number of trajectories with initial $0$ mm distance from vessels in the second tract. This effect is probably due to the threshold chosen during the vessel segmentation part. A too conservative threshold would include some noise which has been interpreted as small vessels by our procedure. However, the optimization strategy was able to find alternative paths and to provide final trajectories which complied with our hard constraints. Focusing on Figure 3.4c, the high concentration of $\delta_v^{EP}$ initial values below, but in proximity of the defined threshold, confirms the neurosurgeon's intention to provide a minimum distance value around $4$ mm in the first tract of the trajectories. This requirement has been satisfied by both optimization approaches. Lastly, since only $9$ real inter-electrode conflicts have been detected, no statistical difference has been found between OMTP and OSTP. As expected, the OMTP strategy leads to alternative trajectories which preferentially increase the insertion angle rather than the minimum vessel distances, according to the weights expressed in the cost function (eq. 3.4). All the trajectories proposed satisfied the hard constraints applied in the optimiza-

tion.

The multi-trajectory strategy presented and implemented in OMTP was able to resolve these inter-electrode conflicts and propose alternative solutions which satisfy all the constraints. The strategy implemented overcame the limitations of the previous multi-trajectory planner [45] by reducing the computational cost with a selective brute force approach. The graph construction allowed these electrodes to be split into independent subgroups (as reported in 3.3.3, the largest subgroup reported among all patients' trajectories comprised 4 electrodes), decreasing the computational effort by reducing the number of combinations to explore. This method allowed us to run our optimization algorithm in a reasonable time on the 3D Slicer platform that, to our understanding, does not offer the possibility of multi-core parallelization or GPU acceleration.

## 3.5 Conclusion

We presented an automated multi-trajectory planner able to assist neurosurgeons during the different planning phases. We collected and analyzed in terms of quantitative indexes, $253$ manually planned trajectories of patients who successfully underwent SEEG surgery. The optimization strategy allowed these indexes to be improved in $98\%$ the cases by managing inter-electrode conflicts through an efficient selective brute force approach. The evaluated indexes showed an improvement in terms of safety compared to the MP trajectories, nonetheless, one of the major limitations of this work is the absence of a qualitative validation of the proposed new trajectories. In this regard, our architecture sets the basis for future developments and improvements to the different stages of the procedures and allows for future extended clinical trials and validation. In addition, future studies will focus on the analysis of MP trajectories to identify additional parameters that have not been included in our model yet and to select constraint values based on quantitative information.

Finally, the use of the 3D Slicer platform as a development environment improves the planner flexibility and the possibility to integrate and modify the workflow according to custom tools developed at other centers. Future efforts will focus on the integration of SEEG tools such as the "seeg electroDE rEconstruction TOol" (DEETO) [7], and SEEG-Assistant [145] which allow the automatic segmentation of implanted electrodes from post-operative CT and offer other dedicated tools useful for viewing SEEG signals.

CHAPTER 4

# Experience-based SEEG planning: from retrospective data to automated electrode trajectories suggestions

This chapter introduces a novel methodology to exploit the knowledge from the analysis of retrospective data (**C2**). Retrospective manually planned trajectories represent an important source of information that can be used to improve the optimization strategy. Additionally, their analysis may reflect surgeons' preferences that go beyond the anatomical requirements proposed in the previous chapter. Hence, we implemented a general methodology for the classification of trajectories, based on the anatomical zones crossed. The spatial relationship between them is also considered, and the resulting trajectory atlas, obtained by the analysis of 1100 retrospective trajectories, provides anatomical and spatial priors for the exploration of specific brain regions, based on the surgical habits of the clinical center from which the data comes from. A preliminary validation on 10 patients shows that the trajectory atlas constructed can be used to reproduce the exploratory paths commonly used by the surgeons, representing a new initialization method for the automated planning module presented in the previous Chapter. The quantitative result showed promising results with

respect to the safety indexes computed.

Based on this work, a journal paper has been published as [176]: Scorza, D., Amoroso, G., Cortès, C., Artetxe, A., Bertelsen, À., Rizzi, M., ... Kabongo, L. "Experience-based SEEG planning: from retrospective data to automated electrode trajectories suggestions". In *Healthcare technology letters*, 5(5), 167-171, 2018.

## 4.1 Introduction

Automated planning in SEEG has been focusing on the optimization of electrode trajectories based on requirements such as the maximization of the distance from vessels, the minimization of entry angle, increase of GM sampling and conflict avoidance. Optimization approaches usually involve one electrode at a time, except for conflict resolution strategies where the whole set of trajectories is considered. In [214] the authors proposed a method able to optimize the trajectories and maximize the gray matter volume recorded. However their study was limited to three electrodes at a time. Only Sparks et al. [186] propose a method which computes the minimum number of electrodes able to cross all the required regions selected by the surgeon. Nevertheless, this method has the drawback of being very dependent on the atlas used and could lead to solutions that may not be aligned with real clinical decisions. Additionally, as shown in a recent study [199], the planning strategy of different centers may differ due to the hardware used for electrode placement, the imaging protocol and the center experience. Therefore, even if the safety and efficacy requirements are similar, there are no standardized rules that guide all clinical centers and a more tailored approach may provide a better answer to specific center requirements. In Scorza et al. [177], electrodes are manually initialized by surgeons by placing rough entry and target points (respectively EP and TP), while the atlas is only used to maintain the initial anatomical zones during optimization. In this way, the initialization guarantees to respect the clinical practice but requires a manual intervention that may be time consuming.

In this work, we propose a new methodology able to analyze retrospective data from successful SEEG implants and extract the most common trajectories used for the exploration of specific brain zones in a given medical center. The main assumption of this work is that, despite SEEG is a patient specific surgery based on individual anatomy and brain activity, it is possible to identify planning strategies and trajectories that are commonly used to explore multiple brain areas and to provide an adapted model for

the center practice. In this way, our system can suggest an initial plan for a new patient, which the neurosurgeon can further adjust manually or be adapted to the specific anatomy thanks to an optimization framework as the ones previously described. As far as we know, this is the first attempt to model SEEG practice combining surgeon knowledge with specific center retrospective data. The final application will provide trajectory suggestions aligned with the clinical experience, and may be a valid assistant especially for junior surgeons. Preliminary experiments show that, after optimization, the initialized trajectories reach similar values in terms of safety that those that have been manually planned by neurosurgeons. Finally, we were able to cluster the trajectories into various planning strategies that have been positively recognized by a surgeon as commonly adopted in the center.

## 4.2 Methodology

SEEG is a very tailored surgery, influenced by the specific anatomy and the particular case of each patient. Most of the time, the procedure does not require to reach a precise target. Instead, a set of regions needs to be sufficiently sampled to identify the epileptogenic network. Nevertheless, it is possible to identify exploratory patterns or sets of trajectories aimed to explore the same brain regions in different patients. With the aim of identifying and modeling similar trajectories, we need to extrapolate the clinical targets among all the zones an electrode may cross. Actually, the electrode end-point does not necessarily match with the clinical target, it can be any of the zones that it crosses, and clinical knowledge is required here to clearly define the target. Hence, we can associate a generic trajectory descriptor $d = [l_e; l_t]$, where $l_e$ and $l_t$ represent the labels of clinically relevant target regions crossed, accordingly to an anatomical atlas. In this work, retrospective data are collected and analyzed with the aim of modeling the clinical practice of a center and use this knowledge for the initialization of new plans. We generically define a surgical plan $M$ as a set of trajectories $M = \{t_0, t_1, \dots t_Q\}$, with $Q = |M|$, where each trajectory $t \in M$ is defined at least by an entry and a target point, respectively $t = (\mathbf{EP}; \mathbf{TP})$, representing their Euclidean coordinates in the patient image space.

### 4.2.1 Problem statement

Given the MRI image of a new patient and a planning strategy selected by the surgeon, the goal of the system is to provide a set of trajectories based on surgeons' past experience adapted to current patient specific anatomy.

The planning strategy defines a reduced set of trajectories aimed for the exploration of specific brain regions. Those trajectories will be then modified or optimized to adapt them to the specific patient anatomy.

### 4.2.2 Solution strategy

The following steps were conducted for the implementation of the proposed system:

1. Trajectory descriptor and exploratory patterns: analysis of retrospective cases in subject space, identification of similar trajectories among patients and their normalization on an average brain space.
2. Mean trajectories definition ($\overline{T}$): spatial clustering in the average brain space of similar trajectories to produce mean trajectories $\overline{T}$ for the exploration of specific brain regions.
3. Planning strategies definition ($S$): analysis of the spatial relationship between mean trajectories and their clustering, based on the macro-anatomical regions that they explore.
4. Plan adaptation: mapping of the selected planning strategy from a common average brain space to the subject space.

Finally, the trajectories obtained may be optimized similarly as described in [177].

### 4.2.3 Trajectory descriptor and exploratory patterns

We collected the retrospective data of $N$ patients who successfully underwent SEEG procedure. The inputs for our analysis are an MRI-T1W image and the original trajectories planned by the surgeon in subject space. All data have been processed by the Freesurfer (FS) pipeline [66], which co-registers the patient with the MNI-305 space and labels the different brain zones using a probabilistic atlas segmentation [67]. For each patient, we collect the manual plan $MP_p = \{t_0, t_1, t_Q\}$ with $p = 1, \ldots, N$ and $q = |MP_p|$ planned by a surgeon, where $t_i = ((\mathbf{EP}; \mathbf{TP})) \in MP_p$, with $i = 0, \ldots Q$, represents the trajectories defined by the entry and target point coordinates in the subject space.

Trajectories were regularly sampled with a method similar to the one described in [145]. For each $t_{i,p}$, we estimate the position of the electrode contacts based on the nominal electrode geometry and the trajectory length. At each sample point, we simulate a spherical region with 3 mm radius,

simulating the recording volume of an electrode lead. We retrieve all the voxel values inscribed in the spherical volume, corresponding to the labels of specific anatomical regions, accordingly with the anatomical atlas used (figure 4.1).

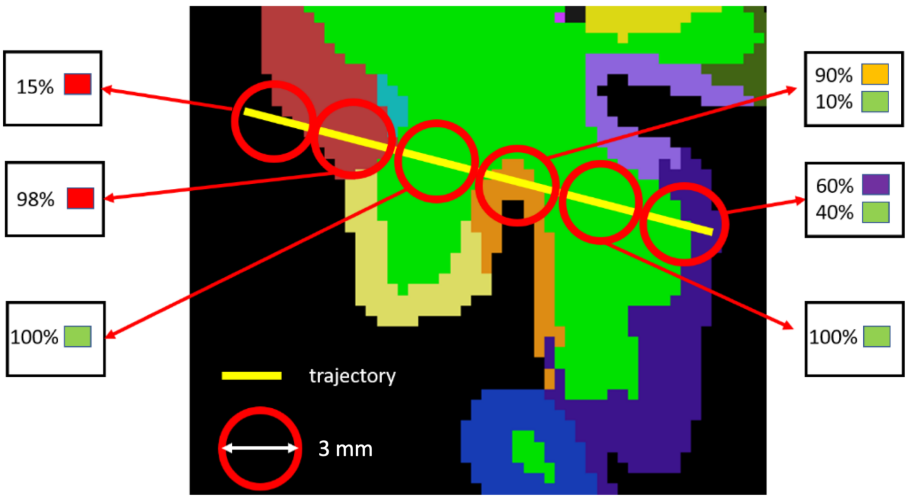


**Figure 4.1:** *2-D representation of the atlas probing procedure: the red circles represent the estimated recording zone of each electrode. We considered the voxels inscripted in each recording volume (in 3D they represent spherical volumes), and assigned to the descriptor the label of the prevalent recorded zone.*

Each trajectory is represented by an initial descriptor $l_{i,p} = \{l_0, l_1, \dots l_I\}$, composed by the labels of all the different zones crossed, from EP to TP. By considering all the labels, it is hard to identify similar trajectories. In two different patients, trajectories aimed to explore the same regions can end up with slightly different descriptors because of the different anatomy, a different planning approach, the result of the anatomical segmentation or a combination of them. Therefore, we divided the atlas labels into two sets $\epsilon$ and $\tau$, containing the labels of anatomical brain regions that are considered as meaningful entry and target zone to be crossed by the first or the second tract of the trajectory respectively. The $\epsilon$ set contains the labels of lateral cortical regions, while $\tau$ the labels of mesial cortical regions and internal structures (e.g. *Superior-temporal, Rostral-Cingulate and Hippocampus* respectively, according to the Desikan-Kiliany atlas). The definition of the two sets $\epsilon$ and $\tau$ resulted from the analysis of the most explored zones in our samples, their anatomical positions and the surgeons suggestions.
Based on this division, we defined a new reduced descriptor $d_{i,p} = \{l_e; l_t\}$,

with $l_e \in \epsilon$ and $l_t \in \tau$, composed only by two relevant regions which are considered the clinical targets of the $t_{i,p}$. A graphical example of the procedure is reported in figure 4.2.

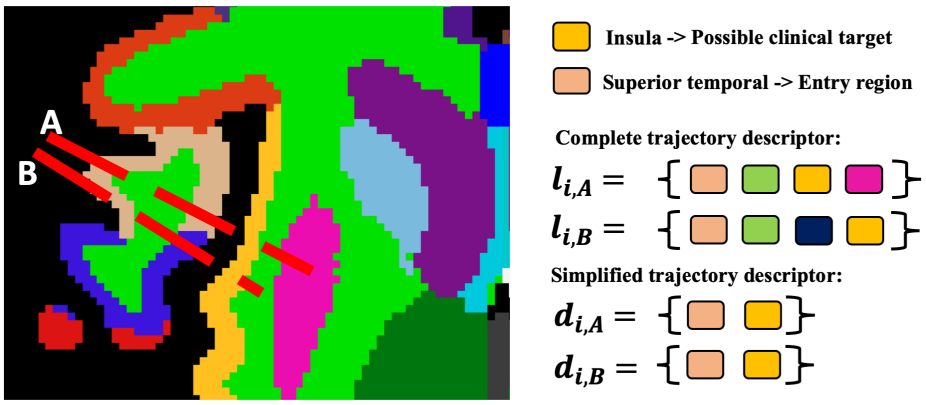


**Figure 4.2:** *Trajectory representation through a reduced anatomical descriptor: two similar trajectories from patients A and B are planned to explore the insular region (yellow), entering from the superior temporal gyrus (light pink). By using the reduced descriptor, we consider only the clinically relevant entry and target regions, which classify them in the same group.*

Finally, sets of similar trajectories $g(l_e; l_t) = \{t_{i,p}\}$ if $d_{i,p} = \{l_e; l_t\}$ were built from all patient data and represent exploratory patterns to explore two regions $[l_e; l_t]$ extracted by the set of labels $\epsilon$ and $\tau$ respectively.

### 4.2.4 Mean trajectory definition

Once similar trajectories have been grouped in subject space, their coordinates were transformed to the MNI-305 space by using the registration matrix provided by the FS pipeline. Since we based our analysis on an anatomical atlas, we must assume that, due to their size, some regions are explored with several electrodes for higher coverage. Therefore, for a given plan $MP_p$ we may find a variable number of trajectories $t_{i,p}$ with the same descriptor $g(l_e; l_t)$. To keep the spatial relationship between those trajectories, we used a k-means algorithm to automatically cluster entry and target coordinates into a number $K$ of groups, and generate a set of mean trajectories $\bar{t}_k$, with $k = 0, \dots K$, where each $\bar{t}_k = (\overline{\mathbf{EP}}_k; \overline{\mathbf{TP}}_k)$ are the mean euclidean coordinates of all $t_{i,p} \in g(l_e; l_t)_k$. The number of groups $K$ is defined as the maximum number of trajectories aimed to explore the same

regions $l_e$ and $l_t$ in a single plan, among all plans $MP_p$, with $p = 1, \ldots, N$. To avoid an erroneous definition of groups due to particular cases, a $\bar{t}_k$ is considered significant only if contains at least $5\%$ of trajectories described by $g(l_e; l_t)$. Otherwise the maximum number of clusters $K$ is decreased by 1 and the k-means algorithm applied iteratively. Figure 4.3 shows an example of the procedure for trajectories commonly used to explore the insular region.
The final set of mean trajectories $\overline{T} = \{\bar{t}_0, \bar{t}_1, \ldots \bar{t}_T\}$, with $T = |\overline{T}|$, is composed by trajectories defined as $\bar{t} = \{\overline{\mathbf{EP}}, \overline{\mathbf{TP}}, (l_e, l_t)\}$, with $l_e \in \epsilon$ and $l_t \in \tau$.

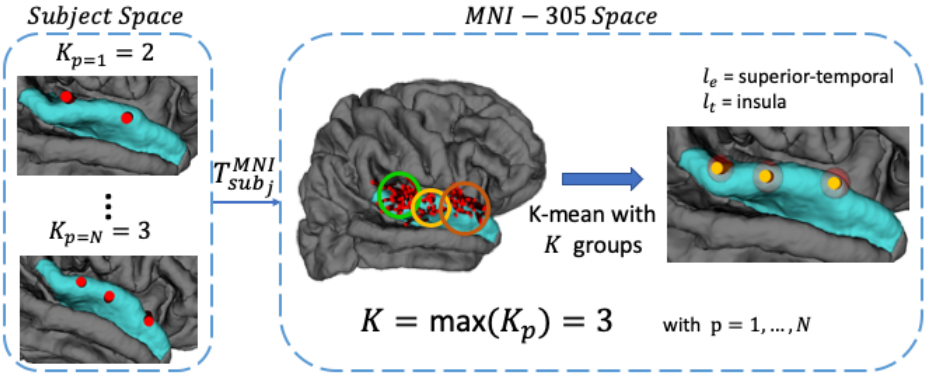


**Figure 4.3:** *Mean trajectories for a single pattern $g(l_e; l_t)$ obtained with K-means algorithm: insular exploration (region b) are usually performed from the superior-temporal (region a), with a maximum of 3 electrodes in the same plan, $K = 3$.*

### 4.2.5 Planning strategies

The definition of a mean trajectory set $\overline{T}$ allows to analyze the manual plans $MP_p$ by means of studying the combination of trajectories used for macro-regions explorations. For each mean trajectory $\bar{t} \in \overline{T}$, we can retrieve the original trajectory $t_i, p \in MP_p$ which contributed to its definition. On that basis, we defined a binary descriptor $f_p$ of fixed length $|(\overline{T})|$ for each plan $MP_p$, representing the presence or absence of a trajectory that contributed to the definition of the corresponding $\bar{t} \in \overline{T}$.
Considering that each $MP_p$ may have a variable number of trajectories, we considered the plan as hierarchical related in the sense that an MP with a lower number of trajectories may be completely included in another, which provide a more extended exploration. Therefore, we used a hierarchical

clustering method which operates on the basis of an empirical coefficient of similarity (the Jaccard distance) computed over the binary descriptors $f_p$ (figure 4.4).

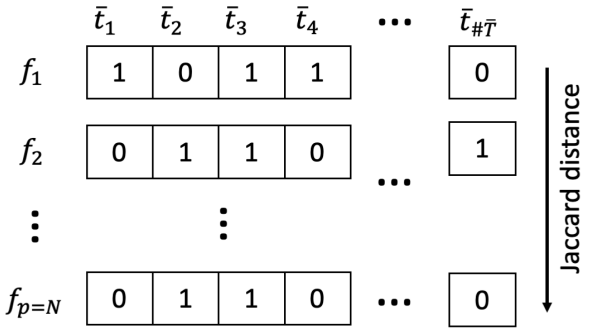


**Figure 4.4:** *Binary vector representation $f_p$ for each plan $MP_p$, representing the presence or absence of a mean trajectory. The Jaccard distance is computed to measure the similarity between binary vectors.*

The generated dendrogram (figure 4.9) organized the plans based on their similarity, making possible to group them into a number $S$ of clusters by the selection of a cut-threshold. Each group of plans $g_j$, with $j = 1, \dots S$, corresponded to similar manual plans which completely or partially shared the same trajectories used to generated specific $\bar{t} \in \overline{T}$. Finally, we could define $S$ planning strategies $s_j$, representing different combinations of $\bar{t} \in \overline{T}$ used to explore multiple brain regions. A mean trajectory $\bar{t}$ was included in $s_j$ only if it was represented in at least two plans $MP_p \in g_c$.

### 4.2.6 Clinical scenario and validation

To construct the trajectory atlas we used $75$ anonymized patient data sets provided by Niguarda Hospital (Milan, Italy), which included a total of $1100$ manually planned trajectories annotations. For each patient, MR images were acquired using the hospital system $1.5T$ (Intera Achieva, Philips Medical System, The Netherlands, T1 3D FFE sagittal images, $0.90mm \times 1.07mm \times 0.90mm$ voxel dimensions, without any inter-slice gap, then reconstructed and reformatted on the axial plane with $560 \times 560 \times 220$ matrix, $0.45mm \times 0.45mm \times 0.9mm$ voxel dimensions). The FS pipeline was used to obtain the cortical reconstructed surface and the probabilistic atlas seg-

mentations (the Desikan-Killiany atlas, with 75 labels per hemisphere, was used in this study). The pipeline also provides the affine registration matrix used to map patients and trajectories from the subject space to the average space (MNI-305).

As a preliminary validation of our method, we used a test set composed by $10$ patients that were not included in the generation of the trajectory atlas. Each patient was elaborated by the FS pipeline to obtain the anatomical parcellation and the registration with the MNI-305 average brain space. For each patient's plan $MP_p$ of the test set, we visually determined the corresponding mean trajectories $\bar{t} \in \overline{T}$ in the trajectory atlas, and reproduced the original $MP_p$ planned by the surgeon. The selected $\bar{t} \in \overline{T}$ where registered to the patient space by inverting the registration matrix previously obtained, and guaranteeing the crossing of the two relevant anatomical regions aimed to be crossed by $\bar{t}$. Therefore, for each patient $p$, we obtained an initialized plan $IP_p = \{t_0, t_1, \dots t_Q\}$, with $Q$ corresponding to the number of mapped trajectories.
We computed the euclidean distances $d_{EP}^{\alpha,\beta}$ and $d_{TP}^{\alpha,\beta}$ between EP and TP coordinates respectively, being $\alpha \in MP_p$ and $\beta \in IP_p$ corresponding manual and initialized trajectories. We considered that a trajectory was correctly mapped when $d_{EP}^{\alpha,\beta} \leq 2\sigma(\bar{t}_{EP})$ and $d_{TP}^{\alpha,\beta} \leq 2\sigma(\bar{t}_{TP})$, being $\bar{t} \in \overline{T}$ the corresponding trajectory in the atlas, and $\sigma$ the dispersion around the mean $\overline{EP}$ and $\overline{TP}$ obtained in the atlas construction. The value of $\sigma$ varies based on the trajectories used to define $\bar{t}$. The metric obtained represent a quality measure of the mapping procedure from the atlas space to the subject space. Figure provide a graphical representation of the process described.

The initialized trajectories may not comply with clinical criteria (e.g. safe distance to vessels), and therefore they need to be optimized to produce valid initial plans and adapt to the specific patient anatomy. For the optimization we used the method presented in [177] (Chapter 3), and verified the compliance in terms of distance from vessels and insertion angle. We evaluated initial quantitative values comparing manual planned (MP) trajectories, the corresponding initialized trajectories (IP), and their optimized solution OMP and OIP respectively. Finally, the groups obtained by the hierarchical clustering have been presented and qualitatively evaluated by a surgeon. Results are reported in the following section.

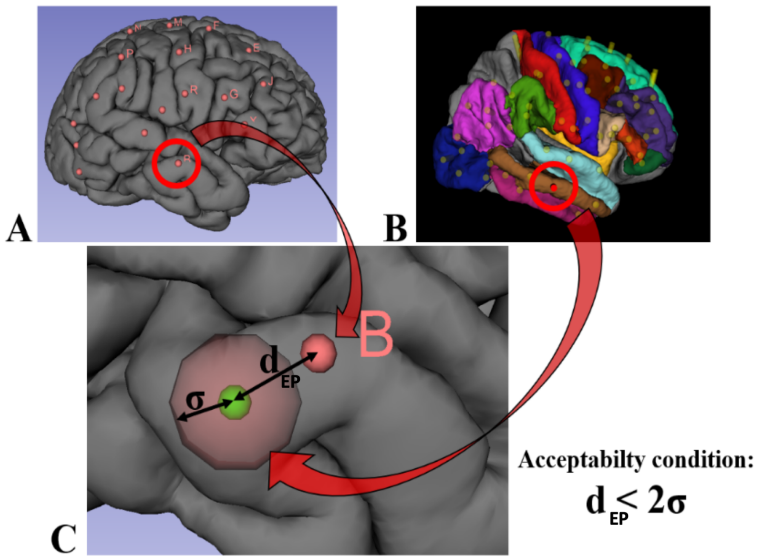


**Figure 4.5:** *Validation experiment for the initialization procedure: corresponding trajectories are selected between the patient p with the manual plan $MP_p$ (figure A) and the trajectory atlas (figure B). After the registration, the Euclidean distance between corresponding EPs is computed, and compared with the $\sigma$ associated to the $\bar{t} \in \overline{T}$ selected in the atlas. If the distance $d_{EP} < 2\sigma$, the trajectory is considered correctly mapped.*

## 4.3 Results

### 4.3.1 Exploratory patterns and mean trajectories

The analysis of the planned trajectories based on the Desikan-Killiany atlas reduced the possible target regions used to classify the trajectories. We did not take into account the white matter, while other structures such as ventricles, brain stem or cerebellum, where automatically excluded since they were classified as outliers. Following the clinician's advice, electrodes crossing the *insula* and ending in the *putamen* were included in the Insular pattern. In the same way, we consider as a single target point the *hippocampus* and the *para-hippocampus*, since it is not possible to explore the last without crossing the *hippocampus*, and on the other side by prolonging the trajectory we easily reach the *para-hippocampus*, increasing the recorded information. Finally, since our data had poor representation of occipital trajectories, we joined the occipital zones of *lingual cortex*, *cuneus*, *precuneus* and *pericalcarine*, assuming that the spatial distribution of those were more important than the specific description pattern in terms of entry and target zones.

By grouping the trajectories with the reduced descriptors presented in section 4.2.3, we found 30 exploratory patterns $pt_{a,b}$, for a total of 61 mean trajectories $\overline{T}$ that represent the mean coordinates of the most representative trajectories in our data. Figure 4.6 shows the mean trajectories in the average space.

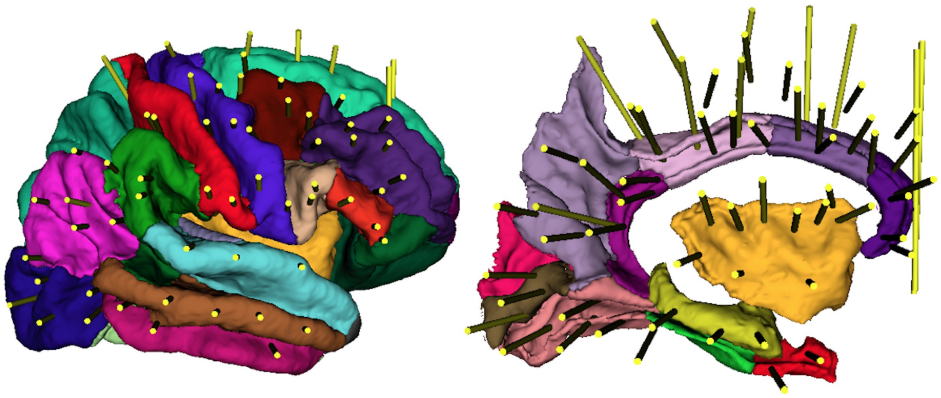

**Figure 4.6:** *A sagittal view of the mean trajectories computed in the average space: dimensions have been enlarged for visualization purposes.*

To test the viability of our method, we mapped the recognized trajecto-

ries on 10 patients that were not included in the initial database as explained in section 4.2.6, for a total of 95 initialized trajectories. By computing the initial euclidean distance with their corresponding manually planned trajectories at EP and TP in subject space, we found that the 90% of the initialized ones satisfy the criteria presented in 4.2.6. Finally, to test the viability of our initialization method, we compared the values of distance from vessels at the entry points, distance from vessels in the second tract and insertion angle before and after the optimization for both groups (MP and IP). The results are shown in image 4.7.

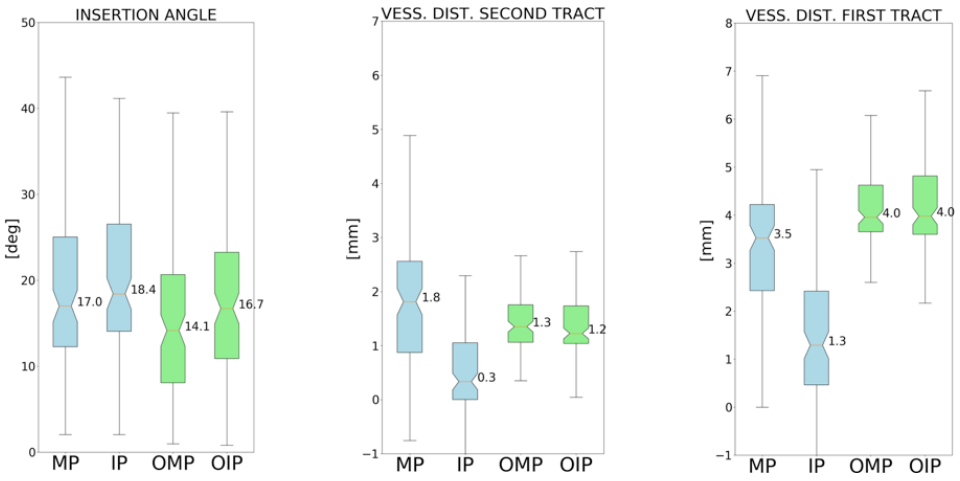


**Figure 4.7:** *Comparison of quantitative indexes between Manual Planning (MP), Initialized Planning (IP) trajectories and their optimized versions (OMP and OIP). The mean values of insertion angle and distance from vessels (first and second tract as reported in [177]) present no statistical difference between OIP and OMP*

Even if the mapped trajectories (IP) could not be considered safe in terms of indexes, the optimization performed provides a better solution (OIP group) with respect to the manually planned (MP) trajectories and a comparable solution with respect to the optimized ones (OMP), making this a valid method to initialize an optimization strategy provided by an automated planner. No statistical difference has been found between the indexes of the two groups OMP and OIP after optimization.

### 4.3.2 Planning clustering and strategies definition

The hierarchical clustering method applied and the cutting-threshold chosen led to 8 different clusters composed by similar plans. The cut-threshold has been chosen empirically, in order to balance the number of groups and

its components.

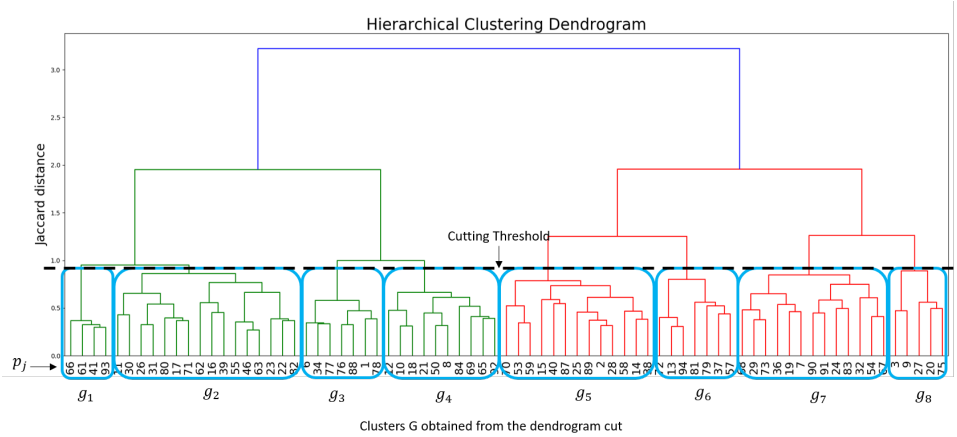


**Figure 4.8:** *Dendrogram obtained by the hierarchical clustering performed using the Jaccard distance. The cutting threshold defined 8 groups.*

Therefore, for each cluster obtained we selected those trajectories which appear in at least two plans and generate the planning strategies $cl_g$. The clusters were evaluated by a neurosurgeon, who recognized the main trends in the trajectories proposed. Therefore, we were able to name each cluster, as reported in figure 4.9.

Since SEEG is a patient-specific procedure, the clusters obtained do not completely match with actual patient plans. Additionally, some of the clusters (e.g. *Fronto-central*) resulted to be over-populated, since we preferred a reduced number of clusters with more trajectories rather than more groups to be combined. From a usability point of view, we considered that removing trajectories from a suggested strategy would be easier for the surgeon than to combine different cluster and then refine the plan. However, they seem to be a good representation of the planning strategies adopted in the center to explore specific macro-areas of the brain. Notice that the results have been obtained from a reduced set of data, with unbalanced distribution of plans. However, the system was able to group the plans into clinically meaningful clusters, that can be used as an initial starting point for a new patient planning. By the use of those clusters, the clinician should only remove or add few specific trajectories, while the rest would be directly mapped to the patient anatomy. Nonetheless, the use of a cluster is not mandatory, since there may be specific patients where the direct choice of single trajectories from the $\overline{T}$ set would provide a faster initialization.

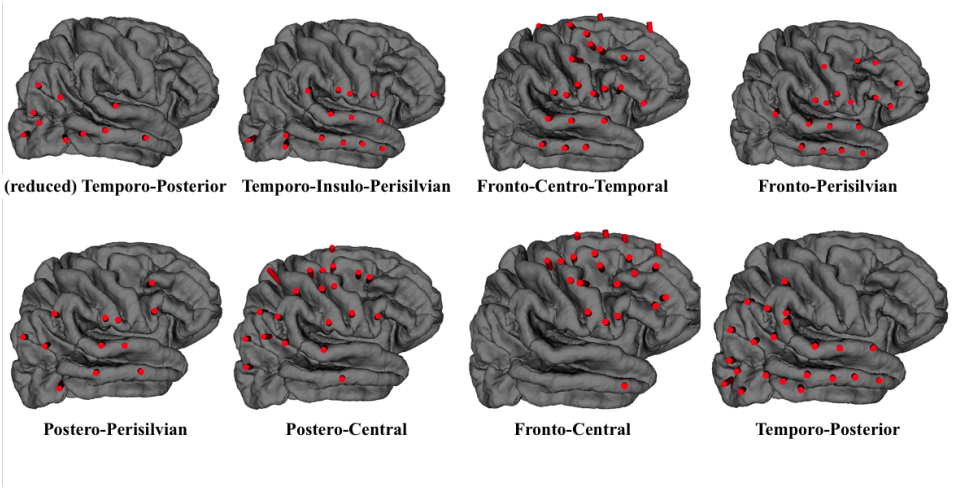


**Figure 4.9:** *Lateral view of the 8 clusters obtained, with the labels defined according to the surgeon suggestions*

## 4.4 Conclusion

In this work, we presented a novel methodology that merges clinical knowledge with the analysis of retrospective data of a given clinical center. The approach presented has been able to identify and model the most used trajectories, and define specific planning strategies by clustering similar plans. To the best of our knowledge, this is the first application that provides a trajectory initialization method adapted to a single center strategy based on its retrospective data analysis. The final application allows to easily visualize and select the most common trajectories, and cluster electrodes commonly used for a specific exploration. Preliminary results show that mean trajectories can be successfully mapped to patient plans that were not included to build our model, and provide a meaningful initialization for an automated planner as the work presented in [177]. The cluster obtained have been positively recognized by surgeons as exploratory strategies used in their center and we were able to map $90\%$ of the trajectories. Finally, those initialized trajectories have been correctly optimized by the automated planner, adapting to the subject anatomy and reaching quantitative results comparable or superior than manually planned trajectories, in terms of safety. An extended validation with surgeons is still needed to assess the viability of those trajectories. Current limitations of this approach are represented by the need of FS pipeline and of a large amount of data. Since the trajectories extracted represent the most common trajectories used in the center, a

new patient plan would be unlikely initialized completely by a chosen set and surgeons will still have to manually plan few trajectories depending on specific patient requirements (e.g. lesions). Nonetheless, the method presented provides a model of the clinical practice mostly based on the data provided by the center. The database constructed for this work will store new patient information and their planned trajectories, allowing our model to continuously adapt while new patients are added. To improve our model, especially regarding the planning strategies proposed, Diffusion Weighted Imaging (DWI) and tractography may be used to identify specific brain networks and generate more specific electrode clusters to map them. Similarly, in the future, we would like to include other functional imaging techniques as functional-MRI and/or EEG-signals. Future work will be focused on the generalization of this methodology and to provide a more complete validation.

CHAPTER 5

# Data-based automated planning system for StereoElectroEncephaloGraphy: a center-based scenario

In this chapter, we present the complete decision-support system developed based on the previous implemented algorithms, described in chapter 3 and chapter 4. The system proposed has been designed for the integration of the optimization strategy with the results raised by the analysis of retrospective trajectories. Therefore, it consists in an adaptable system, which modify its strategy based on the trajectories chosen by the user. However, we improved the optimization model to include new components in the cost function, and modified the optimization parameters to match with the surgeons preferences. A retrospective qualitative review on more than 200 trajectories is also reported, showing promising results with respect the approximation presented.

Part of this work has been submitted to *Annals of Biomedical Engineering* as: Scorza, D., Rizzi, M., De Momi, E., Cortés, C., Bertelsen, À., Cardinale, F. "Data-based automated planning system for StereoElectroEncephaloGraphy: a center-based scenario" and is currently under-revision.

## 5.1 Introduction

Accurate trajectory planning became a crucial part for the success of keyhole interventions in neurosurgery, especially for the stereotactic insertion of one or multiple needle-shaped surgical instruments (e.g. biopsies, Deep Brain Stimulation, SEEG). Precise targeting and critical structure avoidance represent key factors to reduce the risk of complications and the efficacy of the intervention. Many authors proposed solutions to quantify the risk of planned trajectories and assist the surgeons in planning the optimal trajectory. Interactive methods were proposed in [92, 146, 163], which precompute the risk based on the segmentation of vessels, ventricles, and other vital structures. The result is then proposed to surgeons in the form of color maps, usually projected on the skull surface, to assist them in the selection of the optimal path. In [44], the authors coded the risk measures represented by color maps into linguistic terms by the use of fuzzy logic. For DBS intervention, where the targets are represented by specific subcortical nuclei (*subthalamic nucleus* and *globus pallidus* and *thalamus*), automated trajectory planning solutions have been explored. In [20, 61] the user needs to select the target and a series of surgical constraints that compose a weighted sum global cost function used in the optimization procedure. Nonetheless, the selection and combination of weights and constraints values represents a difficult task, and different choices may lead to very different results. In [125], the authors involved surgeons from three different institutions to assess the generalization of their method. In [60], a retrospective analysis is performed to study and analyze the criteria guiding DBS trajectory planning, collecting data from two different centers. Results from both studies [60, 125] suggest that, even if they used different approaches, the rules guiding the planning in DBS surgery can be generalized. Still, most recent works in DBS planning evaluated alternative optimization methods to avoid the selection of weights *a priori*, using for example Pareto-based approximations [87]. They also introduced additional planning features to increase the implant efficacy, by selecting the most feasible target point using anatomo-clinical atlases and volume of tissue activated [48].
Regarding SEEG planning, safe trajectories need to maximize their distance from vessels [120], avoid specific critical structures (e.g. *Cerebellum*, *Ventricles* and *brain-stem*), and reduce their insertion angle with respect to the the normal vector to the skull surface [29]. With respect to other neurosurgical interventions, SEEG requires to plan multiple trajectories and a minimum distance between tools must be guaranteed to avoid collisions and to provide the most uniform sampling as possible. In the

last years, multi-trajectory planning algorithms have greatly advanced in the representation of those constraints by means of cost functions and implemented multi-trajectory strategies capable of providing a viable solution in a feasible time-span [45, 177, 187, 214]. In [186], the authors presented an anatomy-driven multi-trajectory planning solution which added spatial priors by the selection of candidate target points within an anatomical brain region, improving spatial coverage. However, this requires a higher interaction level, since the user is required to specify both the target region and the candidate point. As suggested in recent validation studies [198, 199], the accurate representation of the surgical planning process has additional difficulties in SEEG interventions because of the great variability between the clinical workflow of different centers and surgeons.
Guided by the same hypothesis, in [176] we analyzed a series of retrospective trajectories from a single center and classified them into the most common exploratory patterns used. Even if a limited retrospective validation was provided, the results suggested that such work may be effective in the initialization of optimization methods, combining the knowledge from past cases and a representation of commonly used trajectories to select for a new case. However, the automated planning framework presented in [177] required additional improvements in order to correctly account for gray matter (GM) recordings, and only a retrospective quantitative validation was conducted. Additional experiments conducted jointly with neurosurgeons enhanced the need to modify some cost-functions to better account for their preferences.

In this work, we propose a novel system based on [176, 177], able to exploit the knowledge extracted by previously planned cases into an optimization framework which adapts the trajectories to the patient anatomy. With respect to our previous publications, the contributions are manifold:

1. the extension and integration of a retrospective trajectories analysis method [176] into a CAP solution;
2. the development of an interactive Graphical User Interface (GUI) for the definition of initial trajectories, which acts as anatomo-spatial priors onto the specific patient anatomy and are used as initial seeds in the optimization module;
3. the extension of the optimization framework [177] to modify its strategy based on the trajectory type to be optimized;
4. the introduction of a new operator to maximize the GM recorded by

a trajectory, as well as the modification of already implemented cost-function to better account for surgeons' preferences.

The system was customized with the data provided by a single high-volume center [33], and tested by two neurosurgeons (MR and FC) of the same institution acting as internal raters.
The experiments were designed to assess the capability of the initialization module in representing the trajectories commonly used by the surgeons, extracted from the analysis of retrospective data, and the efficacy of the new optimization strategy provided. With respect to our previous works, we report the qualitative and quantitative results obtained on more than $200$ trajectories, on $15$ retrospective patients' data sets.

## 5.2 Methods

We generically define a surgical plan $M$ as a set of trajectories $M = \{t_0, t_1, \dots t_Q\}$, with $Q = \#M$, where each trajectory $t \in M$ is defined at least by an entry and a target point, respectively $t = (\mathbf{EP}; \mathbf{TP})$, representing their Euclidean coordinates in the patient image space. The decision-support system (DSS) developed for the assistance during SEEG surgical planning is composed by two parts (Figure 5.1):

1. *the initialization module* (section 5.2.1) implements a procedure to automatically extract the most common trajectories used by the center, analyzing the trajectories of previously implanted electrodes [176]. The procedure can be run periodically and the results are stored and proposed through a graphical user interface (GUI). The latter allows the user to define trajectory seeds in an average brain space, defined as $\overline{t} = \{\overline{\mathbf{EP}}; \overline{\mathbf{TP}}; (l_e; l_t); \Lambda\}$ where $\overline{\mathbf{EP}}$ and $\overline{\mathbf{TP}}$ are the Euclidean coordinates of EP and TP in the average brain space, $(l_e; l_t)$ the labels of two relevant brain regions to be crossed (according to an anatomical atlas) and $\Lambda$ the "*type*" of trajectory (as it will explained in section 5.2.1). The combination of chosen seed trajectories is registered to the patient specific anatomy, defining an initial plan $IP = \{t_0, \dots t_N\}$, with $N = \#IP$ as input for the optimization procedure.

2. *The automated planning module* (section 5.2.2) provides the optimization strategy to adapt the initial trajectory seeds in $IP$. The procedure optimizes a set of indexes such as the distance from vessels, the gray matter recordings and the insertion angle. The final optimized plan $OPT$ are proposed to the surgeon for revision.

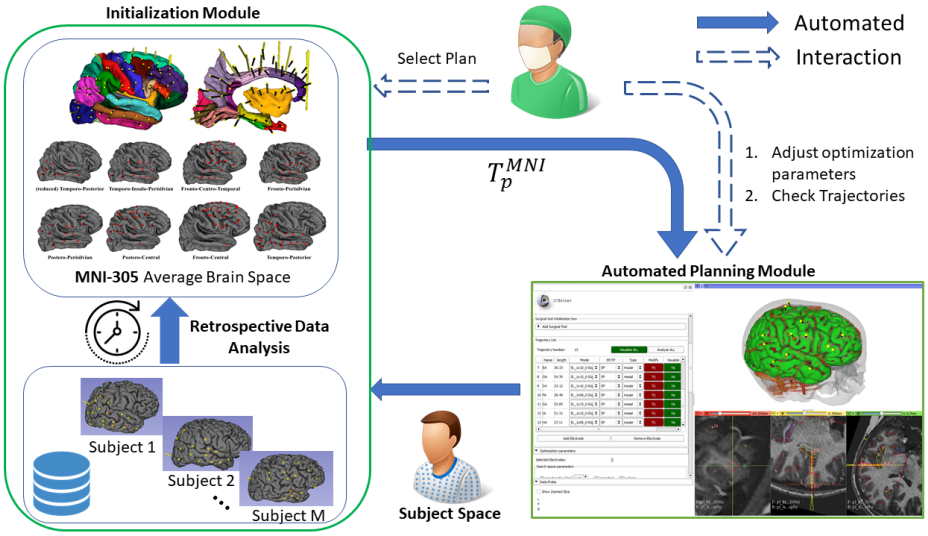


**Figure 5.1:** *Overview of the SEEG data-based planning system architecture. The initialization module is built on the analysis of trajectories from past cases, that are stored in a database. The user selects the trajectories represented on an average brain in the MNI-305 space, which are transformed to the specific patient anatomy as seed trajectories. The automated planning module adapts them based on the clinical criteria defined and the medical images provided. After revision, accepted trajectories are saved in the initialization module database.*

The two module are designed as part of a unique system[1], able to store new patient data and allow periodic updates to refine the output proposed to the surgeon.

### 5.2.1 Initialization module

The initialization module is built on the analysis of retrospective cases, exploiting the knowledge contained in previously planned cases and to assist the surgeon in the initialization of new patients' plans. Section 5.2.1 reports the methodology already presented in [176] and its extension with respect trajectory profiles, while section 5.2.1 its application for new patient's cases.

[1] A video of the system can be found at: *https://www.youtube.com/watch?v=I-99SUxKHyY*

**Retrospective data analysis**

A retrospective database is built containing $P$ image patient's data sets and their corresponding manual plans $MP_p$, with $p = 1, 2, \dots P$, composed by surgeons' manually planned (MP) trajectories for past SEEG interventions. As reported in [176], we register each patient's T1W Magnetic Resonance Image (MRI) to the Montreal National Institute brain space (MNI-305), and provide a segmentation according to an anatomical atlas (e.g. Desikan-Kiliany atlas [49]). Each patient's MRI is consequently segmented into a number $L$ of anatomical brain regions labels.
Since the goal of the procedure is to record the brain activity, we assume that each trajectory is aimed to cross at least 2 cortical regions (lateral and mesial), corresponding to the first cortical regions found from the entry and target points respectively. Therefore, we divide the atlas labels into two sets $\epsilon$ and $\tau$, containing the labels of anatomical brain regions to be crossed by the first or the second tract of the trajectory respectively. The $\epsilon$ set contains the labels of lateral cortical regions, while $\tau$ the labels of mesial cortical regions (e.g. *Superior-temporal and Hippocampus* respectively, according to the Desikan-Kiliany atlas). To each trajectory $t_{i,p}$ we assigned 2 labels $\{l_e; l_t\}$, $l_e \in \epsilon$ and $l_t \in \tau$ and grouped them in $G$ sets of type $g(l_e; l_t) = \{t_{i,p}\}$, which collects trajectories aimed to explore the same regions from all patients.
Since anatomical brain zones could be broads, we assume that surgeons may want to explore the regions with more than one trajectory for same patient plan $MP_p$. To keep this spatial relationship between trajectories of the same group, we transformed all $t_{i,p} \in g(l_e; l_t)$ from the corresponding subject space to the MNI-305 space and clustered them by the usage of a k-means algorithm into $g_k(l_e; l_t)$ groups, with $k = 1, \dots K$ and $K$ corresponding to the maximum number of trajectories belonging to $g(l_e; l_t)$ in a single plan $MP_p$ among all available plans. This allows to maintain the spatial relationship among similar trajectories, obtaining a mean trajectory $\overline{t}_k = \{\overline{\mathbf{EP}}_k; \overline{\mathbf{TP}}_k\}$ from each group $g_k(l_e; l_t)$, with $k = 0, \dots K$, corresponding to the mean Euclidean coordinates of EPs and TPs $\forall\, t_{i,p} \in g_k(l_e; l_t)$ in MNI space, specifying for instance a different way to cross the same regions.
The final set of mean trajectories $\overline{T} = \{\overline{t}_0, \overline{t}_1, \dots, \overline{t}_T\}$, $T = |\overline{T}|$ identified the most common paths used by our clinical center to explore specific brain regions. Implementation details were presented in [176].

Additionally, by qualitatively analyzing the regions crossed by MP trajectories and by discussing it with our clinical partners, we were able to

identify three different trajectory types $\Lambda$, which require different optimization strategies and specific adjustments. They are named according to the deepest sampled region:

1. *Midline trajectories* ($\Lambda_1$): they are prolonged as much as possible, from the brain convexity to the mesial surface of the hemisphere.
2. *Insular trans-opercular trajectories* ($\Lambda_2$): they reach the insular cortex, overcoming it as much as needed to guarantee at least two contacts deeper than the opercular cortical ribbon.
3. *Mesio-temporal trajectories* ($\Lambda_3$): they sample the temporal convexity, reaching the hippocampus and prolonged as much as possible to the inner temporal surface. These type of trajectories may violate the ventricular avoidance constraint (section 5.2.2).

Each mean trajectory is completely described as $\bar{t} = \{\overline{\mathbf{EP}}; \overline{\mathbf{TP}}; (l_e; l_t); \Lambda\}$, with $\overline{\mathbf{EP}}$ and $\overline{\mathbf{TP}}$ the mean Euclidean coordinates of EP and TP in the MNI space, $(l_e; l_t)$ the labels of two anatomical regions to be explored by the trajectory and $\Lambda_i$, with $i = 1, 2, 3$, the trajectory type to guide the optimization procedure (section 5.2.2). All the mean trajectories $\bar{t}_k$ obtained by $g(l_e; l_t)$ are usually described by the same profile $\Lambda_i$.

Finally, as proposed in [176], we hierarchically clustered the $MP_p$ plans based on their similarity with respect to the trajectories used and define $S$ different planning strategies. Each planning strategy $s_j$ , with $j = 1, \dots S$, correspond to a subset of trajectories $s_j \subset \overline{T}$ that could be found in more than two $MP_p$ belonging to the same cluster and represent combination of mean trajectories $\bar{t} \in \overline{T}$ commonly used to record the activity of multiple structure in a macro brain area (e.g. *Fronto-Central exploration, Temporo-Posterior exploration*; we report the strategy names defined by the surgeons in table 5.1). Each planning strategy $s_j$ may have a variable number $|s_j|$ of $\bar{t}$.

The procedure reported allows to be executed periodically with the introduction of new data, and allows additional profiles to be added if necessary. It has to be noticed that, a different set of data would lead to a different set of mean trajectory, which should represent the common patterns used at the center from which the data come from. Those results are presented to the surgeon by the GUI interface presented in the following section.

#### Application and Graphical User Interface

A GUI application (Figure 5.2) is built to represent the mean trajectories $\bar{t} \in \overline{T}$ as cylinders on an average brain in the MNI-305 space. Each new patient

is registered to the MNI space and segmented according to an anatomical atlas.

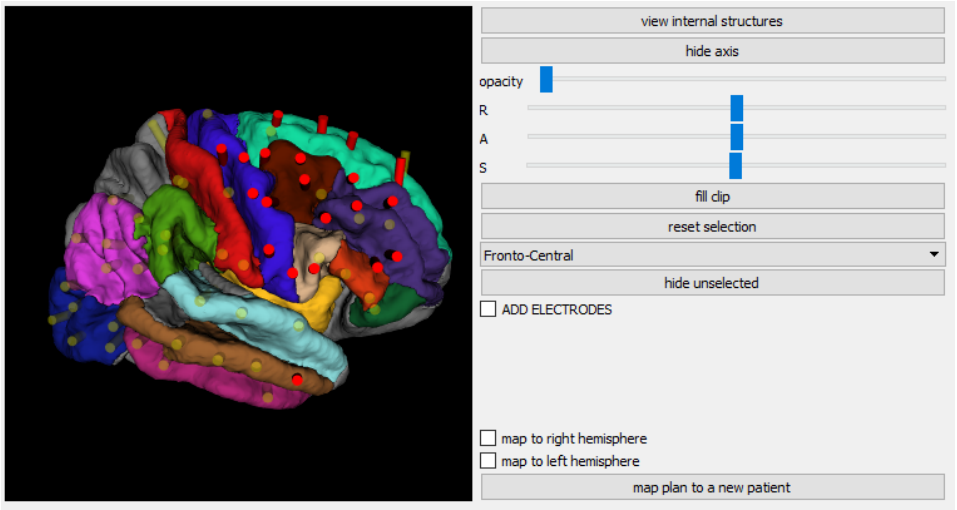


**Figure 5.2:** *GUI application for the selection of initial trajectory seeds in the average brain space. A Fronto-Central exploration strategy has been selected and the corresponding trajectories visualization enhanced (in red).*

The user can select a planning strategy, $s_j$, as a starting point based on the patient-specific hypothesis on EZ. By selecting an $s_j$, the trajectories $\overline{t_i} \in s_j$ are enhanced for visualization purposes, and the user can modify the initial proposal by removing and/or selecting other $\overline{t_i} \in \overline{T}$. For each $\overline{t_i}$, it is possible to visualize the target regions $(l_e; l_t)$ associated, $l_e \in \epsilon$ and $l_t \in \tau$.
Once the user has selected the desired combination of trajectories, they are transformed from the MNI space to the patient's images space through the inverse transform obtained by the registration procedure. EPs and TPs are automatically iteratively adjusted by finding the intersection with the closest gyrus point of the cortical surface and verifying the trajectory crosses with the corresponding regions.
The final $IP = \{t_0, \ldots t_N\}$, with $N = |IP|$, represents a set of trajectory seeds in the form $t = \{\mathbf{EP}_0; \mathbf{TP}_0; (l_e; l_t); \Lambda\}$ where $\mathbf{EP}_0$ and $\mathbf{TP}_0$ are the initial Euclidean coordinates of EP and TP in subject space, $(l_e; l_t)$ the labels of the target brain regions to be crossed by the trajectory and $\Lambda$ trajectory type. The automated planning module, explained in the following section, uses the seeds trajectories as anatomical and spatial priors for the optimization procedure and adapts its strategy based on the trajectory type

$\Lambda$.

### 5.2.2 Automated planning module

The automated planning module entails three steps consisting in 1) image processing, 2) path optimization and 3) trajectory check. As presented in [177], the image processing step processes the patient's medical images and provides the image and surface inputs for the optimization procedure.
With respect to our previous implementation, the optimization has been improved accordingly with the integration of the initialization module and thanks to series of iterative experiments conducted in collaboration with the medical staff.
The input data of the optimization module are reported as following:

- the distance map volume [42], computed from the vessels binarization;
- the cortical surface, segmented between sulci and gyrus regions;
- the skull surface;
- the T1W MRI segmented according to an anatomical atlas;
- the Hippocampus surface;
- an initial plan $IP$ composed by initial trajectory seeds for the optimization.

For each $t_i \in IP$, $i = 1, 2, \ldots |IP|$, we generate a search space $sp_i$ composed by the trajectories obtained by the combination of possible EPs and TPs.
The set $S^i_{EP} = \{\mathbf{EP}_0, \mathbf{EP}_1, \ldots, \mathbf{EP}_E\}$, with $E = |S^i_{EP}|$, of possible EPs is composed by the vertices coordinates of the cortical surface gyrus region around $\mathbf{EP}_0$, which satisfy $g_e \leq r^i_{EP}$, with $g_e$ the geodesic distance computed between the vertices coordinates $\mathbf{EP}_e$ and $\mathbf{EP}_0$, $e = 0, 1, \ldots E$, and $r^i_{EP}$ a user defined search radius around $\mathbf{EP}_0$ for the trajectory $t_i$. The use of the geodesic distance instead of the Euclidean one guarantees to consider only the connected region around $\mathbf{EP}_0$ and reduces the possibilities of changing gyrus during the optimization process, especially in case of large $r^i_{EP}$.
TPs are generated differently based on the trajectory type $\Lambda$: $\Lambda_1$ and $\Lambda_3$ (*Midline* and *Mesio-temporal*) trajectories use the mesial part of the cortical and hippocampus surfaces respectively, composing the target points set

$S^i_{TP} = \{\mathbf{TP}_0, \dots \mathbf{TP}_R\}$, with $R = |S^i_{TP}|$, of vertices coordinates which satisfy $d_r = \|\mathbf{TP}_r - \mathbf{TP}_0\| \leq r^i_{TP}$, with $r = 0, 1, \dots R$, $r^i_{TP}$ a user defined search radius around $\mathbf{TP}_0$ and $d_r$ the Euclidean distance between vertices. In this case, the Euclidean distance is used since at TP we do not have the surface connectivity requirement as at the EP. Additionally, the use of the two surfaces guarantees that all the trajectories reach their maximum length in order to increase recording information. On the other side, TPs of $\Lambda_2$ (*insular*) trajectories are defined by generating a spherical point grid of radius $r^i_{TP}$ with $0.5$ mm resolution around $\mathbf{TP}_0$.
The candidate search space $sp_i = \{tr_0, tr_1, \dots tr_J\}$, with $J = E * R$, is composed by the combination of the two sets of Euclidean coordinates $EP_i$ and $TP_i$.
For each trajectory $tr_j \in sp_i$, $j = 0, 1, \dots J$, we compute the labels $l_j = \{l_0, l_1, \dots l_I\}$ crossed, with $I = |l_j|$, according to the anatomical atlas. All trajectories crossing dangerous regions (*cerebellum*, *ventricles* with the exception of $\Lambda_3$ type, or *brain-stem*) are discarded, as well as $tr_j$ of $\Lambda_1$ and $\Lambda_3$ type that do not cross their target regions $(l_e; l_t)_i$ associated to the initial seed. Trajectories of type $\Lambda_2$ have an additional requirement consisting in placing their TP overcoming the deeper target region, guaranteeing at least two electrode leads in a non-cortical regions.
To compute the insertion angle, we used an oriented bounding box tree to decompose the skull surface into a hierarchical structure, used to identify the collision point $\mathbf{k}_j$ between the skull element and the prolonged trajectory $tr_j$. The insertion angle $\theta_j$ between the vector $\vec{\mathbf{v}_j} = \mathbf{TP}_j - \mathbf{k}_j$ and the normal to the skull surface $\vec{n}(k_j)$ is computed as:

$$\theta_j = \arccos\left(\frac{(\vec{\mathbf{v}_j} \cdot \vec{n}(\mathbf{k}_j))}{\|\vec{\mathbf{v}_j}\| \cdot \|\vec{n}(\mathbf{k}_j)\|}\right) \tag{5.1}$$

All trajectories exceeding a user defined $\theta^{max}_i$ are discarded.
As explained in [177], for safety reasons with respect to the distance from vessels, we divide the trajectory into two tracts: the first tract is considered from $\mathbf{k}_j$ to an intermediate point $\mathbf{m}_j$ at a user-defined distance $\zeta$ from the cortical $\mathbf{EP}_j$, while the second tract goes from $\mathbf{m}_j$ to $\mathbf{TP}_j$. This approach allows the user to define two different minimum distance thresholds, $\delta v^{EP}_i$ and $\delta v^{TP}_i$, respectively for the first and second tract, with $\delta v^{TP}_i \leq \delta v^{EP}_i$.
Therefore, we collect the distance map voxel values $\mathbf{dv}^{EP}_j = \{v_0, \dots v_X\}$, with $X = |\mathbf{dv}^{EP}_j|$, and $\mathbf{dv}^{TP}_j = \{v_0, \dots v_Y\}$, with $Y = |\mathbf{dv}^{TP}_j|$, intersected by the first and second tract of $tr_j$ respectively and discard $\forall\, tr_j \mid \delta^{EP}_{min} \leq \delta v^{EP}_i$ or $\forall\, tr_j \mid \delta^{TP}_{min} \leq \delta v^{TP}_i$, with $\delta^{EP}_{min} = \min(\mathbf{dv}^{EP}_j)$ and $\delta^{TP}_{min} = \min(\mathbf{dv}^{TP}_j)$
Additionally, to avoid crossing sulci regions in the first tract or to place the

$\mathbf{EP}_j$ too close to the boundary region between gyrus and sulci, we discard all $tr_j$ with a minimum distance inferior to a user-defined threshold $\delta s_i^{EP}$. At this point, if $sp_i = \emptyset$, we alternatively increase the search radius by 1 mm or relax the constraint value which has caused most rejections and repeat the procedure until we find at least an acceptable trajectory or we exceed the maximum number of iterations $iter_{max}$.
Otherwise, we compute the component of our cost function: the cumulative distance from vessels $f_v(tr_j)$, the insertion angle index $f_\theta(tr_j)$ and the grey matter index $GM(tr_j)$.
The first is a weighted sum of cumulative distances $f_v^{EP}(tr_j)$ and $f_v^{TP}(tr_j)$ for the first and second tract, computed as in equation 5.2:

$$f_v^x(tr_j) = \frac{1}{N+1} \cdot \Big[ \sum_{i=1}^{N} \Big( \frac{v_i - \delta_{min}^x}{\delta_{max}^x - \delta_{min}^x} \Big) + \frac{\delta_{min}^x - \delta v_i^x}{\delta v_i^x} \Big] \tag{5.2}$$

with $x$ substitute alternatively the index $EP$ or $TP$ depending on the trajectory tract considered, $v_i \in \mathbf{dv}_j^x$ the voxel value of distance from vessel, $i = 0, \dots N$, $N = |\mathbf{dv}_j^x|$. The final $f_v(tr_j)$ results in a weighted combination of the individual score of the two components:

$$f_v(tr_j) = \omega_v^{EP} * f_v^{EP} + \omega_v^{TP} * f_v^{TP} \tag{5.3}$$

with $\omega_v^{EP}, \omega_v^{TP} \in [0, 1]$ and $\omega_v^{EP} + \omega_v^{TP} = 1$ are user-defined weights.
The insertion angle index is computed as following:

$$f_\theta(tr_j) = \frac{\theta_{max} - \theta_{tr_j}}{\theta_{max}} \tag{5.4}$$

Finally, based on the trajectory length and the electrode leads geometry, we estimate the position of electrode contacts $C = \{\mathbf{c}_0, \dots \mathbf{c}_Z\}$, with $Z = |C|$ along the $tr_j$. For each contact $c \in C$, we assume a spherical recording volume of radius $r_c = 3$ mm and collect the voxels values $A(c)$ of the anatomical atlas intersected by the spherical volume. The grey matter index $GM(tr_j)$ is computed as:

$$GM(tr_j) = \frac{1}{C} \cdot \sum_{c=0}^{C} \frac{\sum_{a=0}^{|A(c)|} [a \in g]}{|A(c)|} \tag{5.5}$$

where here $[a \in g]$ are willing to use the "*Iverson Bracket notation*", $a \in A(c)$ is an anatomical label associated to the corresponding voxel value and $g$ is a set composed by all cortical regions, accordingly to the anatomical

atlas used.
The final cost function is expressed as following:

$$f(tr_j) = \omega_v \cdot f_v(tr_j) + \omega_\theta \cdot f_\theta(tr_j) + \omega_{GM} \cdot GM(tr_j) \tag{5.6}$$

with $\omega_v, \omega_\theta, \omega_{GM} \in [0, 1]$ and $\omega_v + \omega_\theta + \omega_{GM} = 1$. The search space $sp_i$ is ordered by ranking the trajectories from the highest to the lowest $f(tr_j)$, and the corresponding $tr_{j=0} \in sp_i$ is assigned to the electrode $i$.

Once the last electrode has been optimized, a selective brute force method similar to the one presented in [177] is used to solve possible conflicts that may occur. With respect to the previous version, here the user defines two distances $\gamma^{EP}_{min}$ and $\gamma^{TP}_{min}$ representing the minimum allowed Euclidean distances between electrodes in the first and second tract respectively. Generally, $\gamma^{EP}_{min} \geq \gamma^{TP}_{min}$, since at the EP we need to guarantee enough space to place the screws through which the electrode is inserted. Hence, a conflict between two electrodes $m$ and $n$ is found when $\gamma^{EP}_{m,n} \leq \gamma^{EP}_{min}$ or $\gamma^{TP}_{m,n} \leq \gamma^{TP}_{min}$. If a conflict occurs, we efficiently explore the search spaces $sp_m$ and $sp_n$ taking advantage of the ordered ranking scheme and find the first acceptable combination of trajectories. However, since we are working with a discrete number of solutions defined by each $sp_i$, it may occur that the conflict cannot be avoided. In such cases, we select the electrode with the highest score between the pair involved in the conflict and eliminate the other, raising a warning to the user. The final optimized plan $OPT = \{t_0, \dots t_O\}$, with $O = |OPT| \leq |IP|$, contains the optimized trajectories proposed by the system, requiring the revision of the surgeon. A schematic representation of the optimization strategy described is presented in figure 5.3.

### 5.2.3 Experimental protocol and validation

Patients were operated on at the "Claudio Munari" Centre for Epilepsy and Parkinson Surgery, ASST GOM Niguarda, Milan, Italy. No complications have been reported. MP trajectories were planned using the Voxim (IVS Technology GmbH, Chemnitz, Germany) software application.
The initialization module has been obtained by the analysis of $75$ patients, for a total of more than $\sim 1100$ trajectories. All the patients were processed with the Freesurfer pipeline [66], which includes the registration of each patient with the MNI-305 space and the probabilistic segmentation of cortical and non-cortical brain structures. We obtained $G = 30$ anatomical groups, corresponding to $\overline{t_i}$ mean trajectories, $i = 1, \dots 61$ and $s_j$ planning strategies, $j = 1, \dots 8$. In general, the number of $\overline{t_i} \in s_j$ was higher than

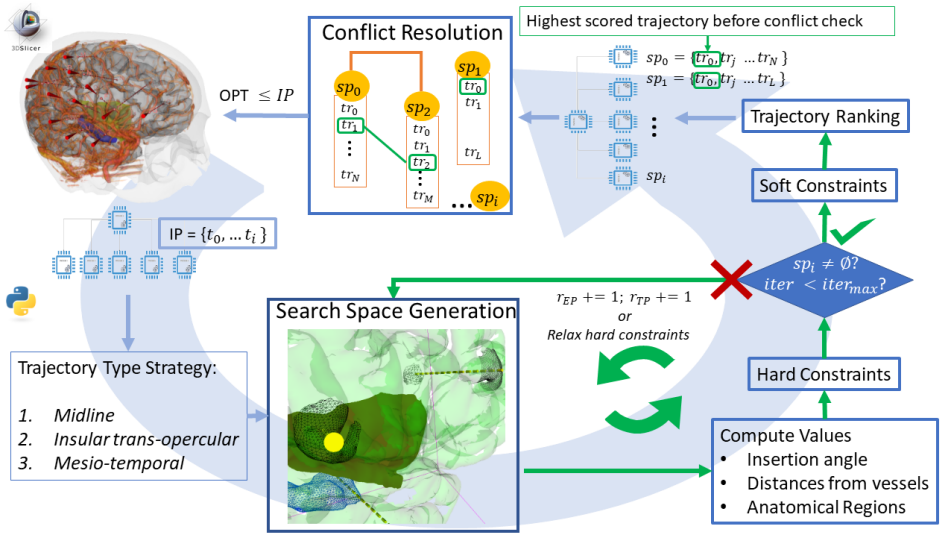


**Figure 5.3:** *Optimization strategy overview: for each trajectory seed in the initialized plan $IP$, a search space is created based on the trajectory type. Each seed enters in the optimization loop until a solution can be found or the maximum number of iteration is reached. The optimization is run in parallel based on the number of processor of the hosting machine. Once all the seeds have been processed, we check for conflicts and the final optimized plan $OPT$ is proposed to the surgeons for revision.*

| Planning Strategies $s_j$ | ID | $\lvert s_j \rvert$ |
|---|---|---|
| Temporo-Posterior | TP | 22 |
| Temporo-Posterior (reduced) | rTP | 10 |
| Temporo-Insulo-Perisilvian | TIP | 14 |
| Fronto-Centro-Temporal | FCT | 23 |
| Fronto-Perisilvian | FP | 18 |
| Postero-Perisilvian | PP | 23 |
| Postero-Central | PC | 21 |
| Fronto-Central | FC | 21 |

**Table 5.1:** *We report the names assigned to the planning strategies $s_j$, with $j = 1, 2, \ldots, 8$ represented in the initialization module. For each $s_j$, we report the number of $\overline{t_i} \in s_j$.*

the mean number of manually planned trajectories (the data analyzed from the database showed a mean of $\sim 14$ electrodes per patient, while the mean number of $\overline{t_i} \in s_j$ was $\sim 19$). However, we intentionally defined $s_j$ to include more trajectories following the hypothesis that removing one is easier than adding a new one. Table 5.1 reports the name of each $s_j$, as well as the number of $\overline{t_i}$ in each cluster.

For the validation, we randomly selected a total of $15$ patients' data sets who successfully underwent SEEG electrode implantation in the last three years and who were not included in the database used to generate the initialization module. Two expert neurosurgeons, FC and MR, have been involved in the validation. We conducted two different experiments: the first (section 5.2.3) was focused on the initialization module, while the second (section 5.2.3) on the qualitative and quantitative evaluation of the trajectories proposed by the system.

#### Experiment 1

The first experiment focused on the capability of the initialization module in representing the exploration strategies more commonly adopted at Niguarda hospital. Since it presents only the most common trajectories extracted by the analysis of our database, we must assume that manual plans $MP$ have additional trajectories not suggested by the module. Indeed, trajectories targeted to explore brain lesions and, therefore, not representing a common path, were unlikely to be included in $\overline{T}$. The experiment focused on verifying the number of trajectories that the final user was able to initialize with our module, and to assess the need of all the planning strategies proposed.

| Constraint values | | Optimization Parameters | |
|---|---|---|---|
| $\delta_v^{EP}$ | 2.5 mm | $\omega_v^{EP}$ | 0.7 |
| $\delta_v^{TP}$ | 1.0 mm | $\omega_v^{TP}$ | 0.3 |
| $\delta_s^{EP}$ | 2.5 mm | $\zeta$ | 12 mm |
| $\theta_{max}$ | 30° | $r_{EP}$ | 8 mm |
| $\gamma^{EP}$ | 12 mm | $r_{TP}$ | 5 mm |
| $\gamma^{TP}$ | 5 mm | $\omega_v$ | 0.6 |
| | | $\omega_\theta$ | 0.2 |
| $iter_{max}$ | 5 | $\omega_{GM}$ | 0.2 |

**Table 5.2:** *Default values applied to the constraints and optimization parameters*

For each patient $p_k$, $k = 1, 2, \dots 15$, the surgeon defined a new plan $IP_k$ through the initialization module, using the original manually planned trajectories $MP_k$ as a visual reference.
The procedure was as following:

1. the surgeon selects a planning strategy $s_j$ as a starting point (optional);
2. additional trajectories $\overline{t_i} \in \overline{T} \notin s_j$ could be selected, as well as $\overline{t_i} \in s_j$ could be removed based on the EZ hypothesis;
3. the selected trajectories were automatically mapped to the corresponding patient hemisphere.

For practical reasons, in case of bilateral patients, we chose the hemisphere with more trajectories. We defined a counter variable $c_j$ to count how many times a planning strategy $s_j$ was used as starting point by the surgeon. For each patient $p_k$, we also computed two indices $\alpha_a$ and $\alpha_r$ representing respectively the percentage of added and removed $\overline{t_i}$ with respect to $|s_j|$. We report also the number of trajectories $|MP_k|$ and $|IP_k|$ for comparison.

#### Experiment 2

We processed the initialized plans $IP_k$ with the optimization procedure described in section 5.2.2. The parameters used for the optimization are reported in table 5.2, modified with respect to previous versions to account for the new constraints added and the iterative experiments conducted in collaboration with clinicians. FC and MR reviewed and evaluated the proposed plans $OPT_k$, by classifying each trajectory into three groups: *accepted*, *intermediate* and *rejected*. The *accepted* group represents all the trajectories that were considered feasible "*as they are*", without requiring

any modification. For instance, it represents trajectories with no angular or vascular transgression (minimum distance of $2.5$ mm), and sufficient GM recordings. The *intermediate* group represents those trajectories close to the clinical choice, but required a minimal modification (e.g. an increment in length). The *rejected* group contains trajectories that were not clinically acceptable. Trajectories were reviewed in 3D Slicer, with the functionalities exposed by the planner module [178], on not-processed patient's images.
As a second analysis, we compared the quantitative values of all relevant indexes $\delta_{min}^{EP}$, $\delta_{min}^{TP}$, $\theta$, $GM$ between the three groups $MP$, $IP$ and $OPT$. Since such data were non-normally distributed (Shapiro-Wilk test, p-value $\leq 0.05$), we compare group-specific indexes by means of Kruskal-Wallis test and the relative post-hoc analysis with Conover-Iman test. The data were processed using the SciPy python package [140].

#### Imaging Protocol

Magnetic Resonance (MR) datasets were acquired with an Achieva® 1.5 T magnet (Philips Healthcare; Best, The Netherlands). All patients underwent 3D Fast Field Echo T1 Weighted (FFE T1W) imaging (contiguous axial slices with $560$ x $560$ matrix, $0.46$ x $0.46$ x $0.9$ mm voxel, with no inter-slice gap). Images for 3D Cone-Beam-Computed-Tomography Digital-Subtraction-Angiography (3D CBCT DSA) were obtained by means of the O-armTM 1000 System (Medtronic; Minneapolis, MN, USA) [31]. The reconstructed 3D volume is a $200$ x $150$ mm cylinder, described by $192$ axial slices ($512$ x $512$ matrix, $0.415$ x $0.415$ x $0.833$ mm voxels).
The T1W MRI was processed with the Freesurfer pipeline [66] to obtain the cortical surface and Desikan-Kiliany atlas segmentation. The image processing module presented in [177] was used to segment the 3D CBCT DSA through a manual thresholding and compute the distance map, as well as to compute the skull surface, segment between gyrus and sulci regions and generate the surface of hippocampus and insula regions.

## 5.3 Results

#### Experiment 1

Table 5.3 presents the number of times $c_j$ a planning strategy $s_j$ has been selected as a starting point to reproduce a patient plan, as well as the percentage indices $\alpha_a$ and $\alpha_r$ of the trajectories added or removed by the surgeon with respect to $|s_j|$ . In this validation set, three $s_j$ were never chosen as the best option for initialization. The other five strategies were equally

| ID | $c_j$ | $\alpha_r$ [%] | $\alpha_a$ [%] |
|---|---|---|---|
| TP | 2 | 31.8 | 4.5 |
| rTP | Never | / | / |
| TIP | 2 | 28.6 | 42.8 |
| FCT | 3 | 52.1 | 23.2 |
| FP | 3 | 35.2 | 14.8 |
| PP | Never | / | / |
| PC | Never | / | / |
| FC | 3 | 53.9 | 22.2 |

**Table 5.3:** *We report the number of times a planning strategy was used as a starting point for a new patient plan. The percentage of trajectories added/removed is also reported*

chosen, depending on the patient case. As expected, no planning strategy could reproduce a real patient case "*as it is*": all selected $s_j$ needed a manual intervention and, in general, the surgeon had to remove $\sim 40\%$ of $\overline{t_i} \in s_j$ and add $\sim 20\%$ of $\overline{t_i} \in \overline{T} \notin s_j$. Patient initialization took around $4$ and $10$ minutes based on the patient case and number of electrodes, including checking that the trajectory were correctly mapped on the patient's anatomy.

In table 5.4, we report for each case the planning strategy selected, the number of electrodes that were manually planned $|MP_k|$ and the number of trajectories $|IP_k|$ that the surgeon was able to initialize through the module. Planning strategy was not adopted in $2$ patients with bilateral implantation, and few electrodes on each hemisphere (respectively $7$ and $9$ trajectories). In these cases the surgeon considered the use of the planning strategy redundant.
However, the surgeons were able to identify around $\sim 95\%(205/216)$ of the total $MP$ trajectories.

#### Experiment 2

In the second experiment, we evaluated the overall capability of our system to optimize and propose clinically valid trajectories. The system was able to optimize the $\sim 98\%$ $(201/205)$ trajectories of the $IP$ plans: in one case, an error was raised due to an erroneous initial position, while the other three represented conflicts between electrode pairs that could not be solved. In table 5.5, we report the evaluations of the two surgeons of all trajectories in $OPT$. Both surgeons considered as clinically feasible approximately $\sim 81\%$ of the proposed trajectories $(164/201)$ with an inter-raters reliabil-

| k | Hemisphere | $s_j$ | $\lvert MP_k \rvert$ | $\lvert IP_k \rvert$ |
|---|---|---|---|---|
| 1 | RH | FP | 13 | 13 |
| 2 | RH | FCT | 18 | 18 |
| 3 | RH | FCT | 17 | 16 |
| 4 | RH | FC | 15 | 15 |
| 5 | RH | TIP | 19 | 19 |
| 6 | RH | FC | 14 | 14 |
| 7 | RH | FP | 13 | 13 |
| 8 | RH | FCT | 17 | 15 |
| 9 | LH | FP | 13 | 13 |
| 10 | bila (RH) | FC | 14 | 14 |
| 11 | bila (RH) | / | 7 | 7 |
| 12 | RH | TP | 15 | 14 |
| 13 | bila (RH) | / | 9 | 8 |
| 14 | LH | TIP | 14 | 13 |
| 15 | RH | TP | 18 | 13 |
| | | | **216** | **205** |

**Table 5.4:** *Comparison of the number of trajectories in the original $MP$ and in the initialized $IP$ for each patient. The hemisphere and the initial $s_j$ chosen is also reported.*

| | Accepted | Intermediate | Rejected |
|---|---|---|---|
| MR | 164 | 16 | 21 |
| FC | 164 | 11 | 26 |

**Table 5.5:** *Qualitative evaluation results from 2 expert neurosurgeons.*

ity of $75\%$. Their evaluation concurred for $156$ trajectories, however in $26$ cases they classified them differently between the *Accepted* and *Rejected* groups, while the remaining $22$ cases between the *Intermediate* and *Rejected* groups.
Most of the trajectories in the *Intermediate* group were trajectories of $\Lambda_1$ and $\Lambda_3$ type, a couple of mm shorter with respect to the extension required. By considering this group, which require a minimal manual adjustment by the user, the success rate of the system raises to $\sim 88\%$. Rejected trajectories were mainly caused by an erroneous vascular segmentation, that did not include all the vascular structures during the binarization. The second rejection cause consisted in erroneous EPs, which caused an unnatural positioning of a specific type of trajectories.

Finally, we quantitatively compared the three different groups $IP$, $MP$ and $OPT$ with respect to the most relevant indexes: distance from vessels, insertion angle and grey matter recording (figure 5.4). Regarding the distance from vessels, we found statistically significant differences among all groups, regardless of the tract considered. As expected, $IP$ trajectories did not satisfy the minimum requirements defined by the user $\delta v^{EP}$ and $\delta v^{TP}$, since during the mapping procedure we did not consider any vascular information. After the optimization, the $OPT$ group showed the best results, with a median value statistically higher and a reduced inter-quartile range than $MP$. No statistical difference between groups was found with respect to the insertion angle $\theta$ or $GM$ index. The trajectories were optimized on a desktop computer running Windows 10, Intel(R) Cose(TM) i5-7500U CPU @ 3.40GHz with 12GB of RAM DDR3, showing a mean time of $584.74 \pm 415$ seconds.

## 5.4 Discussion

The planning of an SEEG intervention is a very tedious and time consuming task, requiring the surgeon to carefully analyze the patient images and to find safe and optimal paths for electrode insertions. Recent validation experiments involving external reviewers have shown the great variability in the SEEG practice between centers and surgeons [198, 199], suggesting that a more customized approach may provide more tailored results with respect to the clinical practice.
In this manuscript we presented a novel data-based CAP solution, adapted to the medical routine of a clinical center by exploiting the knowledge extracted by its retrospective data. The methodology presented allows the user to periodically feed the database with new cases and, consequently, to

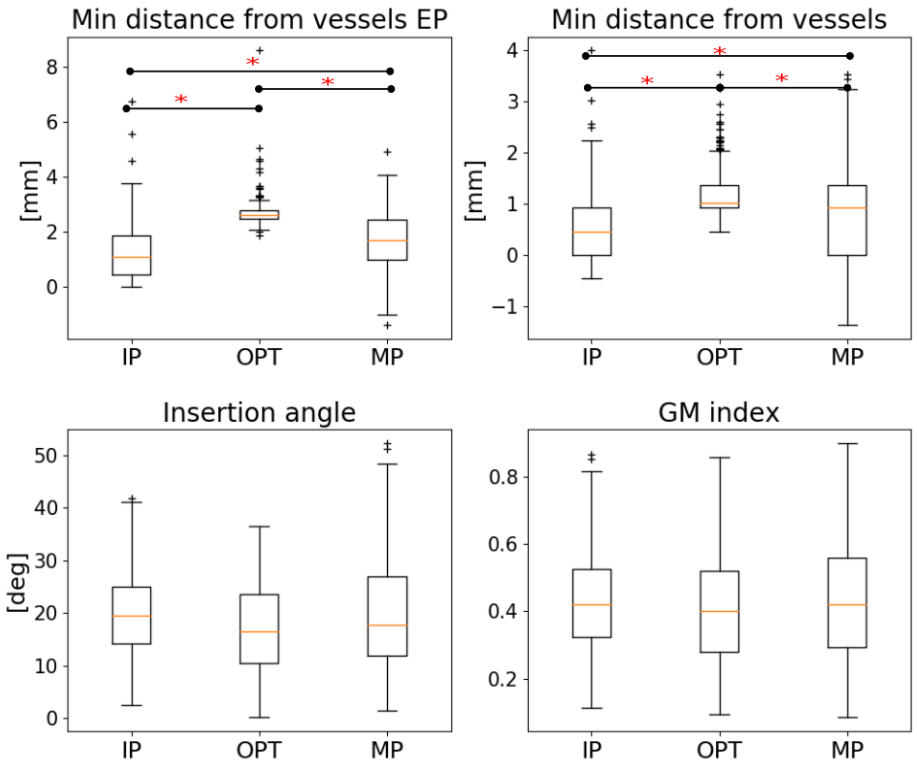


**Figure 5.4:** *Quantitative results for each relevant index considered during the optimization. We compared the values of the three groups, reporting significative differences (p-value* $\leq 0.01$*).*

refine the trajectories proposed by the system.
We extended our previous work [176] by adding the concept of trajectory profiles and integrating it as an initialization module in a CAP solution. The optimization framework proposed in [177] have been improved to account for those data, as new functionalities have been added such as the GM maximization, the composition of the vessel cost functions as a weighted sum of the first and second tract and a conflict resolution strategy which account for the screw dimensions at the EP. In this version, we also proposed a parallel architecture which reduced considerably the optimization time.

The system has been validated with the help of two neurosurgeons working in a high volume center, in a retrospective scenario composed by $15$ patients' data sets. They revised $\sim 200$ optimized trajectories, considering more than $\sim 80\%$ of them as clinically feasible. Only $12\%$ of the proposed trajectories were found unfeasible, while the remaining required minor modifications. The results obtained are very promising, being comparable or superior to other reported similar studies [45, 186, 214] and suggesting that this architecture can be more effective in reproducing and automating the planning process.

As regards the initialization module, its usage was found intuitive and user-friendly, requiring only the selection of $\overline{t_i} \in \overline{T}$. Indeed, the surgeon was able to select and map $\sim 95\%$ of the $MP$ trajectories used as visual references, meaning that the analysis performed on the retrospective cases produced representative results of the clinical practice.
Despite this, the effectiveness of planning strategies $s_j$ is unclear: three of them (*reduced Temporo-Posterior*, *Postero-Perisylvian* and *Postero-Central*), corresponding to less represented groups based on the hierarchical clustering performed [176], were never used for patient initialization suggesting that they could be removed. Still, the others strategies always required considerably modifications. A solution would be to provide a higher number of less populated planning strategies and to allow their combination when defining a new plan or, as it happened in two cases, to simply select the required trajectories without the usage of any strategy.

The other three trajectories were discarded because of conflicts: The system was not able to solve conflicts in three cases: trajectory pairs converged to very close $EPs$ and $TPs$ during the optimization, with a reduced number of available states and preventing the conflict resolution strategy to find a solution. It is worth to notice that the number of electrodes "*per patient*" implanted in our center is, in general, higher than other reported studies [187, 199, 214], making the system more prone to this type of problems.

The qualitative validation showed that most of the proposed trajectories were found acceptable by the two surgeons. Regarding the *intermediate* and *rejected* groups, FC rejected more trajectories that were considered as intermediate by MR. In particular, in some cases one of them considered that the EP was placed too close to a sulci, or gave more importance to the minimum distance from vessels in the second tract than the other.
Short trajectories of the *intermediate* group were caused by inaccurate segmentation of the cortical and hippocampal structures. It may happen that the surface boundaries obtained by the segmentation does not completely overlap with the anatomical boundaries represented in the image. Therefore, cases of sub-segmentation would prevent the trajectories to reach their maximum extensions.
As regards the *rejected* group, the principal causes were an erroneous vascular segmentation, where vascular structures were not included in the segmented volume, and unfeasible EPs. The latter characterized especially *midline* trajectories ($\Lambda_1$) with the EP at the level of the fronto-central gyri above the superior-temporal line of the skull. The optimization strategy provided a solution similar to the majority of trajectories, which have their main direction perpendicular to the sagittal plane. In those cases, a minimal brain shift can provoke the lack of gyrus targeting at the EP, when the trajectory is too much tangential to the brain as in this type of explorations and caused the surgeons to reject such solutions.
In a minority of cases (2 trajectories), the rejection was caused by the relaxation strategy performed during the optimization, which decreased the minimum acceptable distance from vessels.

Despite the problems raised by the qualitative analysis, quantitative comparison between groups showed better performances for $OPT$ trajectories. Even if these results confirmed the efficacy of the optimization strategy, which is able to adapt the $IP$ to the patient anatomy and reach similar results as $MP$, it must be stressed that those indexes are computed on the segmentation provided and must be interpreted carefully. The parallel architecture considerably reduced the processing time, which could be additionally reduced by running the optimization on a computer with a higher number of CPUs. However, we must stress that the processing time does not correspond to computer-time for the surgeon, since once started, the procedure it is completely automated.

The first limitation of the work is represented by the retrospective nature of the study, especially regarding the validation of the initialization module. However, the results obtained set the basis for a future perspective study, to evaluate the efficacy of the whole system as a tool to reduce the time and

the work-load of the surgeons. In such scenario, we will be able to provide additional details regarding any modification required with respect to the proposed trajectories, as well as comparing the planning time needed using our system or a more traditional method.
The usage of internal raters rather than externals (as in [199]) rely on the nature of the system: we customized our initialization and planning strategy based on the data provided by the center, making internal reviewers the natural choice to evaluate the likelyhood of our results compared with their own clinical practice.

Future improvements of the system will be focused on the definition of new trajectory profiles, such as *superior midline* and *lesional* trajectories. The database will be enriched with new data, as well as new analysis will be performed jointly with the medical staff to identify new profiles or include additional information that could be exploited during the optimization. Finally, a major unsolved problem regards the vessel segmentation: the majority of rejections were caused by unsegmented vessels that, consequently, were not considered during the optimization. On going work is exploring deep learning techniques to improve the vessel segmentation phase [58], that will be integrated in the image processing module.

## 5.5 Conclusion

In this work we propose a novel data-based planning system for SEEG, able to reproduce the clinical practice and propose effective and safe trajectories for brain exploration. The architecture presented provides two main advantages: first, we can adapt to the specific criteria and preferences of a clinical center and second, we can continuously improve our system by performing new analysis and increasing the amount of information contained in the database. The validation presented confirms its capability of reproducing the planning strategies adopted at Niguarda hospital, as well as to provide clinically feasible trajectories in more than $\sim 80\%$ of the cases. The study sets the basis for a learning system based on data, that could be extended and integrated with new image processing algorithm and optimization strategies derived by the analysis of retrospective cases.

CHAPTER 6

# Conclusions

Planning is a crucial step in any keyhole percutaneous procedure, which requires a deep study of the anatomical site to be operated and the elaboration of the most effective and safe strategy to maximize the final outcome. Since surgeons do not have a direct view of the surgical site, this must be done preoperatevely by the analysis of the patient's image data. Additionally, the time required for carefully plan a complex surgery as well as the lack of commercial systems providing advanced assistance tools, opens to a wide research field focused on modelling the decision-making process that guides the surgical practice.

In particular, SEEG offers a very challenging scenario, due to the amount of constraints and requirements that must be considered simultaneously. Additionally, the necessity of high precision and the large amount of electrodes per patient makes the planning process a tedious and time consuming task. Therefore, this PhD thesis addresses the following clinical needs:

- the development of an automated planning framework able to generate safe and optimal trajectories, adapted to the specific anatomy of the patient and following the rules guiding the surgical practice;
- the adaptation of the system to the specific work-flow of the clinical

center and its improvement by including the knowledge embedded in retrospective data available.

The work presented in this dissertation addresses those needs. In Chapter 2, an extended literature review reported the mathematical basis and the theory on which the decision making process has been modelled in surgical planning applications. The analysis of the different works validated **H1**, showing that different percutaneous interventions can be modelled through similar constraints. Therefore, Chapter 3 reported the first working prototype built for SEEG planning, able to optimize trajectories based on the analysis of patient images and maximize the most important safety requirements (**H2**). Chapter 4 presented a novel methodology to exploit retrospective data (**H3**), to account for additional surgeons preferences extrapolated by the analysis of manually planned trajectories. Chapter 5 presented the complete decision-support system developed for trajectory planning, which integrates and extends the previous components and modifies the optimization strategy based on the trajectories retrospectively analyzed (**H4**).

## 6.1 Thesis contributions

The Phd research has been focused on the development of a decision-support system focused on the planning of SEEG trajectories. The tools developed along the thesis allow the automated planning of electrode trajectories based on the preferences expressed by the final user and the knowledge extracted by the analysis of retrospective data.

The first contribution (**C1**) of the thesis is represented by the extended literature review presented in Chapter 2, which introduces the user to the general concepts of trajectory planning modelling in percutaneous surgical applications. To the author knowledge, it is the first survey which revises this topic from a methodological point of view, reporting the different methods and clinical applications and analyzing how clinical requirements have been translated into geometrical constraints. Based on that, in Chapter 3, the first prototype of a SEEG planning method has been presented, following the concepts expressed in the first chapter. We designed it with a modular architecture, using 3D Slicer as a development framework. It was composed by three different modules focused on (i) the image processing of the patient images, (ii) the optimization of trajectories starting from initial trajectory seeds and (iii) an advanced visualization framework for trajectory revision. The latter offered the classical *probe-eye-view* visualization

mode and the possibility of generating MIP images on the electrode perpendicular plane. A GMM-MRF segmentation method provided the surgeon with an additional tool to segment the vessels in the 2D MIP image. The algorithm proposed allowed the anatomy-driven optimization of electrode trajectories, maximizing the distance from vessels, the insertion angle, and guaranteeing a minimum distance between the electrodes. To this purpose, a novel heuristic algorithm based on graph modelling was presented, able to reduce the computational complexity derived by the number of possible states that each electrode could reach. The method has been proved to be more efficient than a classical brute force approach. A retrospective quantitative evaluation was performed using manually planned trajectories on 20 patients: the planning algorithm optimized and improved trajectories in $98\%$ of cases. We were able to resolve and optimize the remaining $2\%$ by applying electrode specific constraints based on manual planning values. In addition, we found that the global parameters used discards $68\%$ of the manual planned trajectories, even when they represent a safe clinical choice. The latter suggests that additional constraints and optimization values must be used to better reproduce the clinical practice.

The second contribution (**C2**) relies on the novel method proposed in Chapter 4, focused on the exploitation of the embedded knowledge contained in the retrospective manually planned trajectories available. The results obtained in the work presented in Chapter 3 suggested that studying the clinical practice by means of retrospective planned trajectories could provide useful information to improve our optimization strategy. Additionally, we wanted to improve the initialization procedure of our planning module, to reduce the interaction required to the user. The method presented classified manually planned trajectories based on the relevant anatomical regions crossed, according to the anatomical atlas used for brain parcellation. We analyzed the data from $75$ anonymized patients, obtaining 30 exploratory patterns and 61 mean trajectories represented in an average brain space. A preliminary validation on a test set showed that we were able to correctly map $90\%$ of those trajectories and, after optimization, they had comparable or better values than manually planned trajectories in terms of distance from vessels and insertion angle. Finally, by detecting and analyzing similar plans, we were able to identify $8$ planning strategies, which represent tailored sets of trajectories that neurosurgeons used to deal with the different patient cases. In this way, we could reduce the level of interaction requested to the user to the selection of a planning strategy, instead of initializing each electrode trajectory or defining specific parameter values

to run the optimization.

The last contribution of the thesis (**C3**) regards the decision-support system for SEEG planning presented in Chapter 5, integrating the previous developments. The system described was composed by an initialization module able to extrapolate a set of trajectories from the analysis of retrospective data, which were proposed to the surgeon by a simple dedicated graphical user interface. The module allowed the initialization of new patient cases, by registering them to the specific anatomy and providing spatial and anatomical priors to the optimization strategy. The latter was modified with respect to the initial version, adapting its strategy based on the type of trajectory to optimize. We introduced the concept of trajectory profile, meaning a set of specific parameters depending on the anatomical zones to explore. The final cost functions included the maximization of the distance from vascular structure (sulci avoidance), the minimization of the insertion angle and the maximization of the recorded grey matter. The heuristic algorithm presented in Chapter 3 for conflict resolution among the electrodes was updated to guarantee a larger inter-electrode distance at the target point, taking into account the screw dimensions. Two neurosurgeons working in a high-volume hospital validated our system, on $15$ retrospective patient data sets and reviewed more than $200$ trajectories. The surgeons were able to reproduce $\sim 95\%$ of their manually planned trajectories through the use of the initialization module. After the automated planning module optimization, both surgeons considered $\sim 81\%$ of the optimized trajectories clinically feasible. Quantitative comparison of distance from vessels, insertion angle and grey matter recording index showed that the optimized trajectories reached superior or comparable values with respect to the original manual plans. The decision-support system presented is able to propose a relevant number of clinically feasible trajectories for SEEG, adapting its optimization strategy thanks to the analysis of retrospective data. The architecture presented sets the basis of an adaptable surgical planning solution for SEEG. The results suggest that a tailored center-based solution increase the acceptability of the proposed trajectories.

## 6.2 Impact, limitations and future challenges

SEEG has been proved to be a safe surgery [27, 143], which can provide great support in the localization of the epileptogenic zone. At the same time, the intervention is part of a very complex scenario where a multidisciplinary team collaborates in the analysis of different source of data:

video-telemetry, neuroimaging and neuro-psychological. The planning of electrode trajectories is defined around the EZ hypotheses, and a careful study of the patient's anatomy is required to identify the optimal insertion paths to guarantee his/her safety, increasing the work load of surgeons.

Although SEEG was introduced in the late 50s, only over the last decade the procedure has been adopted in an increasing number of clinical centers, probably with the spread of robotic assistants and advances in the medical imaging field [211]. In this context, decision support systems aimed to reduce the planning work load and to assist the surgeons in the definition of optimal trajectories has gained importance.

This has been the main topic of this doctoral research, which investigated the methodologies focused on SEEG trajectory planning modelling, with the goal of providing automated tools based on image analysis and optimization theory. Other authors have proposed similar systems for SEEG [45, 186, 214] and other disciplines [90, 125], demonstrating their efficacy with respect to the traditional clinical practice. However, as evidenced in [198, 199], there is no simple or obvious solution in the definition of surgical trajectories, and there is a great variability between the experience and the medical workflows of clinical centers.

Following this idea, the methods presented have been designed to be adaptable to the clinical practice of the center by the analysis of its own data. The advantages of this approach are manifolds:

- the system developed can be continuously improved by including new or different trajectories, as well as further studies can lead to additional parameters to consider;
- the methodology presented (Chapter 4) may be applied to any center, having its retrospecting data available, allowing the adaptation of the system to its specific workflow;
- the initialization module can act as a transfer learning system, allowing to set trajectory-specific parameters from a center to another, as well as helping junior surgeons in the definition of exploratory strategies.

The system has been implanted at Niguarda hospital, for further validations and improvements. The results obtained in the retrospective qualitative validation are very promising, however they highlighted specific improvements that will be object of study in the future.

Despite the promising results of the system proposed along the thesis, we must address a series of limitations that should be considered and discussed. First of all, all the results presented are based on retrospective analysis: despite retrospective studies may be very useful and effective for the evaluation of a CAP solution, especially when combined with a qualitative evaluation performed by experienced users, they still lack of realism. Both external or internal raters, which analyze a retrospective data set, may be biased by the fact that such trajectories won't be implanted. Also, additional clinical considerations which may raise by the discussion with neurologists and epileptologists cannot be taken into account, while they surely influence the final electrode positions. A prospective study, similar to the one proposed in [198], would allow to really evaluate the benefits or improvements points with respect to the real clinical practice. To this purpose, we are planning to conduct a prospective study on a set of patient, comparing the final planning solution obtained by the usage of our system with respect to a traditional planning method. An external rater from the institution should evaluate the planning proposed by two independent surgeons, considering all the clinical aspects of the cases. To this purpose, a specific software module has been already developed, which allows to export the computed trajectories in a format compatible with the software of the surgical robot used.

A second limitation of this work is the fact that bending of electrodes has not been considered. As presented in Chapter 2, only few works have considered the deformation between the tools and soft tissues in their planning frameworks. Commonly, such estimations rely on FEM-based approaches, which are likely to increase the computational complexity of the problem and, consequently, the planning time. Despite this, electrode bending is an outstanding problem in SEEG [29], that should be further analysed. An alternative approximation could be the study of hidden variables that may cause deviation between the planned and implanted trajectory, such as the insertion angle, the thickness of the skull or the distance between the skull and the cortical entry point. The analysis of the retrospective data collected, compared with the segmentation of the electrodes provided by the post-operative images, could lead to new considerations aimed to mitigate the bending factors, which may be taken into account during the trajectory optimization step. In the future, this would be object of study.

Finally, the thesis has been focused on the modelling of the surgical planning decision process, and no particular novel algorithms have been presented regarding the image processing part. The latter has been solved by the usage of already developed software packages such as Freesurfer

[66], able to provide a satisfactory reconstruction the cortical surface as well the segmentation of different structures based on atlases. Despite this, the usage of external software tools may introduce errors which directly affect the final planning, and an accurate evaluation of the pre-processing steps must be performed and acknowledge the limitations of those. For instance, in the validation presented in chapter 5, we found that part of the trajectories could not reach their maximum length due to errors in the reconstruction steps or sub-segmentation of specific zones such as the hippocampus.
Especially in SEEG, a robust and precise vascular segmentation will increase the quality of the proposed trajectories, as reflected by ours results and other studies [198, 200]. Thanks to the image modality used by our partner institution [31], simple methods based on intensity thresholds and morphological filtering allowed a satisfactory segmentation of the vascular tree. However, the final result is far from perfect, and require the user to select the threshold for each case, making the method very subjective. Assuming these limitations, we firstly developed a specific module able to enhance the vascular visualization during the trajectory check phase [178], to ensure a correct quality control of the solutions proposed by our system. Despite this, ongoing work is exploring deep learning techniques to improve the vascular segmentation used for the automated planning [58].

This work has only scratched the surface of SEEG modelling. As regard the application presented in this thesis, only structural image modalities were used. The integration with functional elements such as fMRI and EEG signals could provide great support to the actual system, possibly allowing the automatic definition of the EZ hypothesis and the selection of the most appropriate electrode set. Much work is still required to integrate these tools with post-operative signal analysis, to relate electrical activity with the anatomical positions of the electrodes and provide a complete platform for SEEG assistance.

Finally, it must be stressed that scientific models (as the one described in this thesis) are just representation of the reality [74]. Especially in the biomedical domain, in those applications which involve patients, models (and the applications built on them) must be used carefully, understanding their limits and the approximations behind them. The final result cannot be trust "*a priori*", but should always be reviewed by an experienced user able to judge the proposed solution.

# Scientific publications

Part of the methodologies reported in this PhD dissertation were presented in the following peer-reviewed publications.

## Journal publications

**Scorza, D.**, El Hadji, S., Cortés, C., Bertelsen, À., De Momi, E. "Surgical planning assistance in keyhole minimally invasive surgery: a systematic review". In *Medical Image Analysis*, to be submitted.

**Scorza, D.**, Rizzi, M., De Momi, E., Cortés, C., Bertelsen, À., Cardinale, F. "Data-based automated planning system for StereoElectroEncephaloGraphy: a center-based scenario". In *Annals of Biomedical Engineering*, under-revision.

El Hadji, S., Moccia, S., **Scorza, D.**, Francesco, C., Baselli, G., De Momi, E. "Cerebrovasculature segmentation via fully convolutional neural network for SEEG trajectory planning". In *International journal of computer assisted radiology and surgery*, under revision.

**Scorza, D.**, Amoroso, G., Cortès, C., Artetxe, A., Bertelsen, À., Rizzi, M., ... Kabongo, L. "Experience-based SEEG planning: from retrospective data to automated electrode trajectories suggestions". In *Healthcare technology letters*, 5(5), 167-171, 2018.

**Scorza, D.**, De Momi, E., Plaino, L., Amoroso, G., Arnulfo, G., Narizzano, M., ... Cardinale, F. "Retrospective evaluation and SEEG trajectory analysis for interactive multi-trajectory planner assistant". In *International journal of computer assisted radiology and surgery*, 12(10), 1727-1738, 2017.

Cardinale, F., Rizzi, M., d'Orio, P., Casaceli, G., Arnulfo, G., Narizzano, M., **Scorza, D.**... Sberna, M. "A new tool for touch-free patient registration for robot-assisted intracranial surgery: application accuracy from a phantom study and a retrospective surgical series". In *Neurosurgical focus*, 42(5), E8, 2017.

Cortès, C., de los Reyes-Guzmàn, A., **Scorza, D.**, Bertelsen, À., Carrasco, E., Gil-Agudo, Á., ... Flòrez, J. "Inverse kinematics for upper limb compound movement estimation in exoskeleton-assisted rehabilitation", in *BioMed research international*, 2016.

## Conference proceedings

El Hadji, S., Moccia, S., **Scorza, D.**, Michele, R., Francesco, C., Baselli, G., De Momi, E. "Brain-vascular segmentation for SEEG planning via a 3Dfully-convolutional neural network". In *Engineering in Medicine and Biology Conference*, 2019.

Favaro, A., Cerri, L., **Scorza, D.**, De Momi, E. "Automatic multi-trajectory planning solution for steerable catheters". In *2018 International Symposium on Medical Robotics (ISMR)* (pp. 1-6), 2018, March.

**Scorza, D.**, S. Moccia, G. De Luca, L. Plaino, F. Cardinale, Leonardo S. Mattos, L. Kabongo, E. De Momi, "Safe electrode trajectory planning in SEEG via MIP–based vessel segmentation," in *Medical Imaging 2017: Image–Guided Procedures, Robotic Interventions, and Modeling*, vol. 10135, page 101352C. International Society for Optics and Photonics, 2017.

Bertelsen, Á., **Scorza, D.**., Cortés, C., Onativia, J., Escudero, Á., Sánchez, E., Presa, J. "Collaborative Robots for Surgical Applications". In *Iberian Robotics conference* (pp. 524-535). Springer, Cham, 2017.

# List of Abbreviations

| | |
|---|---|
| SEEG | StereoElectroEncephaloGraphy |
| ILAE | International League Against Epilepsy |
| DRFE | Drug Resistant Focal Epilepsy |
| EZ | Epileptogenic Zone |
| MRI | Magnetic Resonance Imaging |
| MRA | Magnetic Resonance Angiography |
| PET | Positron Emission Tomography |
| SPECT | Single Photon Emission Computed Tomography |
| CBCT | Cone Beam Computed Tomography |
| CE-CBCT | Contrast Enhanced CBCT |
| DBS | Deep Brain Stimulation |
| MWA | MicroWave Ablation |
| RFA | RadioFrequency Ablation |
| LiTT | Laser interstitial Thermal Therapy |
| CRYO | CryoAblation |
| SP | Screw Placement |
| EP | Entry Point |
| TP | Target Point |
| GM | Gray Matter |
| MP | Manual Plan or Manually Planned |
| IP | Initialized Plan |
| OPT | Optimized Plan |
| DSS | Decision Support System |

# List of Figures

## List of Figures

# List of Tables

**List of Tables**

# Bibliography

[1] Niki Abolhassani, Rajni Patel, and Mehrdad Moallem. Needle insertion into soft tissue: A survey. *Medical engineering & physics*, 29(4):413–431, 2007.

[2] Seyed-Ahmad Ahmadi, Tassilo Klein, Nassir Navab, Ran Roth, Reuben R Shamir, Leo Joskowicz, Elena DeMomi, Giancarlo Ferrigno, Luca Antiga, and Roberto Israel Foroni. Advanced planning and intra-operative validation for robot-assisted keyhole neurosurgery in robocast. In *2009 International Conference on Advanced Robotics*, pages 1–7. IEEE, 2009.

[3] Hasan Al-Marzouqi, Jack H Noble, Frank M Warren, Robert F Labadie, J Michael Fitzpatrick, and Benoit Dawant. Planning a safe drilling path for cochlear implantation surgery using image registration techniques. In *Medical Imaging 2007: Visualization and Image-Guided Procedures*, volume 6509, page 650933. International Society for Optics and Photonics, 2007.

[4] Inga Altrogge, Tim Kröger, Tobias Preusser, Christof Büskens, Philippe L Pereira, Diethard Schmidt, Andreas Weihusen, and Heinz-Otto Peitgen. Towards optimization of probe placement for radio-frequency ablation. In *International Conference on Medical Image Computing and Computer-Assisted Intervention*, pages 486–493. Springer, 2006.

[5] Inga Altrogge, Tobias Preusser, Tim Kröger, Christof Büskens, Philippe L Pereira, Diethard Schmidt, and Heinz-Otto Peitgen. Multiscale optimization of the probe placement for radiofrequency ablation. *Academic radiology*, 14(11):1310–1324, 2007.

[6] Johan Andersson. A survey of multiobjective optimization in engineering design. *Department of Mechanical Engineering, Linktjping University. Sweden*, 2000.

[7] Gabriele Arnulfo, Massimo Narizzano, Francesco Cardinale, Marco Massimo Fato, and Jaakko Matias Palva. Automatic segmentation of deep intracerebral electrodes in computed tomography scans. *BMC bioinformatics*, 16(1):99, 2015.

[8] John Ashburner. Spm: a history. *Neuroimage*, 62(2):791–800, 2012.

[9] Claire Baegert, Caroline Villard, Pascal Schreck, and Luc Soler. Multi-criteria trajectory planning for hepatic radiofrequency ablation. In *International Conference on Medical Image Computing and Computer-Assisted Intervention*, pages 676–684. Springer, 2007.

[10] Claire Baegert, Caroline Villard, Pascal Schreck, and Luc Soler. Precise determination of regions of interest for hepatic rfa planning. In *Medical Imaging 2007: Visualization and*

## Bibliography

*Image-Guided Procedures*, volume 6509, page 650923. International Society for Optics and Photonics, 2007.

[11] Claire Baegert, Caroline Villard, Pascal Schreck, Luc Soler, and Afshin Gangi. Trajectory optimization for the planning of percutaneous radiofrequency ablation of hepatic tumors. *Computer Aided Surgery*, 12(2):82–90, 2007.

[12] R Baissalov, George A Sandison, D Reynolds, and K Muldrew. Simultaneous optimization of cryoprobe placement and thermal protocol for cryosurgery. *Physics in Medicine & Biology*, 46(7):1799, 2001.

[13] Saeed M Bakhshmand, Roy Eagleson, and Sandrine de Ribaupierre. Multimodal connectivity based eloquence score computation and visualisation for computer-aided neurosurgical path planning. 4:152–156, 2017.

[14] J. Bancaud, J: Talairach. *La Stereo-Electroencephalographie dans l' Épilepsie.* Editeurs, Masson & Cie, 1965.

[15] Meike Becker, Ralf Gutbell, Igor Stenin, and Stefan Wesarg. Towards automatic path planning for multi-port minimally-traumatic lateral skull base surgery. In *Workshop on Clinical Image-Based Procedures*, pages 59–66. Springer, 2012.

[16] Meike Becker, Stefan Hansen, Stefan Wesarg, and Georgios Sakas. Path planning for multi-port lateral skull base surgery based on first clinical experiences. In *Workshop on Clinical Image-Based Procedures*, pages 23–30. Springer, 2013.

[17] Esia Belbachir, Ehsan Golkar, Bernard Bayle, and Caroline Essert. Automatic planning of needle placement for robot-assisted percutaneous procedures. *International journal of computer assisted radiology and surgery*, 13(9):1429–1438, 2018.

[18] Alim Louis Benabid, Stephan Chabardes, John Mitrofanis, and Pierre Pollak. Deep brain stimulation of the subthalamic nucleus for the treatment of parkinson's disease. *The Lancet Neurology*, 8(1):67–81, 2009.

[19] Eren Berber. The first clinical application of planning software for laparoscopic microwave thermosphere ablation of malignant liver tumours. *HPB*, 17(7):632–636, 2015.

[20] Silvain Bériault, Fahd Al Subaie, D Louis Collins, Abbas F Sadikot, and G Bruce Pike. A multi-modal approach to computer-assisted deep brain stimulation trajectory planning. *International journal of computer assisted radiology and surgery*, 7(5):687–704, 2012.

[21] Silvain Bériault, Fahd Al Subaie, Kelvin Mok, Abbas F Sadikot, and G Bruce Pike. Automatic trajectory planning of dbs neurosurgery from multi-modal mri datasets. In *International Conference on Medical Image Computing and Computer-Assisted Intervention*, pages 259–266. Springer, 2011.

[22] Silvain Bériault, Simon Drouin, Abbas F Sadikot, Yiming Xiao, D Louis Collins, and G Bruce Pike. A prospective evaluation of computer-assisted deep brain stimulation trajectory planning. In *Workshop on Clinical Image-Based Procedures*, pages 42–49. Springer, 2012.

[23] Nikolaos G. Bourbakis and Mariette Awad. A 3-d visualization method for image-guided brain surgery. *IEEE Transactions on Systems, Man, and Cybernetics, Part B (Cybernetics)*, 33(5):766–781, 2003.

[24] Edward B Bromfield, José E Cavazos, and Joseph I Sirven. Basic mechanisms underlying seizures and epilepsy. In *An Introduction to Epilepsy [Internet]*. American Epilepsy Society, 2006.

[25] Ellen JL Brunenberg, Anna Vilanova, Veerle Visser-Vandewalle, Yasin Temel, Linda Ackermans, Bram Platel, and Bart M ter Haar Romeny. Automatic trajectory planning for deep brain stimulation: a feasibility study. In *International Conference on Medical Image Computing and Computer-Assisted Intervention*, pages 584–592. Springer, 2007.

[26] Torsten Butz, Simon K Warfield, Kemal Tuncali, Stuart G Silverman, Eric van Sonnenberg, Ferenc A Jolesz, and Ron Kikinis. Pre-and intra-operative planning and simulation of percutaneous tumor ablation. In *International Conference on Medical Image Computing and Computer-Assisted Intervention*, pages 317–326. Springer, 2000.

[27] Francesco Cardinale, Giuseppe Casaceli, Fabio Raneri, Jonathan Miller, and Giorgio Lo Russo. Implantation of stereoelectroencephalography electrodes: a systematic review. *Journal of Clinical Neurophysiology*, 33(6):490–502, 2016.

[28] Francesco Cardinale, Giuseppa Chinnici, Manuela Bramerio, Roberto Mai, Ivana Sartori, Massimo Cossu, Giorgio Lo Russo, Laura Castana, Nadia Colombo, Chiara Caborni, et al. Validation of freesurfer-estimated brain cortical thickness: comparison with histologic measurements. *Neuroinformatics*, 12(4):535–542, 2014.

[29] Francesco Cardinale, Massimo Cossu, Laura Castana, Giuseppe Casaceli, Marco Paolo Schiariti, Anna Miserocchi, Dalila Fuschillo, Alessio Moscato, Chiara Caborni, Gabriele Arnulfo, et al. Stereoelectroencephalography: surgical methodology, safety, and stereotactic application accuracy in 500 procedures. *Neurosurgery*, 72(3):353–366, 2012.

[30] Francesco Cardinale, Anna Miserocchi, Alessio Moscato, Massimo Cossu, Laura Castana, Marco Paolo Schiariti, Francesca Gozzo, Guglielmo Pero, Luca Quilici, Alberto Citterio, et al. Talairach methodology in the multimodal imaging and robotics era. *Stereotaxy and epilepsy surgery*, pages 245–272, 2012.

[31] Francesco Cardinale, Guglielmo Pero, Luca Quilici, Mariangela Piano, Paola Colombo, Alessio Moscato, Laura Castana, Giuseppe Casaceli, Dalila Fuschillo, Luciana Gennari, et al. Cerebral angiography for multimodal surgical planning in epilepsy surgery: description of a new three-dimensional technique and literature review. *World neurosurgery*, 84(2):358–367, 2015.

[32] Francesco Cardinale, Michele Rizzi, Piergiorgio dâOrio, Giuseppe Casaceli, Gabriele Arnulfo, Massimo Narizzano, Davide Scorza, Elena De Momi, Michele Nichelatti, Daniela Redaelli, et al. A new tool for touch-free patient registration for robot-assisted intracranial surgery: application accuracy from a phantom study and a retrospective surgical series. *Neurosurgical focus*, 42(5):E8, 2017.

[33] Francesco Cardinale, Michele Rizzi, Elena Vignati, Massimo Cossu, Laura Castana, Piergiorgio dâOrio, Martina Revay, Martina Della Costanza, Laura Tassi, Roberto Mai, Ivana Sartori, Lino Nobili, Francesca Gozzo, Veronica Pelliccia, Valeria Mariani, Giorgio Lo Russo, and Stefano Francione. Stereoelectroencephalography: retrospective analysis of 742 procedures in a single centre. *Brain*, 07 2019.

[34] M Jorge Cardoso, Marc Modat, Robin Wolz, Andrew Melbourne, David Cash, Daniel Rueckert, and Sebastien Ourselin. Geodesic information flows: spatially-variant graphs and their application to segmentation and fusion. *IEEE transactions on medical imaging*, 34(9):1976–1988, 2015.

[35] Chun-Cheng R Chen, Michael I Miga, and Robert L Galloway. Optimizing needle placement in treatment planning of radiofrequency ablation. In *Medical Imaging 2006: Visualization, Image-Guided Procedures, and Display*, volume 6141, page 614124. International Society for Optics and Photonics, 2006.

[36] Rendong Chen, Fang Lu, Kaifeng Wang, Dexing Kong, et al. Semiautomatic radiofrequency ablation planning based on constrained clustering process for hepatic tumors. *IEEE Transactions on Biomedical Engineering*, 65(3):645–657, 2017.

[37] D Louis Collins, Colin J Holmes, Terrence M Peters, and Alan C Evans. Automatic 3-d model-based neuroanatomical segmentation. *Human brain mapping*, 3(3):190–208, 1995.

## Bibliography


[38] D Louis Collins, Peter Neelin, Terrence M Peters, and Alan C Evans. Automatic 3d intersubject registration of mr volumetric data in standardized talairach space. *Journal of computer assisted tomography*, 18(2):192–205, 1994.

[39] D Louis Collins, Alex P Zijdenbos, Wim FC Baaré, and Alan C Evans. Animal+ insect: improved cortical structure segmentation. In *Biennial International Conference on Information Processing in Medical Imaging*, pages 210–223. Springer, 1999.

[40] Yunfei Cui, Zhiqiang Geng, Qunxiong Zhu, and Yongming Han. Multi-objective optimization methods and application in energy saving. *Energy*, 125:681–704, 2017.

[41] N Daemi, Alireza Ahmadian, Alireza Mirbagheri, AH Ahmadian, Hooshang Saberi, F Amidi, and Javad Alirezaie. Planning screw insertion trajectory in lumbar spinal fusion using preoperative ct images. In *2015 37th Annual International Conference of the IEEE Engineering in Medicine and Biology Society (EMBC)*, pages 3639–3642. IEEE, 2015.

[42] Per-Erik Danielsson. Euclidean distance mapping. *Computer Graphics and image processing*, 14(3):227–248, 1980.

[43] Benoit M Dawant, Steven L Hartmann, J-P Thirion, Frederik Maes, Dirk Vandermeulen, and Philippe Demaerel. Automatic 3-d segmentation of internal structures of the head in mr images using a combination of similarity and free-form transformations. i. methodology and validation on normal subjects. *IEEE transactions on medical imaging*, 18(10):909–916, 1999.

[44] Alejandro De León-Cuevas, Saúl Tovar-Arriaga, Arturo González-Gutiérrez, and Marco Antonio Aceves-Fernández. Risk map generation for keyhole neurosurgery using fuzzy logic for trajectory evaluation. *Neurocomputing*, 233:81–89, 2017.

[45] Elena De Momi, Chiara Caborni, Francesco Cardinale, Giuseppe Casaceli, Laura Castana, Massimo Cossu, Roberto Mai, Francesca Gozzo, Stefano Francione, Laura Tassi, et al. Multitrajectories automatic planner for stereoelectroencephalography (seeg). *International journal of computer assisted radiology and surgery*, 9(6):1087–1097, 2014.

[46] Elena De Momi, Chiara Caborni, Francesco Cardinale, Laura Castana, Giuseppe Casaceli, Massimo Cossu, Luca Antiga, and Giancarlo Ferrigno. Automatic trajectory planner for stereoelectroencephalography procedures: a retrospective study. *IEEE Transactions on Biomedical Engineering*, 60(4):986–993, 2012.

[47] Zhong-Shan Deng and Jing Liu. Computerized planning of multi-probe cryosurgical treatment for tumor with complex geometry. In *ASME 2007 International Mechanical Engineering Congress and Exposition*, pages 97–101. American Society of Mechanical Engineers, 2007.

[48] Olga Dergachyova, Yulong Zhao, Claire Haegelen, Pierre Jannin, and Caroline Essert. Automatic preoperative planning of dbs electrode placement using anatomo-clinical atlases and volume of tissue activated. *International journal of computer assisted radiology and surgery*, 13(7):1117–1128, 2018.

[49] Rahul S Desikan, Florent Ségonne, Bruce Fischl, Brian T Quinn, Bradford C Dickerson, Deborah Blacker, Randy L Buckner, Anders M Dale, R Paul Maguire, Bradley T Hyman, et al. An automated labeling system for subdividing the human cerebral cortex on mri scans into gyral based regions of interest. *Neuroimage*, 31(3):968–980, 2006.

[50] P-F D'Haese, Ebru Cetinkaya, Peter E Konrad, Chris Kao, and Benoit M Dawant. Computer-aided placement of deep brain stimulators: from planningto intraoperative guidance. *IEEE transactions on medical imaging*, 24(11):1469–1478, 2005.

[51] Pierre-François D'Haese, Srivatsan Pallavaram, Rui Li, Michael S Remple, Chris Kao, Joseph S Neimat, Peter E Konrad, and Benoit M Dawant. Cranialvault and its crave tools: a clinical computer assistance system for deep brain stimulation (dbs) therapy. *Medical image analysis*, 16(3):744–753, 2012.

[52] Mario Di Silvestre, Patrizio Parisini, Francesco Lolli, and Georgios Bakaloudis. Complications of thoracic pedicle screws in scoliosis treatment. *Spine*, 32(15):1655–1661, 2007.

[53] Dennis J Dlugos. The early identification of candidates for epilepsy surgery. *Archives of neurology*, 58(10):1543–1546, 2001.

[54] Gerald D Dodd, Mark S Frank, Manohar Aribandi, Shailendra Chopra, and Kedar N Chintapalli. Radiofrequency thermal ablation: computer analysis of the size of the thermal injury created by overlapping ablations. *American Journal of Roentgenology*, 177(4):777–782, 2001.

[55] John S Duncan. Imaging and epilepsy. *Brain: a journal of neurology*, 120(2):339–377, 1997.

[56] Tiziano DâAlbis, Claire Haegelen, Caroline Essert, Sara Fernández-Vidal, Florent Lalys, and Pierre Jannin. Pydbs: an automated image processing workflow for deep brain stimulation surgery. *International journal of computer assisted radiology and surgery*, 10(2):117–128, 2015.

[57] Lars C Ebert, Martin Fürst, Wolfgang Ptacek, Thomas D Ruder, Dominic Gascho, Wolf Schweitzer, Michael J Thali, and Patricia M Flach. Automatic entry point planning for robotic post-mortem ct-based needle placement. *Forensic science, medicine, and pathology*, 12(3):336–342, 2016.

[58] Sara EL HADJI, Sara Moccia, Davide Scorza, Rizzi Michele, Cardinale Francesco, Giuseppe Baselli, Elena DE MOMI, et al. Brain-vascular segmentation for seeg planning via a 3dfully-convolutional neural network. In *Engineering in Medicine and Biology Conference*, 2019.

[59] Dario J Englot. A modern epilepsy surgery treatment algorithm: incorporating traditional and emerging technologies. *Epilepsy & Behavior*, 80:68–74, 2018.

[60] Caroline Essert, Sara Fernandez-Vidal, Antonio Capobianco, Claire Haegelen, Carine Karachi, Eric Bardinet, Maud Marchal, and Pierre Jannin. Statistical study of parameters for deep brain stimulation automatic preoperative planning of electrodes trajectories. *International journal of computer assisted radiology and surgery*, 10(12):1973–1983, 2015.

[61] Caroline Essert, Claire Haegelen, and Pierre Jannin. Automatic computation of electrodes trajectory for deep brain stimulation. In *International Workshop on Medical Imaging and Virtual Reality*, pages 149–158. Springer, 2010.

[62] Caroline Essert, Claire Haegelen, Florent Lalys, Alexandre Abadie, and Pierre Jannin. Automatic computation of electrode trajectories for deep brain stimulation: a hybrid symbolic and numerical approach. *International journal of computer assisted radiology and surgery*, 7(4):517–532, 2012.

[63] Caroline Essert, Maud Marchal, Sara Fernandez-Vidal, Tiziano DâAlbis, Eric Bardinet, Claire Haegelen, Marie-Laure Welter, Jérôme Yelnik, and Pierre Jannin. Automatic parameters optimization for deep brain stimulation trajectory planning. In *Proceedings of MICCAI workshop DBSMC*, volume 12, pages 20–29, 2012.

[64] Carlos Faria, Wolfram Erlhagen, Manuel Rito, Elena De Momi, Giancarlo Ferrigno, and Estela Bicho. Review of robotic technology for stereotactic neurosurgery. *IEEE reviews in biomedical engineering*, 8:125–137, 2015.

[65] Alberto Favaro, Akash Lad, Davide Formenti, Davide Danilo Zani, and Elena De Momi. Straight trajectory planning for keyhole neurosurgery in sheep with automatic brain structures segmentation. In *Medical Imaging 2017: Image-Guided Procedures, Robotic Interventions, and Modeling*, volume 10135, page 101352E. International Society for Optics and Photonics, 2017.

[66] Bruce Fischl. Freesurfer. *Neuroimage*, 62(2):774–781, 2012.

## Bibliography


[67] Bruce Fischl, David H Salat, Evelina Busa, Marilyn Albert, Megan Dieterich, Christian Haselgrove, Andre Van Der Kouwe, Ron Killiany, David Kennedy, Shuna Klaveness, et al. Whole brain segmentation: automated labeling of neuroanatomical structures in the human brain. *Neuron*, 33(3):341–355, 2002.

[68] Bruce Fischl, André Van Der Kouwe, Christophe Destrieux, Eric Halgren, Florent Ségonne, David H Salat, Evelina Busa, Larry J Seidman, Jill Goldstein, David Kennedy, et al. Automatically parcellating the human cerebral cortex. *Cerebral cortex*, 14(1):11–22, 2004.

[69] Robert S Fisher, Carlos Acevedo, Alexis Arzimanoglou, Alicia Bogacz, J Helen Cross, Christian E Elger, Jerome Engel Jr, Lars Forsgren, Jacqueline A French, Mike Glynn, et al. Ilae official report: a practical clinical definition of epilepsy. *Epilepsia*, 55(4):475–482, 2014.

[70] Robert S Fisher, Walter Van Emde Boas, Warren Blume, Christian Elger, Pierre Genton, Phillip Lee, and Jerome Engel Jr. Epileptic seizures and epilepsy: definitions proposed by the international league against epilepsy (ilae) and the international bureau for epilepsy (ibe). *Epilepsia*, 46(4):470–472, 2005.

[71] Robert S Fisher, J Helen Cross, Jacqueline A French, Norimichi Higurashi, Edouard Hirsch, Floor E Jansen, Lieven Lagae, Solomon L Moshé, Jukka Peltola, Eliane Roulet Perez, et al. Operational classification of seizure types by the international league against epilepsy: Position paper of the ilae commission for classification and terminology. *Epilepsia*, 58(4):522–530, 2017.

[72] Alejandro F Frangi, Wiro J Niessen, Koen L Vincken, and Max A Viergever. Multiscale vessel enhancement filtering. In *International conference on medical image computing and computer-assisted intervention*, pages 130–137. Springer, 1998.

[73] Moti Freiman, Leo Joskowicz, Noah Broide, Miriam Natanzon, E Nammer, Ofek Shilon, Lior Weizman, and Jacob Sosna. Carotid vasculature modeling from patient ct angiography studies for interventional procedures simulation. *International journal of computer assisted radiology and surgery*, 7(5):799–812, 2012.

[74] Roman Frigg and Stephan Hartmann. Models in science. 2006.

[75] Chaowei Gao, Li Chen, Bochao Hou, Xiaojing Liu, and Chuanbin Guo. Precise and semi-automatic puncture trajectory planning in craniofacial surgery: A prototype study. In *2014 7th International Conference on Biomedical Engineering and Informatics*, pages 617–622. IEEE, 2014.

[76] Nicolas Gerber, Brett Bell, Kate Gavaghan, Christian Weisstanner, Marco Caversaccio, and Stefan Weber. Surgical planning tool for robotically assisted hearing aid implantation. *International journal of computer assisted radiology and surgery*, 9(1):11–20, 2014.

[77] J Goerres, A Uneri, T De Silva, M Ketcha, S Reaungamornrat, M Jacobson, S Vogt, G Kleinszig, Greg Osgood, JP Wolinsky, et al. Spinal pedicle screw planning using deformable atlas registration. *Physics in Medicine & Biology*, 62(7):2871, 2017.

[78] J Goerres, A Uneri, M Jacobson, B Ramsay, T De Silva, M Ketcha, R Han, A Manbachi, S Vogt, G Kleinszig, et al. Planning, guidance, and quality assurance of pelvic screw placement using deformable image registration. *Physics in Medicine & Biology*, 62(23):9018, 2017.

[79] Jorge Gonzalez-Martinez, Jeffrey Mullin, Sumeet Vadera, Juan Bulacio, Gwyneth Hughes, Stephen Jones, Rei Enatsu, and Imad Najm. Stereotactic placement of depth electrodes in medically intractable epilepsy. *Journal of neurosurgery*, 120(3):639–644, 2014.

[80] Josephine Granna, Arya Nabavi, and Jessica Burgner-Kahrs. Toward computer-assisted planning for interstitial laser ablation of malignant brain tumors using a tubular continuum robot. In *International Conference on Medical Image Computing and Computer-Assisted Intervention*, pages 557–565. Springer, 2017.

[81] Josephine Granna, Arya Nabavi, and Jessica Burgner-Kahrs. Computer-assisted planning for a concentric tube robotic system in neurosurgery. *International journal of computer assisted radiology and surgery*, 14(2):335–344, 2019.

[82] Gianpiero Gravante, Seok L Ong, Matthew S Metcalfe, Andrew Strickland, Ashley R Dennison, and David M Lloyd. Hepatic microwave ablation: a review of the histological changes following thermal damage. *Liver international*, 28(7):911–921, 2008.

[83] Ned Greene. Environment mapping and other applications of world projections. *IEEE Computer Graphics and Applications*, 6(11):21–29, 1986.

[84] Marc Guénot, Jean Isnard, Philippe Ryvlin, Catherine Fischer, François Mauguière, and Marc Sindou. Seeg-guided rf thermocoagulation of epileptic foci: feasibility, safety, and preliminary results. *Epilepsia*, 45(11):1368–1374, 2004.

[85] Ting Guo, Andrew G Parrent, and Terry M Peters. Automatic target and trajectory identification for deep brain stimulation (dbs) procedures. In *International Conference on Medical Image Computing and Computer-Assisted Intervention*, pages 483–490. Springer, 2007.

[86] Noura Hamzé, Alexandre Bilger, Christian Duriez, Stéphane Cotin, and Caroline Essert. Anticipation of brain shift in deep brain stimulation automatic planning. In *2015 37th Annual International Conference of the IEEE Engineering in Medicine and Biology Society (EMBC)*, pages 3635–3638. IEEE, 2015.

[87] Noura Hamzé, Jimmy Voirin, Pierre Collet, Pierre Jannin, Claire Haegelen, and Caroline Essert. Pareto front vs. weighted sum for automatic trajectory planning of deep brain stimulation. In *International Conference on Medical Image Computing and Computer-Assisted Intervention*, pages 534–541. Springer, 2016.

[88] R Han, A Uneri, T De Silva, M Ketcha, J Goerres, S Vogt, G Kleinszig, Greg Osgood, and JH Siewerdsen. Atlas-based automatic planning and 3d–2d fluoroscopic guidance in pelvic trauma surgery. *Physics in Medicine & Biology*, 64(9):095022, 2019.

[89] Mihály Héder. From NASA to EU: The evolution of the TRL scale in public sector innovation. *The Innovation Journal*, 22(2):1–23, 2017.

[90] A Helck, Christian Schumann, J Aumann, K Thierfelder, FF Strobl, M Braunagel, M Niethammer, Dirk-André Clevert, Ralf-Thorsten Hoffmann, M Reiser, et al. Automatic path proposal computation for ct-guided percutaneous liver biopsy. *International journal of computer assisted radiology and surgery*, 11(12):2199–2205, 2016.

[91] Paul Herghelegiu, Vasile Manta, and Eduard Gröller. Needle-stability maps for brain-tumor biopsies. In *15th International Conference on System Theory, Control and Computing*, pages 1–5. IEEE, 2011.

[92] Paul-Corneliu Herghelegiu, Vasile Manta, Radu Perin, Stefan Bruckner, and E Gröller. Biopsy planner–visual analysis for needle pathway planning in deep seated brain tumor biopsy. In *Computer graphics forum*, volume 31, pages 1085–1094. Wiley Online Library, 2012.

[93] Jan Herzog, Urban Fietzek, Wolfgang Hamel, Andre Morsnowski, Frank Steigerwald, Bettina Schrader, Dieter Weinert, Gerd Pfister, Dieter Müller, Hubertus M Mehdorn, et al. Most effective stimulation site in subthalamic deep brain stimulation for parkinson's disease. *Movement disorders*, 19(9):1050–1054, 2004.

[94] Gregory L Holmes and Yezekiel Ben-Ari. Seizing hold of seizures. *Nature medicine*, 9(8):994, 2003.

[95] Danying Hu, Yuanzheng Gong, Blake Hannaford, and Eric J Seibel. Path planning for semi-automated simulated robotic neurosurgery. In *2015 IEEE/RSJ International Conference on Intelligent Robots and Systems (IROS)*, pages 2639–2645. IEEE, 2015.

## Bibliography

[96] Shijia Huang, Jie Yu, Ping Liang, Xiaoling Yu, Zhigang Cheng, Zhiyu Han, and Qinying Li. Percutaneous microwave ablation for hepatocellular carcinoma adjacent to large vessels: a long-term follow-up. *European journal of radiology*, 83(3):552–558, 2014.

[97] Bahman Jabbari, Michael B Russo, and Michelle L Russo. Electroencephalogram of asymptomatic adult subjects. *Clinical neurophysiology*, 111(1):102–105, 2000.

[98] Amir Jaberzadeh and Caroline Essert. Pre-operative planning of multiple probes in three dimensions for liver cryosurgery: comparison of different optimization methods. *Mathematical Methods in the Applied Sciences*, 39(16):4764–4772, 2016.

[99] Mark Jenkinson, Christian F Beckmann, Timothy EJ Behrens, Mark W Woolrich, and Stephen M Smith. Fsl. *Neuroimage*, 62(2):782–790, 2012.

[100] Shan Jiang, Xiaoyan Liu, and Yongchun Song. 3d trajectory planning based on fem with application of brachytherapy. In *2009 2nd International Conference on Biomedical Engineering and Informatics*, pages 1–5. IEEE, 2009.

[101] Xin Kang, Hongliang Ren, Jing Li, and Wai-Pan Yau. Statistical atlas based registration and planning for ablating bone tumors in minimally invasive interventions. In *2012 IEEE International Conference on Robotics and Biomimetics (ROBIO)*, pages 606–611. IEEE, 2012.

[102] Tina Kapur, Steve Pieper, Andriy Fedorov, Jean-Christophe Fillion-Robin, Michael Halle, Lauren O'Donnell, Andras Lasso, Tamas Ungi, Csaba Pinter, Julien Finet, et al. Increasing the impact of medical image computing using community-based open-access hackathons: The na-mic and 3d slicer experience, 2016.

[103] Tero Karras. Maximizing parallelism in the construction of bvhs, octrees, and k-d trees. In *Proceedings of the Fourth ACM SIGGRAPH/Eurographics conference on High-Performance Graphics*, pages 33–37. Eurographics Association, 2012.

[104] Rostislav Khlebnikov, Bernhard Kainz, Judith Muehl, and Dieter Schmalstieg. Crepuscular rays for tumor accessibility planning. *IEEE transactions on visualization and computer graphics*, 17(12):2163–2172, 2011.

[105] Scott Kirkpatrick, C Daniel Gelatt, and Mario P Vecchi. Optimization by simulated annealing. *science*, 220(4598):671–680, 1983.

[106] Arno Klein and Jason Tourville. 101 labeled brain images and a consistent human cortical labeling protocol. *Frontiers in neuroscience*, 6:171, 2012.

[107] Shawn Klein, Cari M Whyne, Raphael Rush, and Howard J Ginsberg. Ct-based patient-specific simulation software for pedicle screw insertion. *Clinical Spine Surgery*, 22(7):502–506, 2009.

[108] Dejan Knez, Boštjan Likar, Franjo Pernuš, and Tomaž Vrtovec. Automated pedicle screw size and trajectory planning by maximization of fastening strength. In *International Workshop and Challenge on Computational Methods and Clinical Applications for Spine Imaging*, pages 3–13. Springer, 2015.

[109] Dejan Knez, Boštjan Likar, Franjo Pernuš, and Tomaž Vrtovec. Computer-assisted screw size and insertion trajectory planning for pedicle screw placement surgery. *IEEE transactions on medical imaging*, 35(6):1420–1430, 2016.

[110] Dejan Knez, Janez Mohar, Robert J Cirman, Boštjan Likar, Franjo Pernuš, and Tomaž Vrtovec. Manual and computer-assisted pedicle screw placement plans: a quantitative comparison. In *International Workshop on Computational Methods and Clinical Applications for Spine Imaging*, pages 105–115. Springer, 2016.

[111] Dejan Knez, Janez Mohar, Robert J Cirman, Boštjan Likar, Franjo Pernuš, and Tomaž Vrtovec. Variability analysis of manual and computer-assisted preoperative thoracic pedicle screw placement planning. *Spine*, 43(21):1487–1495, 2018.

[112] Dejan Knez, Imad S Nahle, Tomaž Vrtovec, Stefan Parent, and Samuel Kadoury. Computer-assisted pedicle screw placement planning: Towards clinical practice. In *2018 IEEE 15th International Symposium on Biomedical Imaging (ISBI 2018)*, pages 249–252. IEEE, 2018.

[113] Dejan Knez, Imad S Nahle, Tomaž Vrtovec, Stefan Parent, and Samuel Kadoury. Computer-assisted pedicle screw trajectory planning using ct-inferred bone density: a demonstration against surgical outcomes. *Medical physics*, 2019.

[114] Martin H Krag, Bruce D Beynnon, Malcolm H Pope, and Thomas A DeCoster. Depth of insertion of transpedicular vertebral screws into human vertebrae: effect upon screw-vertebra interface strength. *Journal of spinal disorders*, 1(4):287–294, 1988.

[115] George Le Goualher, Christian Barillot, and Yves Bizais. Modeling cortical sulci with active ribbons. *International Journal of Pattern Recognition and Artificial Intelligence*, 11(08):1295–1315, 1997.

[116] Jongwon Lee, Sungmin Kim, Young Soo Kim, and Wan Kyun Chung. Automated segmentation of the lumbar pedicle in ct images for spinal fusion surgery. *IEEE transactions on biomedical engineering*, 58(7):2051–2063, 2011.

[117] Jongwon Lee, Sungmin Kim, Young Soo Kim, and Wan Kyun Chung. Optimal surgical planning guidance for lumbar spinal fusion considering operational safety and vertebra–screw interface strength. *The International Journal of Medical Robotics and Computer Assisted Surgery*, 8(3):261–272, 2012.

[118] Jongwon Lee, Sungmin Kim, Young Soo Kim, Wan Kyun Chung, and Minjun Kim. Automated surgical planning and evaluation algorithm for spinal fusion surgery with three-dimensional pedicle model. In *2011 IEEE/RSJ International Conference on Intelligent Robots and Systems*, pages 2524–2531. IEEE, 2011.

[119] Kuo Li, Vejay N Vakharia, Rachel Sparks, Lucas GS França, Alejandro Granados, Andrew W McEvoy, Anna Miserocchi, Maode Wang, Sebastien Ourselin, and John S Duncan. Optimizing trajectories for cranial laser interstitial thermal therapy using computer-assisted planning: a machine learning approach. *Neurotherapeutics*, 16(1):182–191, 2019.

[120] Kuo Li, Vejay N Vakharia, Rachel Sparks, Roman Rodionov, Sjoerd B Vos, Andrew W McEvoy, Anna Miserocchi, Maode Wang, Sebastien Ourselin, and John S Duncan. Stereoelectroencephalography electrode placement: Detection of blood vessel conflicts. *Epilepsia*, 60(9):1942–1948, 2019.

[121] Wan Cheng Lim, Weian Guo, and Hongliang Ren. An ablation planning system for computer-assisted interventions. In *2013 International Conference on Collaboration Technologies and Systems (CTS)*, pages 487–490. IEEE, 2013.

[122] Cristian A Linte, Jon J Camp, Kurt E Augustine, Paul M Huddleston, Richard A Robb, and David R Holmes III. Estimating pedicle screw fastening strength via a virtual templating platform for spine surgery planning: a retrospective preliminary clinical demonstration. *Computer Methods in Biomechanics and Biomedical Engineering: Imaging & Visualization*, 3(4):204–212, 2015.

[123] Shaoli Liu, Zeyang Xia, Jianhua Liu, Jing Xu, He Ren, Tong Lu, and Xiangdong Yang. Automatic multiple-needle surgical planning of robotic-assisted microwave coagulation in large liver tumor therapy. *PloS one*, 11(3):e0149482, 2016.

[124] Yuan Liu, Benoit M Dawant, Srivatsan Pallavaram, Joseph S Neimat, Peter E Konrad, Pierre-Francois D'Haese, Ryan D Datteri, Bennett A Landman, and Jack H Noble. A surgeon specific automatic path planning algorithm for deep brain stimulation. In *Medical Imaging 2012: Image-Guided Procedures, Robotic Interventions, and Modeling*, volume 8316, page 83161D. International Society for Optics and Photonics, 2012.

## Bibliography

[125] Yuan Liu, Peter E Konrad, Joseph S Neimat, Stephen B Tatter, Hong Yu, Ryan D Datteri, Bennett A Landman, Jack H Noble, Srivatsan Pallavaram, Benoit M Dawant, et al. Multisurgeon, multisite validation of a trajectory planning algorithm for deep brain stimulation procedures. *IEEE Transactions on Biomedical Engineering*, 61(9):2479–2487, 2014.

[126] William E Lorensen and Harvey E Cline. Marching cubes: A high resolution 3d surface construction algorithm. In *ACM siggraph computer graphics*, volume 21, pages 163–169. ACM, 1987.

[127] David C Lung, Thomas F Stahovich, and Yoed Rabin. Computerized planning for multiprobe cryosurgery using a force-field analogy. *Computer Methods in Biomechanics and Biomedical Engineering*, 7(2):101–110, 2004.

[128] Michael J Mack. Minimally invasive and robotic surgery. *Jama*, 285(5):568–572, 2001.

[129] Emmanouil Magiorkinis, Aristidis Diamantis, Kalliopi Sidiropoulou, and Christos Panteliadis. Highights in the history of epilepsy: the last 200 years. *Epilepsy research and treatment*, 2014, 2014.

[130] Christopher B Maks, Christopher R Butson, Benjamin L Walter, Jerrold L Vitek, and Cameron C McIntyre. Deep brain stimulation activation volumes and their association with neurophysiological mapping and therapeutic outcomes. *Journal of Neurology, Neurosurgery & Psychiatry*, 80(6):659–666, 2009.

[131] Amir Manbachi, Richard SC Cobbold, and Howard J Ginsberg. Guided pedicle screw insertion: techniques and training. *The Spine Journal*, 14(1):165–179, 2014.

[132] J-F Mangin, D Riviere, A Cachia, E Duchesnay, Y Cointepas, D Papadopoulos-Orfanos, Paola Scifo, T Ochiai, F Brunelle, and J Regis. A framework to study the cortical folding patterns. *Neuroimage*, 23:S129–S138, 2004.

[133] John C Mankins. Technology readiness levels. *White Paper, April*, 6:1995, 1995.

[134] Hani J Marcus, Vejay N Vakharia, Rachel Sparks, Roman Rodionov, Neil Kitchen, Andrew W McEvoy, Anna Miserocchi, Lewis Thorne, Sebastien Ourselin, and John S Duncan. Computer-assisted versus manual planning for stereotactic brain biopsy: A retrospective comparative pilot study. *Operative Neurosurgery*, 2019.

[135] R Timothy Marler and Jasbir S Arora. Survey of multi-objective optimization methods for engineering. *Structural and multidisciplinary optimization*, 26(6):369–395, 2004.

[136] Dorota Marszalik and Waldemar Rączka. Surgical tool trajectory optimization in brain tumour resection. In *2019 20th International Carpathian Control Conference (ICCC)*, pages 1–4. IEEE, 2019.

[137] Robert CG Martin, Charles R Scoggins, and Kelly M McMasters. Safety and efficacy of microwave ablation of hepatic tumors: a prospective review of a 5-year experience. *Annals of surgical oncology*, 17(1):171–178, 2010.

[138] Thomas Mendel, Florian Radetzki, David Wohlrab, Karsten Stock, Gunther Olaf Hofmann, and Hansrudi Noser. Ct-based 3-d visualisation of secure bone corridors and optimal trajectories for sacroiliac screws. *Injury*, 44(7):957–963, 2013.

[139] A Mikos, D Bowers, AM Noecker, CC McIntyre, M Won, A Chaturvedi, KD Foote, and MS Okun. Patient-specific analysis of the relationship between the volume of tissue activated during dbs and verbal fluency. *Neuroimage*, 54:S238–S246, 2011.

[140] K Jarrod Millman and Michael Aivazis. Python for scientists and engineers. *Computing in Science & Engineering*, 13(2):9–12, 2011.

[141] Sara Moccia, Elena De Momi, Sara El Hadji, and Leonardo S Mattos. Blood vessel segmentation algorithmsâreview of methods, datasets and evaluation metrics. *Computer methods and programs in biomedicine*, 158:71–91, 2018.

[142] David Moher, Alessandro Liberati, Jennifer Tetzlaff, and Douglas G Altman. Preferred reporting items for systematic reviews and meta-analyses: the prisma statement. *Annals of internal medicine*, 151(4):264–269, 2009.

[143] Jeffrey P Mullin, Michael Shriver, Soha Alomar, Imad Najm, Juan Bulacio, Patrick Chauvel, and Jorge Gonzalez-Martinez. Is seeg safe? a systematic review and meta-analysis of stereo-electroencephalography–related complications. *Epilepsia*, 57(3):386–401, 2016.

[144] C Munari and J Bancaud. The role of stereo-electroencephalography (seeg) in the evaluation of partial epileptic seizures. *The Epilepsies. London: Butterworth & Co*, pages 267–306, 1985.

[145] Massimo Narizzano, Gabriele Arnulfo, Serena Ricci, Benedetta Toselli, Martin Tisdall, Andrea Canessa, Marco Massimo Fato, and Francesco Cardinale. Seeg assistant: a 3dslicer extension to support epilepsy surgery. *BMC bioinformatics*, 18(1):124, 2017.

[146] Nikhil V Navkar, Nikolaos V Tsekos, Jason R Stafford, Jeffrey S Weinberg, and Zhigang Deng. Visualization and planning of neurosurgical interventions with straight access. In *International Conference on Information Processing in Computer-Assisted Interventions*, pages 1–11. Springer, 2010.

[147] John A Nelder and Roger Mead. A simplex method for function minimization. *The computer journal*, 7(4):308–313, 1965.

[148] Soheyl Noachtar and Jan Rémi. The role of eeg in epilepsy: a critical review. *Epilepsy & Behavior*, 15(1):22–33, 2009.

[149] Jack H Noble, Benoit M Dawant, Frank M Warren, and Robert F Labadie. Automatic identification and 3-d rendering of temporal bone anatomy. *Otology & neurotology: official publication of the American Otological Society, American Neurotology Society [and] European Academy of Otology and Neurotology*, 30(4):436, 2009.

[150] Jack H Noble, Omid Majdani, Robert F Labadie, Benoit Dawant, and J Michael Fitzpatrick. Automatic determination of optimal linear drilling trajectories for cochlear access accounting for drill-positioning error. *The International Journal of Medical Robotics and Computer Assisted Surgery*, 6(3):281–290, 2010.

[151] Jack H Noble, Robert B Rutherford, Robert F Labadie, Omid Majdani, and Benoit M Dawant. Modeling and segmentation of intra-cochlear anatomy in conventional ct. In *Medical Imaging 2010: Image Processing*, volume 7623, page 762302. International Society for Optics and Photonics, 2010.

[152] Jack H Noble, Frank M Warren, Robert F Labadie, and Benoit M Dawant. Automatic segmentation of the facial nerve and chorda tympani in ct images using spatially dependent feature values. *Medical physics*, 35(12):5375–5384, 2008.

[153] Mark Nowell, Roman Rodionov, Gergely Zombori, Rachel Sparks, Gavin Winston, Jane Kinghorn, Beate Diehl, Tim Wehner, Anna Miserocchi, Andrew W McEvoy, et al. Utility of 3d multimodality imaging in the implantation of intracranial electrodes in epilepsy. *Epilepsia*, 56(3):403–413, 2015.

[154] Mark Nowell, Rachel Sparks, Gergely Zombori, Anna Miserocchi, Roman Rodionov, Beate Diehl, Tim Wehner, Gianluca Baio, Gianluca Trevisi, Martin Tisdall, et al. Comparison of computer-assisted planning and manual planning for depth electrode implantations in epilepsy. *Journal of neurosurgery*, 124(6):1820–1828, 2016.

## Bibliography

[155] Wieslaw Lucjan Nowinski, Guo Liang Yang, and Tseng Tsai Yeo. Computer-aided stereotactic functional neurosurgery enhanced by the use of the multiple brain atlas database. *IEEE transactions on medical imaging*, 19(1):62–69, 2000.

[156] John L Ochsner. Minimally invasive surgical procedures. *The Ochsner Journal*, 2(3):135–136, 2000.

[157] Jialin Peng, Fangfang Dong, Yunmei Chen, and Dexing Kong. A region-appearance-based adaptive variational model for 3d liver segmentation. *Medical physics*, 41(4):043502, 2014.

[158] Harry H Pennes. Analysis of tissue and arterial blood temperatures in the resting human forearm. *Journal of applied physiology*, 1(2):93–122, 1948.

[159] Steve Pieper, Michael Halle, and Ron Kikinis. 3d slicer. In *2004 2nd IEEE international symposium on biomedical imaging: nano to macro (IEEE Cat No. 04EX821)*, pages 632–635. IEEE, 2004.

[160] Michael JD Powell. An efficient method for finding the minimum of a function of several variables without calculating derivatives. *The computer journal*, 7(2):155–162, 1964.

[161] Hongliang Ren, Enrique Campos-Nanez, Ziv Yaniv, Filip Banovac, Hernan Abeledo, Nobuhiko Hata, and Kevin Cleary. Treatment planning and image guidance for radiofrequency ablation of large tumors. *IEEE journal of biomedical and health informatics*, 18(3):920–928, 2013.

[162] Hongliang Ren, Weian Guo, Shuzhi Sam Ge, and Wancheng Lim. Coverage planning in computer-assisted ablation based on genetic algorithm. *Computers in biology and medicine*, 49:36–45, 2014.

[163] Mario Rincón-Nigro, Nikhil V Navkar, Nikolaos V Tsekos, and Zhigang Deng. Gpu-accelerated interactive visualization and planning of neurosurgical interventions. *IEEE computer graphics and applications*, 34(1):22–31, 2013.

[164] D Rivière, D Geffroy, I Denghien, N Souedet, and Y Cointepas. Brainvisa: an extensible software environment for sharing multimodal neuroimaging data and processing tools. *Neuroimage*, 47, 2009.

[165] Gustavo K Rohde, Akram Aldroubi, and Benoit M Dawant. The adaptive bases algorithm for intensity-based nonrigid image registration. *IEEE transactions on medical imaging*, 22(11):1470–1479, 2003.

[166] Felix Rosenow and Hans Lüders. Presurgical evaluation of epilepsy. *Brain*, 124(9):1683–1700, 2001.

[167] Thomas L Saaty. Decision making with the analytic hierarchy process. *International journal of services sciences*, 1(1):83–98, 2008.

[168] Jean A Saint-Cyr, Tasnuva Hoque, Luiz CM Pereira, Jonathan O Dostrovsky, William D Hutchison, David J Mikulis, Aviva Abosch, Elspeth Sime, Anthony E Lang, and Andres M Lozano. Localization of clinically effective stimulating electrodes in the human subthalamic nucleus on magnetic resonance imaging. *Journal of neurosurgery*, 97(5):1152–1166, 2002.

[169] Ingrid E Scheffer, Samuel Berkovic, Giuseppe Capovilla, Mary B Connolly, Jacqueline French, Laura Guilhoto, Edouard Hirsch, Satish Jain, Gary W Mathern, Solomon L Moshé, et al. Ilae classification of the epilepsies: position paper of the ilae commission for classification and terminology. *Epilepsia*, 58(4):512–521, 2017.

[170] Jörg Schipper, Antje Aschendorff, Iakovos Arapakis, Thomas Klenzner, Christian Barna Teszler, Gerd Jürgen Ridder, and Roland Laszig. Navigation as a quality management tool in cochlear implant surgery. *The Journal of Laryngology & Otology*, 118(10):764–770, 2004.

[171] C Schumann, C Rieder, S Haase, H Hahn, and T Preusser. Interactive access path exploration for planning of needle-based interventions. *Roboter-Assistenten werden sensitiv.*, page 103, 2013.

[172] Christian Schumann, Jennifer Bieberstein, Stefan Braunewell, Matthias Niethammer, and Heinz-Otto Peitgen. Visualization support for the planning of hepatic needle placement. *International journal of computer assisted radiology and surgery*, 7(2):191–197, 2012.

[173] Christian Schumann, Jennifer Bieberstein, Christoph Trumm, Diethard Schmidt, Philipp Bruners, Matthias Niethammer, Ralf T Hoffmann, Andreas H Mahnken, Philippe L Pereira, and Heinz-Otto Peitgen. Fast automatic path proposal computation for hepatic needle placement. In *Medical Imaging 2010: Visualization, Image-Guided Procedures, and Modeling*, volume 7625, page 76251J. International Society for Optics and Photonics, 2010.

[174] Christian Schumann, Christian Rieder, Jennifer Bieberstein, Andreas Weihusen, Stephan Zidowitz, Jan Hendrik Moltz, and Tobias Preusser. State of the art in computer-assisted planning, intervention, and assessment of liver-tumor ablation. *Critical Reviewsâ in Biomedical Engineering*, 38(1), 2010.

[175] Christian Schumann, Christian Rieder, Sabrina Haase, Katrin Teichert, Philipp Süss, Peter Isfort, Philipp Bruners, and Tobias Preusser. Interactive multi-criteria planning for radiofrequency ablation. *International journal of computer assisted radiology and surgery*, 10(6):879–889, 2015.

[176] Davide Scorza, Gaetano Amoroso, Camilo Cortés, Arkaitz Artetxe, Álvaro Bertelsen, Michele Rizzi, Laura Castana, Elena De Momi, Francesco Cardinale, and Luis Kabongo. Experience-based seeg planning: from retrospective data to automated electrode trajectories suggestions. *Healthcare technology letters*, 5(5):167–171, 2018.

[177] Davide Scorza, Elena De Momi, Lisa Plaino, Gaetano Amoroso, Gabriele Arnulfo, Massimo Narizzano, Luis Kabongo, and Francesco Cardinale. Retrospective evaluation and seeg trajectory analysis for interactive multi-trajectory planner assistant. *International journal of computer assisted radiology and surgery*, 12(10):1727–1738, 2017.

[178] Davide Scorza, Sara Moccia, Giuseppe De Luca, Lisa Plaino, Francesco Cardinale, Leonardo S Mattos, Luis Kabongo, and Elena De Momi. Safe electrode trajectory planning in seeg via mip-based vessel segmentation. In *Medical Imaging 2017: Image-Guided Procedures, Robotic Interventions, and Modeling*, volume 10135, page 101352C. International Society for Optics and Photonics, 2017.

[179] Alexander Seitel, Markus Engel, Christof M Sommer, Boris A Radeleff, Caroline Essert-Villard, Claire Baegert, Markus Fangerau, Klaus H Fritzsche, Kwong Yung, Hans-Peter Meinzer, et al. Computer-assisted trajectory planning for percutaneous needle insertions. *Medical physics*, 38(6Part1):3246–3259, 2011.

[180] James A Sethian. Fast marching methods. *SIAM review*, 41(2):199–235, 1999.

[181] Reuben R Shamir, Martin Horn, Tobias Blum, Janh Mehrkens, Yigal Shoshan, Leo Joskowicz, and Nassir Navab. Trajectory planning with augmented reality for improved risk assessment in image-guided keyhole neurosurgery. In *2011 IEEE International Symposium on Biomedical Imaging: From Nano to Macro*, pages 1873–1876. IEEE, 2011.

[182] Reuben R Shamir, Leo Joskowicz, Luca Antiga, Roberto I Foroni, and Yigal Shoshan. Trajectory planning method for reduced patient risk in image-guided neurosurgery: concept and preliminary results. In *Medical Imaging 2010: Visualization, Image-Guided Procedures, and Modeling*, volume 7625, page 76250I. International Society for Optics and Photonics, 2010.

[183] Reuben R Shamir, Leo Joskowicz, Idit Tamir, Elad Dabool, Lihi Pertman, Adam Ben-Ami, and Yigal Shoshan. Reduced risk trajectory planning in image-guided keyhole neurosurgery. *Medical physics*, 39(5):2885–2895, 2012.

## Bibliography

[184] Reuben R Shamir, Idit Tamir, Elad Dabool, Leo Joskowicz, and Yigal Shoshan. A method for planning safe trajectories in image-guided keyhole neurosurgery. In *International Conference on Medical Image Computing and Computer-Assisted Intervention*, pages 457–464. Springer, 2010.

[185] Giovanni F Solitro and Farid Amirouche. Innovative approach in the development of computer assisted algorithm for spine pedicle screw placement. *Medical engineering & physics*, 38(4):354–365, 2016.

[186] Rachel Sparks, Vejay Vakharia, Roman Rodionov, Sjoerd B Vos, Beate Diehl, Tim Wehner, Anna Miserocchi, Andrew W McEvoy, John S Duncan, and Sebastien Ourselin. Anatomy-driven multiple trajectory planning (admtp) of intracranial electrodes for epilepsy surgery. *International journal of computer assisted radiology and surgery*, 12(8):1245–1255, 2017.

[187] Rachel Sparks, Gergely Zombori, Roman Rodionov, Mark Nowell, Sjoerd B Vos, Maria A Zuluaga, Beate Diehl, Tim Wehner, Anna Miserocchi, Andrew W McEvoy, et al. Automated multiple trajectory planning algorithm for the placement of stereo-electroencephalography (seeg) electrodes in epilepsy treatment. *International journal of computer assisted radiology and surgery*, 12(1):123–136, 2017.

[188] Rachel Sparks, Gergely Zombori, Roman Rodionov, Maria A Zuluaga, Beate Diehl, Tim Wehner, Anna Miserocchi, Andrew W McEvoy, John S Duncan, and Sebastien Ourselin. Efficient anatomy driven automated multiple trajectory planning for intracranial electrode implantation. In *International Conference on Medical Image Computing and Computer-Assisted Intervention*, pages 542–550. Springer, 2016.

[189] Susan S Spencer. The relative contributions of mri, spect, and pet imaging in epilepsy. *Epilepsia*, 35:S72–S89, 1994.

[190] J Talairach and J Bancaud. Stereotaxic approach to epilepsy. In *Progress in neurological surgery*, volume 5, pages 297–354. Karger Publishers, 1973.

[191] Daigo Tanaka, Kenji Shimada, Michael R Rossi, and Yoed Rabin. Cryosurgery planning using bubble packing in 3d. *Computer methods in biomechanics and biomedical engineering*, 11(2):113–121, 2008.

[192] Daigo Tanaka, Kenji Shimada, Mike R Rossi, and Yoed Rabin. Computerized planning of prostate cryosurgery with pullback operation. *Computer Aided Surgery*, 13(1):1–13, 2008.

[193] William O Tatum IV. *Handbook of EEG interpretation*. Demos Medical Publishing, 2014.

[194] Katrin Teichert. *A hyperboxing Pareto approximation method applied to radiofrequency ablation treatment planning*. Fraunhofer-Verlag, 2014.

[195] Stephen Tisch, Ludvic Zrinzo, Patricia Limousin, Kailash P Bhatia, Niall Quinn, Keyoumars Ashkan, and Marwan Hariz. Effect of electrode contact location on clinical efficacy of pallidal deep brain stimulation in primary generalised dystonia. *Journal of Neurology, Neurosurgery & Psychiatry*, 78(12):1314–1319, 2007.

[196] M Trope, Reuben R Shamir, Leo Joskowicz, Z Medress, G Rosenthal, A Mayer, N Levin, A Bick, and Yigal Shoshan. The role of automatic computer-aided surgical trajectory planning in improving the expected safety of stereotactic neurosurgery. *International journal of computer assisted radiology and surgery*, 10(7):1127–1140, 2015.

[197] Vejay N Vakharia, Rachel Sparks, Kuo Li, Aidan G O'Keeffe, Anna Miserocchi, Andrew W McEvoy, Michael R Sperling, Ashwini Sharan, Sebastien Ourselin, John S Duncan, et al. Automated trajectory planning for laser interstitial thermal therapy in mesial temporal lobe epilepsy. *Epilepsia*, 59(4):814–824, 2018.

[198] Vejay N. Vakharia, Rachel Sparks, Anna Miserocchi, Sjoerd B. Vos, Aidan O'Keeffe, Roman Rodionov, Andrew W. McEvoy, Sebastien Ourselin, and John S. Duncan. Computer-assisted planning for stereoelectroencephalography (seeg). *Neurotherapeutics*, 2019.

[199] Vejay N Vakharia, Rachel Sparks, Roman Rodionov, Sjoerd B Vos, Christian Dorfer, Jonathan Miller, Daniel Nilsson, Martin Tisdall, Stefan Wolfsberger, Andrew W McEvoy, et al. Computer-assisted planning for the insertion of stereoelectroencephalography electrodes for the investigation of drug-resistant focal epilepsy: an external validation study. *Journal of neurosurgery*, 130(2):601–610, 2018.

[200] Vejay N Vakharia, Rachel Sparks, Sjoerd B Vos, Andrew W McEvoy, Anna Miserocchi, Sebastien Ourselin, and John S Duncan. The effect of vascular segmentation methods on stereotactic trajectory planning for drug resistant focal epilepsy: A retrospective cohort study. *World Neurosurgery: X*, page 100057, 2019.

[201] Vejay N Vakharia, Rachel E Sparks, Kuo Li, Aidan G O'Keeffe, Fernando Pérez-García, Lucas GS França, Andrew L Ko, Chengyuan Wu, Joshua P Aronson, Brett E Youngerman, et al. Multicenter validation of automated trajectories for selective laser amygdalohippocampectomy. *Epilepsia*, 2019.

[202] Rohan Vijayan, Tharindu De Silva, Runze Han, Xiaoxuan Zhang, Ali Uneri, Sophia Doerr, Michael Daniel Ketcha, Alexander Perdomo-Pantoja, Nicholas Theodore, and Jeffrey H Siewerdsen. Automatic pedicle screw planning using atlas-based registration of anatomy and reference trajectories. *Physics in Medicine & Biology*, 2019.

[203] Caroline Villard, Claire Baegert, Pascal Schreck, Luc Soler, and Afshin Gangi. Optimal trajectories computation within regions of interest for hepatic rfa planning. In *International Conference on Medical Image Computing and Computer-Assisted Intervention*, pages 49–56. Springer, 2005.

[204] Caroline Villard, Luc Soler, Afshin Gangi, Didier Mutter, and Jacques Marescaux. Toward realistic radiofrequency ablation of hepatic tumors 3d simulation and planning. In *Medical Imaging 2004: Visualization, Image-Guided Procedures, and Display*, volume 5367, pages 586–595. International Society for Optics and Photonics, 2004.

[205] Caroline Villard, Luc Soler, Nicolas Papier, Vincent Agnus, Sylvain Thery, Afshin Gangi, Didier Mutter, and Jacques Marescaux. Virtual radiofrequency ablation of liver tumors. In *International Symposium on Surgery Simulation and Soft Tissue Modeling*, pages 366–374. Springer, 2003.

[206] Ryan Wicker and Buz Tedla. Automatic determination of pedicle screw size, length, and trajectory from patient data. In *The 26th Annual International Conference of the IEEE Engineering in Medicine and Biology Society*, volume 1, pages 1487–1490. IEEE, 2004.

[207] Wilhelm Wimmer, Frederic Venail, Tom Williamson, Mohamed Akkari, Nicolas Gerber, Stefan Weber, Marco Caversaccio, Alain Uziel, and Brett Bell. Semiautomatic cochleostomy target and insertion trajectory planning for minimally invasive cochlear implantation. *BioMed research international*, 2014, 2014.

[208] Chen Xiaozhao, Huang Jinfeng, Mao Baolin, Yan Chongnan, and Kang Yan. A method of lumbar pedicle screw placement optimization applied to guidance techniques. *Computer Assisted Surgery*, 21(sup1):142–147, 2016.

[209] Liangjing Yang, Rong Wen, Jing Qin, Chee-Kong Chui, Kah-Bin Lim, and Stephen Kin-Yong Chang. A robotic system for overlapping radiofrequency ablation in large tumor treatment. *IEEE/ASME Transactions on Mechatronics*, 15(6):887–897, 2010.

[210] Ziv Yaniv, Patrick Cheng, Emmanuel Wilson, Teo Popa, David Lindisch, Enrique Campos-Nanez, Hernan Abeledo, Vance Watson, Kevin Cleary, and Filip Banovac. Needle-based

interventions with the image-guided surgery toolkit (igstk): From phantoms to clinical trials. *IEEE transactions on biomedical engineering*, 57(4):922–933, 2009.

[211] Brett E Youngerman, Farhan A Khan, and Guy M McKhann. Stereoelectroencephalography in epilepsy, cognitive neurophysiology, and psychiatric disease: safety, efficacy, and place in therapy. *Neuropsychiatric disease and treatment*, 15:1701, 2019.

[212] Jie Yu, Ping Liang, Xiaoling Yu, Fangyi Liu, Lei Chen, and Yang Wang. A comparison of microwave ablation and bipolar radiofrequency ablation both with an internally cooled probe: results in ex vivo and in vivo porcine livers. *European journal of radiology*, 79(1):124–130, 2011.

[213] Paul A Yushkevich, Joseph Piven, Heather Cody Hazlett, Rachel Gimpel Smith, Sean Ho, James C Gee, and Guido Gerig. User-guided 3d active contour segmentation of anatomical structures: significantly improved efficiency and reliability. *Neuroimage*, 31(3):1116–1128, 2006.

[214] Rina Zelmann, Silvain Bériault, MM Marinho, Kelvin Mok, Jeffery A Hall, Nicolas Guizard, Claire Haegelen, Andre Olivier, G Bruce Pike, and D Louis Collins. Improving recorded volume in mesial temporal lobe by optimizing stereotactic intracranial electrode implantation planning. *International journal of computer assisted radiology and surgery*, 10(10):1599–1615, 2015.

[215] Rina Zelmann, Silvain Beriault, Kelvin Mok, Claire Haegelen, Jeff Hall, G Bruce Pike, Andre Olivier, and D Louis Collins. Automatic optimization of depth electrode trajectory planning. In *Workshop on Clinical Image-Based Procedures*, pages 99–107. Springer, 2013.

[216] Weiming Zhai, Jing Xu, Yannan Zhao, Yixu Song, Lin Sheng, and Peifa Jia. Preoperative surgery planning for percutaneous hepatic microwave ablation. In *International Conference on Medical Image Computing and Computer-Assisted Intervention*, pages 569–577. Springer, 2008.

[217] Qi Zhang, Meng Li, Xiaozhi Qi, Ying Hu, Yongmei Sun, and Gang Yu. 3d path planning for anterior spinal surgery based on ct images and reinforcement learning. In *2018 IEEE International Conference on Cyborg and Bionic Systems (CBS)*, pages 317–321. IEEE, 2018.

[218] Rui Zhang, Shuicai Wu, Weiwei Wu, Hongjian Gao, and Zhuhuang Zhou. Computer-assisted needle trajectory planning and mathematical modeling for liver tumor thermal ablation: A review. *MATHEMATICAL BIOSCIENCES AND ENGINEERING*, 16(5):4846–4872, 2019.

[219] Gergely Zombori, Roman Rodionov, Mark Nowell, Maria A Zuluaga, Matthew J Clarkson, Caroline Micallef, Beate Diehl, Tim Wehner, A Miserochi, Andrew W McEvoy, et al. A computer assisted planning system for the placement of seeg electrodes in the treatment of epilepsy. In *International Conference on Information Processing in Computer-Assisted Interventions*, pages 118–127. Springer, 2014.

[220] Maria A Zuluaga, Roman Rodionov, Mark Nowell, Sufyan Achhala, Gergely Zombori, Alex F Mendelson, M Jorge Cardoso, Anna Miserocchi, Andrew W McEvoy, John S Duncan, et al. Stability, structure and scale: improvements in multi-modal vessel extraction for seeg trajectory planning. *International journal of computer assisted radiology and surgery*, 10(8):1227–1237, 2015.